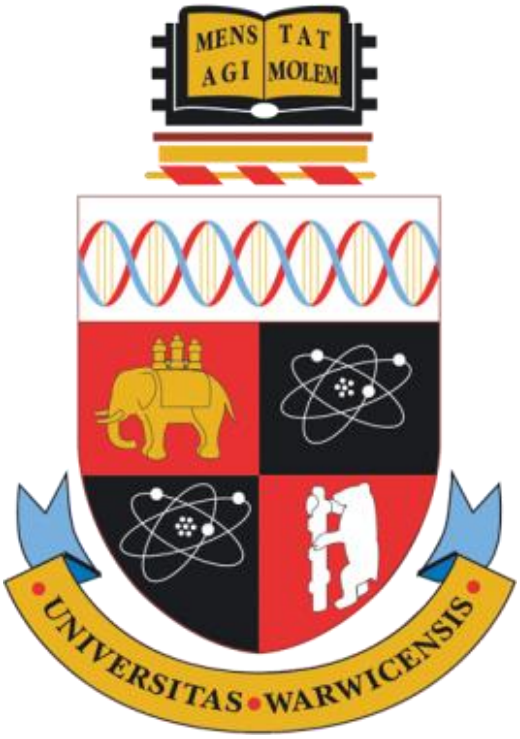

In-situ instrumentation for smart energy storage

by

Joe Fleming

Thesis

Submitted to the University of Warwick for the degree of

Doctor of Philosophy

October 2018

Contents

Contents ..... **i**

List of figures iii

List of tables viii

List of equations ix

List of abbreviations x

Acknowledgements xii

Declaration xii

1 Abstract **1**

2 Introduction **2**

3 Literature review **4**

3.1 Introduction 4

3.2 The Lithium-ion cell 5

3.3 Electronic sensors for *in-situ* monitoring 12

3.4 Optical fibre sensors 23

4 Hypotheses **27**

4.1 Introduction 27

4.2 Hypothesis one 28

4.3 Hypothesis two 29

4.4 Hypothesis three 30

5 Experimental setup, materials and equipment **31**

5.1 Introduction 31

5.2 *In-situ* sensors for Lithium-ion cylindrical and pouch cells 32

5.3 Fibre optic sensors for cylindrical Lithium-ion cells 35

5.4 Analysis methodology 37

6 Instrumentation of pouch cells **43**

6.1 Introduction 43
6.2 Research and development 44
6.3 Chapter conclusions 64

7 Instrumentation of cylindrical cells 66

7.1 Introduction 66
7.2 Research and development 67
7.3 Chapter conclusions 77

8 Optical instrumentation of cylindrical cells 78

8.1 Introduction 78
8.2 Research and development 79
8.3 Chapter conclusions 94

9 Thermo-electrochemical instrumentation of cylindrical cells 95

9.1 Introduction 95
9.2 Research and development 96
9.3 Chapter conclusions 107

10 Thesis conclusions 108

11 Further work 110

12 Reference list 111

13 Appendix 124

13.1 Frequency domain analysis of optical instrumented cylindrical cells 124
13.2 Pouch cell instrumented 126
13.3 18650 frequency data 127

List of figures

Figure 1 An illustration of Lithium-ion cells[4] of different form factors 5
Figure 2 Illustration of hazards associated with a pouch cell and cylindrical lithium-ion cell 8
Figure 3 Temperature sensor output response for Thermocouple, RTD and Thermistors 13
Figure 4 Thermistor instrumentation circuit examples (A) voltage divider circuit (B) Wheatstone Bridge 14
Figure 5 Illustration of a complete instrumentation design for thermistors temperature measurement. 15
Figure 6 Calibration response of sensor proposed by Martiny[27] *et al*. A clear signal noise is apparent within the origin of the data. 17
Figure 7 Thin-Film Thermocouple array and cold junction compensation[31] 18
Figure 8 FBG sensing principle - black lines related to sensing zones[86] 24
Figure 9 Strain resistant FBG assembly[88] 24
Figure 10 Illustration of the pouch cell instrumented experimental cell setup 35
Figure 11 Illustration of an instrumented 18650 experimental setup 37
Figure 12 Illustration of an optical instrumented 18650 cell experimental setup ... 38
Figure 13 Optical System setup for interrogating FBG sensor arrays using an optical circulator, broadband laser source and an optical spectrum analyser 39
Figure 14 Failed conformal coating showing clear track corrosion and delamination 45
Figure 15 Failed sensor versus a coasted sensor embedded into a pouch cell during a CC/CV cycling phase 47
Figure 16 Failed sensor versus a coasted sensor embedded into a pouch cell during a CC/CV cycling phase 47
Figure 17 Distributed thermal sensors (A),(B),(D) and (F) for pouch cell constructions and (C) and (E) for cylindrical cells 49
Figure 18 Thermistor instrumentation circuit conditioning 50
Figure 19 Illustration of poor electrode coating. 52

Figure 20 Anode and cathode mass variations during manufacturing for instrumented cell production units showing a maximum of 0.4% variation from the 53
Figure 21 Cycling aging of a reference vs an instrumented cell at C/10 for a Lithium-ion pouch cell showing negligible aging versus a non-instrumented cell..... 54
Figure 22 *in-situ* Thermistor embedding and testing procedure for a Lithium-ion pouch cell (a) Sensor insertion (b) Hot melt tape applied (C) Unit sealed using heat bars and (D) Complete instrumented cell 55
Figure 23 In-situ temperature response of Lithium-ion cell 1-C rate 56
Figure 24 *In-situ* thermal response of a pouch cell using distributed thermistor elements and corresponding x-ray tomography image 57
Figure 25 Illustration of a 100-cycle capacity extract of instrumented pouch cells vs none instrumented at a rate of C/10 using a CC/CV charge and CC discharge. 58
Figure 26 Illustration of Electrochemical Impedance Spectroscopy (EIS) at 100% and 0% SoC for pristine cells and modified cells 59
Figure 27 (A) sensor removed from pouch (B) Anode material (C) separator material 60
Figure 28 Illustration of sensors removed from an instrumented cell before and after cycling 61
Figure 29 Instrumented pouch cell construction showing modification procedure 62
Figure 30 *In-situ* inspection of an instrumented pouch cell (A) top view of sensor (B) side view of pouch cell and (C) top view of pouch cell 63
Figure 31 Core temperature sensor for a cylindrical cell. The 7-point sensor covers the entire core length 67
Figure 32 Failed Sensor removed from the core a of an 18650 cell 68
Figure 33 3D view and 3D clipped showing sensors entry into an 18650 cell and possible points of failure 68
Figure 34 Instrumented 18650 Cells. (A) shows the top cap drilled through and (B) top cap left intact 69
Figure 35 Long-term 0-100% SoC cycling of an instrumented cell. Data collected over 100 cycles, with axis breaks to improve readability. Consistent and stable cycling behaviour is clearly visible[104,107,108] 70

Figure 36 *In-situ* temperature profile of an 18650 cell during a CC/CV charge and CC discharge cycle..... 71
Figure 37 Lithium-ion battery core and *in-situ* temperature under a high constant current load (2C). Clear difference between the internal and the external cell temperature is visible. The core temperature is significantly higher yet still below the safety limit. 72
Figure 38 Pulsed power rapid discharge of an instrumented 18650 cylindrical cell. Clear and increasing difference between the external and internal temperature is shown. 73
Figure 39 Illustration of Electrochemical Impedance Spectroscopy (EIS) at 100% and 0% SoC for pristine cells and modified cells 75
Figure 40 *In-situ* inspection of instrumented cells showing the assembly procedure, sensor methodology and resulting effects on the sensor extracted 75
Figure 41 XCT 2D scans of an instrumented 18650 cell after the modification procedure 76
Figure 42 *In-situ* x-ray of an instrumented 18650 cell showing room for manoeuvre within the core 80
Figure 43 - (A) assembly detail for instrumented cell and (B) complete system 81
Figure 44 failed sensor insertion techniques using the negative entry side of the cell. 82
Figure 45 *In-situ* sensor consutrction. (A) Sensor removed using a pipe cutter (B) Cap and entry hole exposed (C) Two in one sensor construction (d) complete instrumented cell..... 82
Figure 46 Illustration of the failed FBG sensor calibration at various temperatures 84
Figure 47 Illustration of the FBG two-point calibration and long-term stability of the instrument 84
Figure 48 100 Cycle extract for a stable sensor construction of an 18650 cell 85
Figure 49 Average core temperature, can and drive voltage..... 87
Figure 50 Thermal discharge characteristics extract from Figure 49 87
Figure 51 Thermal charging characteristic extract from Figure 49 88
Figure 52 Illustration of the disturbed *in-situ* thermal data of 18650 cell 88
Figure 53 Discharge capacity comparison of an instrumented vs virgin pouch cell . 89

Figure 54 Illustration of Electrochemical Impedance Spectroscopy (EIS) at 100% and 0% SoC for pristine cells and modified cells at 1 and 100 cycles 91
Figure 55 Illustration of Electrochemical Impedance Spectroscopy (EIS) at 100% and 0% SoC for pristine cells and modified cells 91
Figure 56 CT Scan of a modified cell - (A) instrumented cell assembly (B) top view of cell and entry hole (C) complete instrumented cell (D) top view XCT image and (E) *In-situ* view of optical sensor 93
Figure 57 Failed experimental setup of a 2-in-1 thermo-electrochemical sensor, using a potting compound to form a complete mass 97
Figure 58 Illustration of a failed optical sensor assembly, clearly indicating a measurement cross sensitivity on the fibre 98
Figure 59 A two in one thermo-electrochemical sensor for smart cells'[107] 99
Figure 60 Illustration of the instrumentation methods used within this study[107] .. 100
Figure 61 *In-situ* sensor validation of the two in one sensor using a reference thermocouple[107] 101
Figure 62 Rapid charging protocol and *in-situ* thermal response of an instrumented 18650 cell[107] 102
Figure 63 A failed 2-in-1 thermo-electrical sensor[107] 103
Figure 64 Illustration of the cell potentials of failed a lithium-disc reference electrode embedded into a cylindrical cell[107] 104
Figure 65 Illustration of a Platinum wire reference electrode drift failure over-time[107] 104
Figure 66 Illustration of stable reference electrode potentials using a lithium tongue instrumentation[107] 105
Figure 67 Impedance response of a modified versus virgin cell assembly[107] 106
Figure 68 Illustration of an instrumented cells EIS for a 18650 at 0% SoC for cycle 1 and 100 124
Figure 69 Illustration of an instrumented cells EIS for a 18650 at 100% SoC for cycle 1 and 100 124
Figure 70 Illustration of an instrumented cell versus a virgin cell EIS for a 18650 at 100% SoC 125

Figure 71 Illustration of an instrumented cell versus a virgin cell EIS for a 18650 at 0% SoC 125
Figure 72 Normalised data for EIS study of an instrumented versus a virgin cell at 0% SoC 126
Figure 73 Normalised data for EIS study of an instrumented versus a virgin cell at 100% SoC 126
Figure 74 Nominalised data EIS study of an instrumented 18650 cell at 0% (top figure) and 100% (bottom figure) SoC showing a slight drift in the diffusion region of the device compared to an non-instrumented cell 127

List of tables

Table 1 Thermistors, RTD and Thermocouple characteristics comparison table 13
Table 2 WMG pouch cell production capacity specifications..... 32
Table 3 BD 18650 characteristics..... 33
Table 4 LG INR18650 HG2 18650 characteristics..... 35
Table 5 GEIS configuration for instrumented cell research 40
Table 6 Metris X-TEK XTH 320 LC XCT configuration..... 41
Table 7 Murata NCP03WF104F05RL NTC thermistor element characteristics[117]..... 44
Table 8 Conformal coating testing results for pouch and cylindrical cell formations 46
Table 9 Cyclic data of poor production quality cells during formation 52
Table 10 Cyclic data of poor production quality cells over 10 cycles 52
Table 11 Instrumented pouch cell cycling aging after 35 cycles at C/10..... 53
Table 12 Raw FBG sensor specification..... 79
Table 13 Modified FBG assembly specification..... 85

List of equations

Equation 1 ADC voltage input transfer function from thermistor instrumentation. 50

Equation 2 Steinhart-Hart equation used for converting thermistor resistance to temperature 51

List of abbreviations

18650	18 x 65 mm cylindrical cell
AC	Alternating current
ADC	Analogue to digital converter
ASIC	Application specific integrated circuit
BMS	Battery management system
BTMS	Battery thermal management system
CC	Constant current
CTE	Coefficients of Linear Thermal Expansion
Cu	Copper
CV	Constant voltage
CVD	Chemical vaper disposition
DAQ	Data acquisition
DC	Direct current
DSP	Digital signal processing
EIS	Electrochemical impedance spectroscopy
EMC	Electromagnetic compatibility
EMI	Electromagnetic interference
EV	Electric vehicle
FBG	Fibre Bragg gratings
FEP	Fluorinated Ethylene Propylene
LA	Lead acid
Li	Lithium

Li-ion	Lithium-ion
$LiPF_6$	Lithium Hexafluorophosphate
MEMS	Micro-Electro-Mechanical Systems
NCA	Nickel Cobalt Aluminium oxide
Ni	Nickel
O2	Oxygen
PPM	Parts per million
Pt	Platinum
PTFE	Polytetrafluoroethylene
RTD	Resistance temperature detector
SoC	State of Charge
SoH	State of Health
XCT	X-ray Computed tomography

Acknowledgements

I would like to thank my supervisors Rohit Bhagat, Dave Greenwood and Dave Towers for the advice and support in the completion of this PhD. Furthermore, Tazdin Amietszajew patience, knowledge and continued support in developing my skills has been invaluable for completing this work. I would also like to thank Jaguar Land Rover and the EPSRC for funding this thesis.

Lastly, I thank my iron-lady wife, Georgina for providing invaluable support and encouragement throughout the PhD.

Declaration

This thesis is submitted to the University of Warwick in support of my application for the degree of Doctor of Philosophy. It has been composed by myself and has not been submitted in any previous application for any degree.

Inclusion of published work

The research presented within this thesis is published in the following journals or is under review;

Peer reviewed journals

1. **Fleming, J**., Bhagat, R., Roberts, A. J., Amietszajew, T., Charmet, J., & Greenwood, D. (2019). The design and impact of *in-situ* and operando thermal sensing for smart energy storage. ***Journal of Energy Storage***, 22(October 2018), 36–43. https://doi.org/10.1016/j.est.2019.01.026
2. **Fleming, J.,** Amietszajew, T., Greenwood, D., & Bhagat, R. (2018). Development and evaluation of in-situ instrumentation for cylindrical Li-ion cells using fibre optic sensors. ***HardwareX***, *3*, 100–109
3. McTurk, E., Amietszajew, T., **Fleming, J**., & Bhagat, R. (2018). Thermo-electrochemical instrumentation of cylindrical Li-ion cells. ***Journal of Power Sources***, *379*, 309–316
4. Amietszajew, T., McTurk, E., **Fleming, J**., & Bhagat, R. (2018). Understanding the limits of rapid charging using instrumented commercial 18650 high-energy Li-ion cells. ***Electrochimica Acta*****,** *263*, 346–352.

International conferences (presenter)

1. GRS Batteries: Ventura, California, USA. 2017
2. 233rd ECS: Seattle, Washington State, USA. 2018
3. IDTechex: Santa Clara, California, USA, 2018

Equipment and experimental contributions

1. **X-Ray CT –** Remy Guillaume
2. **Cell Instrumentation -** Tazdin Amietszajew and Euan McTurk

1 Abstract

Lithium-ion technology is an increasing choice for battery powered systems, offering long-lasting, reliable and efficient energy storage. However, significant safety and performance challenges within the technology are still apparent. The current state of the art for monitoring cells performance is typically based on observing full cell voltage and occasional temperature sensor on the skin of a cell. Consequently, it is extremely difficult to track cells' health within complex, especially high-performance, battery systems. Therefore, a new way of characterising cells' is required. Here we show the design and manufacturing methods of transforming normal cells into smart systems. The sensor topologies embedded into the cells were electrical temperature, electro-chemical and optical temperature sensors. This enabled *in-situ* and operando thermal and electrochemical data collection during cells' real-life operations.

In this work, the impact of the sensors upon the cells performance has been shown to be negligible, with over 100 cycles conducted, versus unmodified cells for both pouch and cylindrical formats. This was validated using time and frequency domain analysis. A significant temperature difference was identified between the cell's core and can temperatures of up to 6 °C during discharge and 3 °C during charge phase. Therefore, this work illustrates the necessity of internal cell temperature measurements for thermal management and safety validation. Lastly, with the aid of the *in-situ* measurement tools, certain cells can be further optimised without compromising thermal safety limits, while under particular scenarios safety limits can be breached earlier than the external sensors would indicate, showing how paramount *in-situ* data is to the operational safety.

2 Introduction

The societal drive for high capacity, reliable, long-lasting and scalable renewable energy storage for electric vehicle and off-grid systems is driving the development of battery technology. Previous efforts for large scale energy storage were typically based upon lead-acid (LA) batteries, but LA technology is becoming obsolete for automotive applications, due to the significant technological benefits of other energy storage chemistries.

Lithium-ion cells are a form of rechargeable battery, where lithium ions are the majority charge carriers during operation. The technology is a common choice for high capacity applications, due to several advantages; a high energy density, limited memory effect and high output voltage[1]. However, Lithium-ion cells have several limitations, including; performance temperature sensitivity, risk of explosive failure and operational performance is reduced over time. Despite these limitations, Lithium-ion technology is set to for a rapid boom over the next decade, including, integration into consumer electronics, automotive, energy distribution, medical and military applications.

The rapid expansion of such technology, ahead of a full understanding of its constraints, has led to several high-profile events occurring. Consequently, highlighting the issue that further understanding of the technology is required. Such events include; mass mobile phone recalls by Samsung, Tesla cars catching fire and electronic cigarettes exploding. Each example of failure previously mentioned, use different form factors of Lithium-ion cell, but end with the same result of failure.

The typical method of characterizing a cell is by two factors, the state of charge (SoC) and state of health (SoH), where, the SoH is a particular measure of the performance characteristics such as peak-current delivery, cycle-time and capacity degradation. The SoC is the amount of energy in a cell relative to its capacity, which is dependent upon many factors such as cell chemistry, surrounding environmental conditions and cycle rate, among many factors.

Determining the SoC and SoH parameters is typically performed by a battery management system (BMS). The BMS incorporates sensors, software algorithms and know how knowledge to form accurate SoC and SoH measures. The battery is, however, an extremely complex system and current approaches fail to accurately predict SoC and SoH estimators.

Typically, cells are assembled into modules, which are in turn assembled to form battery packs. Within a module, sensors are attached the surface of a select number of cells[2], monitoring voltage, current and temperature. However, thermal management systems, environmental disturbances and unforeseen events within the module can cause a sensor response to produce false or misleading data[3]. Consequently, measuring the true state of a cell is uncertain, which can lead to unobservable events occurring. Including; thermal hot spots, areas of inactivity or mechanical expansion. Therefore, the strategy of single point surface measurements is not necessarily optimized for providing an accurate indicator of a cell's true condition, thus one of the SoH indicators could be inaccurate

Consequently, this work aims to address the design of reliable and repeatable sensing methodologies for monitoring in-operando performance indicators. The proposed research has significant industrial impact allowing battery packs to be optimised for electrical performance, fault tolerance, robust structure, lifetime optimisation, light-weighting and design for re-manufacture. The data gained will add to internal working knowledge of a cell and could help to validate cell modelling algorithms. An in-operando view of and distributed view of thermal activity could help aid the battery management system for SoH and SoC prediction, battery optimisation and safety analysis.

3 Literature review

3.1 Introduction

This chapter reviews the technology required for this research and describes fundamental principles of several temperature sensing topologies. A description of the Lithium-ion cell and sensor topologies are given. Lastly, the chapter further explores current state of the art methods for a smart cell system.

3.2 The Lithium-ion cell

The construction of a lithium-ion cell has several different forms factors, internal constructions and performance characteristics. Here, is outlined the construction of common form factors and a description of the core assembly components used within the lithium-ion cell system. Figure 1 shows an example of some form factors.

Figure 1 An illustration of Lithium-ion cells[4] of different form factors

Typically, the device is constructed of five core sub-assemblies;

1. Electrolyte
2. Separator
3. Electrodes (Anode and Cathode)
4. Outer enclosure
5. Current collectors.

Additionally, some manufactures choose to include further enhancements to a battery construction. However, such devices can reduce the overall power density, weight and increase overall system cost. The added devices[5] could include a fuse, pressure sensitive venting or diodes .

Electrolyte

The electrolyte solution used in lithium-ion batteries is commonly a mixture of lithium salts in an organic solution, providing a path for ionic charge flow between the electrodes. The Electrolyte mixture used within a cell is dependent upon the operating characterizes required of the battery[4], such as operational temperature range and electrochemical performance. Typically, modifications of the performance

of the electrolyte is achieved by altering the properties of the electrolyte using various additives.

As the electrolyte solution immerses the whole battery system, the materials used in the battery must be able to withstand interactions from electrolyte solution during operation and rest. Furthermore, the electrolyte solution must be stable in the presence of the reducing and oxidising conditions imposed from the negative and positive electrodes respectively[6]. Lastly, the materials used in battery system are protected from corrosion caused from the electrolyte, this is achieved via protective films[7] or operate within a defined electrochemical potential window[8] of the electrolyte, thus reducing the chances that the materials are oxidized or reduced

Separator

The separator as an electrical insulator between the electrodes and provides a path for ionic charge flow, due to the separators low porosity and it is wetted with an electrolyte solution. The separator is can often be combined into a lamination of several different layers, effectively forming a safety mechanism. For example, if the temperature of the cell is too high the porosity of the separator will reduce and stop any flow of charge occurring. The effect of the shutdown can be localized to a region or the entire cell stack, they are commonly referred to as shutdown separators[4].

Current collector

The current collector is typically constructed using a conductive metal such as copper and aluminium. The collector is coated also coated with the electrode material. The purpose is to enable a route for the flow of current into the cell[4].

The entry hole into the cell for the tabs enclosure is sealed using a polymer hot melt adhesive during manufacturing, for pouch cell constructions. While in the case of cylindrical formations the entire enclosure acts as the positive and negative tabs. The current collectors are ultrasonically welded to the can enclosure during manufacturing

Enclosure

The enclosure plays an important role in the battery, the function is to protect the internal battery stack from the environment and hold the stack mechanically stable. The enclosure can be constructed from several different materials such as stainless steel, aluminium or metallised polymer foils for example. Some common form factors of the enclosure are cylindrical or flat pouch cells as shown in Figure 1.

3.2.1 Temperature and Lithium-ion cells

Lithium-ion chemistries are sensitive to temperature[2,9,18–27,10,28–37,11,38–44,12–17] variations which affect performance[22], lead to capacity degradation[12] or even catastrophic failures[13]. The risk of internal overheating is especially increased during cells' performance assessment, when it is especially important to closely monitor thermal responses.

As the current applied to the cells increases, so does the heat generation – Joule (resistive) heating coming from the electrolyte, anode and cathode resistances and exothermic reactions – electrode materials entropy changes, a phenomena unavoidable as part of the cells normal operation[45]. In extreme cases, as the cell internal temperature increases so does the rate of electrolyte decomposition, leading to gas formation and eventually cell rupture[46].

Currently, to monitor cells' operating parameters and estimate their State of Health and charge, they are fitted with sensors that monitor voltage, current flow and surface temperatures. However, in most use cases, especially in automotive applications, battery modules contain an array of tightly packed lithium-ion cells to meet specific power and energy requirements, consequently generating significant amounts of heat during cycling, leading to overheating, performance issues and thermal gradients. However, to maintain optimum temperatures and State of Health prediction a battery thermal management system[47,48] (BTMS) and a battery management system (BMS) are employed.

3.2.2 *In-situ* hazards

Several hazards that could affect the reliability and repeatably of sensing technology embedded into the cell is apparent, Such disturbances include mechanical, chemical and electromagnetic interference, Figure 2 illustrates an example of *in-situ* hazards common to cylindrical and pouch cell formations.

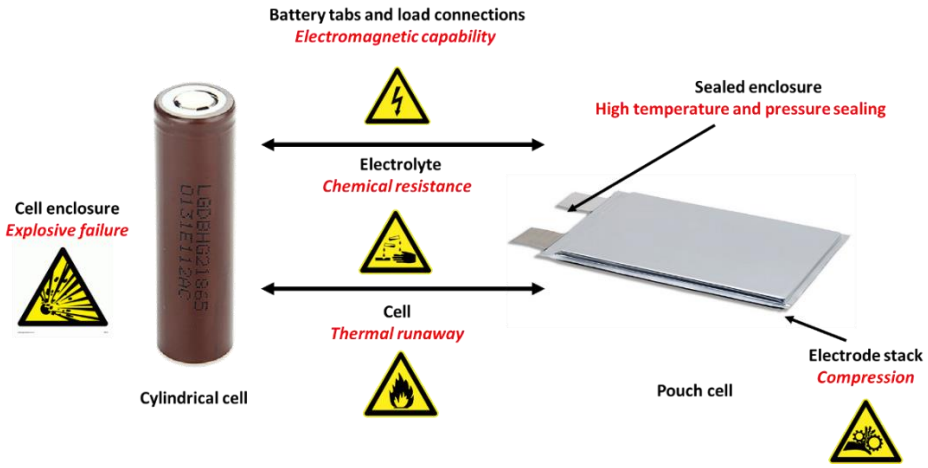

Figure 2 Illustration of hazards associated with a pouch cell and cylindrical lithium-ion cell

Chemical

The electrolyte solution within a battery can become highly corrosive and give rise to hydrofluoric acid in the presence of moisture. Thus, protection will most likely have to be added to the sensing element. Furthermore, un-even distribution of electrolyte could interfere with the electrochemical process of the cell, this could be a concern with embedding sensors with the stack where significant electrochemical activity is occurring. Consequently, leading to areas of inactivity and dry zones within the cell.

Mechanical

For pouch cell constructions, during manufacturing the cells are put under vacuum and/or compression to maintain a tight stack formation, and further compressive techniques may be used during formation and subsequent cycling. Therefore, considerable forces are applied which may affect any *in-situ* sensor. Lastly, the electrode material itself will expand and contract during cycling as the lithium-ions

move from anode to cathode material, causing changes to the material properties, the cell expansion percentage is dependent upon the cell construction. The sensing element would have to be immune to strain or self-calibrate over time.

A further point of failure is also added if a sensor wire is protruding from the cell assembly, this could lead to electrolyte loss and/or foreign elements entering the system.

Electromagnetic

The cell is connected to an electrical system including switching devices which may give rise to electromagnetic noise that could couple to the sensing elements or instrumentation. Consequently, causing false and misleading data to be measured by the system. Introducing signal conditioning circuits can minimize this effect. The method used will depend on the coupling mode (common or differential) and coupling path (inductive or capacitive). It must also be noted that the sensors must not adversely affect other nearby systems. The electromagnetic compliance can be evaluated using standard electromagnetic emissions and immunity testing

3.2.3 Battery management

3.2.3.1 Battery management system

The Lithium-ion cell requires a carefully designed battery management system (BMS) to ensure the cell is operated within very specific and tightly controlled limits, such limits includes a specific charging protocol and operating temperature. Furthermore, several other features such as State-of-charge and State-of-health can be calculated within the battery management system.

3.2.3.2 Battery thermal management system

The aim of the batter thermal management system (BTMS) is to maintain a certain degree of temperature uniformity within the battery module. The technology used to remove excess heat can include liquid/air cooling, heat pipes, cooling plates or phase changing materials[3,49]. A BMS' purpose is to prolong the battery life, predict/prevent failure events and maintain the batteries' flow of energy to the end application.

Within a battery module for an EV system, the battery management system typically monitors the module with one or two sensors due to the cost implications associated with monitoring every cell. These few sensors are used to infer the temperature of all cells within that module. Furthermore, for the monitoring of individuals cells, a battery management system typically monitors voltage, current, power and in some cases temperature[50]. The data from the sensing elements are interpreted using computational algorithms and equivalent circuit modelling data to identify the most appropriate operating profile given the cell's State of Charge, ambient temperature and driving conditions.

However, the approach fails to produce accurate information regarding distributed temperature profiles and unforeseen events occurring within the system. Additionally, due to modelling not taking into account the full cooling effect, cell geometry, mechanical arrangement of cells and external influences[3], the current strategy is not necessarily optimized in providing an accurate state of health estimation. This means unobservable events including thermal hot spots, areas of inactivity or mechanical expansion may be present.

To help avoid failure the cells are often over engineered and run below their maximum performance levels.

3.2.3.3 Charging protocol

The standard method for charging lithium-ion cells is by applying a constant-current (CC) then constant-voltage (CV). This method is widely accepted and used in most battery management systems. However, advanced charge protocols[51–56] including pulse charging (PC), boost phase, and many other variations do exist.

The selection of the protocol to apply to a cell is typically defined by the cell manufacture, hardware limitations within the battery management system, capital cost of the equipment and effect upon cell performance. A clear lack of experimental *in-situ* data in literature is present currently. Meaning such algorithms could be further improved for increased performance using the proposed technology.

3.3 Electronic sensors for *in-situ* monitoring

3.3.1 Temperature

Temperature sensors operate with the hope that the materials respond to a predictable degree and measurably with surrounding temperature changes. Among many ways to sense the change in temperature, three significant technologies are resistance temperature detectors [RTD], thermocouples and thermistors. These three sensors are differentiated by material and operating principles; each device has unique system responses which are crucial for deciding which one is appropriate for the end application.

An RTD is fabricated using a metal formed with a known volume and area. The resistance of the sensing element changes to predictable degree with ambient temperature. RTDs can require significantly more instrumentation such as amplifiers and filtering circuits due to the limited sensitivity. However, the high accuracy and a near linear output are beneficial.

Thermocouples are one of the most common and familiar methods to measure temperature exploiting the Seebeck effect. The technology uses two dissimilar metals that are joined at a common point. Thermocouples measure relative temperature changes, only which makes them unsuitable for some application due to the cold junction requirement. The sensitivity of the device is also low compared to an RTD or thermistor. Additional analogue conditioning circuits are required to perform measurements over the entire operating range of the sensor.

A thermistor is a resistor that's resistance is highly dependent upon the ambient temperature. The device is typically constructed from an oxide material or ceramic, which provides high sensitivity and repeatability though out the temperature range[57]. The problem is the non-linear output of the sensor which adds further firmware resources to the design solution or hardware. The instrumentation requirement is still less compared with a thermocouple and an RTD. A comparison of the three sensor topologies is shown below in Table 1 and illustrated in Figure 3 is a

comparison of the output gain of each sensor versus temperature for all three topologies

Table 1 Thermistors, RTD and Thermocouple characteristics comparison table

	Thermocouple	**RTD**	**Thermistor**
Temperature range	-210 °C to 1750 °C	-240 °C to 650 °C	-40 °C to 250 °C
Accuracy	0.5 to 5°C	0.1 to 1°C	0.05 to 1.5°C
Instrumentation requirements	Cold junction Amplification, Scaling	Power source Scaling	Power Source Scaling

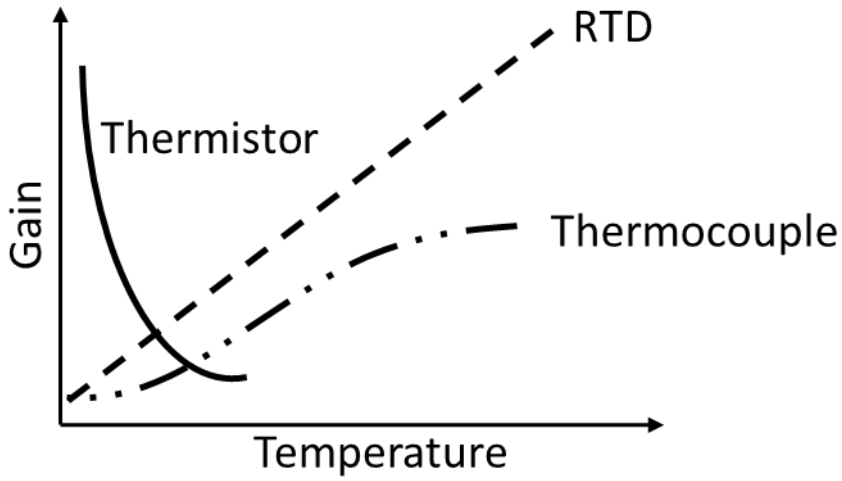

Figure 3 Temperature sensor output response for Thermocouple, RTD and Thermistors

Thermistor Instrumentation

A thermistor is a temperature to resistance converter, to enable the BMS to monitor temperature, the resistance value must be converted into a voltage for the analogue-to-digital converter.

Two methods of converting the thermistor resistance to a voltage is shown below in Figure 4. Both circuits offer the same basic function to convert an unknown resistance to a voltage. However, each circuit requires a different circuit on the output for correct conditioning of the voltage measurement. Both elements R1 act as a linearization circuit, which is beneficial as the output response of the thermistor follows an exponential curve. However, version (B) requires two additional components and correct balancing of the bridge for correct operation.

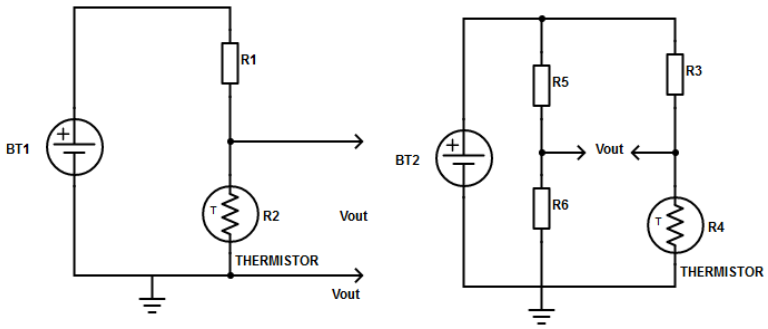

Figure 4 Thermistor instrumentation circuit examples (A) voltage divider circuit (B) Wheatstone Bridge

The complete instrumentation circuit for reliable temperature measurement using a thermistor is shown below in Figure 5. L2 and C2 are a filter for removing unwanted noise from the power supply, L1 is a serial common mode filter. U1 is a buffer op-amp providing a non-loading effect on the thermistor measurement, and a low impedance output for the analogue to digital converter measurement input. Lastly, R4 and C1 are a low pass filter for removing high frequency noise which could have been superimposed onto the signal conditioning path.

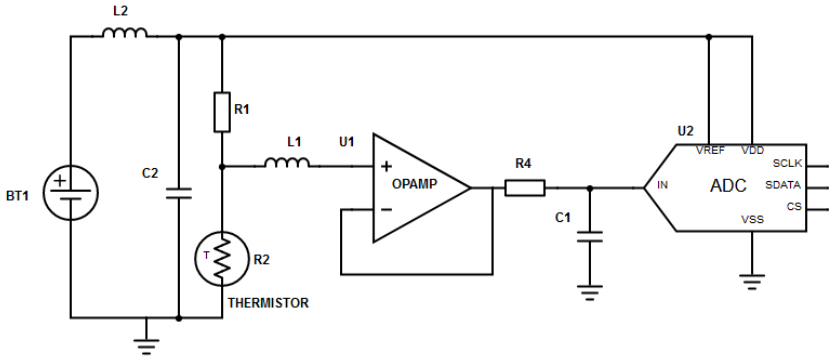

Figure 5 Illustration of a complete instrumentation design for thermistors temperature measurement.

3.3.2 Sensor protection

Devices embedded within or expect to be exposed to harsh environmental conditions often require conformal coatings, protecting sensitive components from chemical, moisture, electrical and mechanical influences. The choice of the correct method for protecting a device depends on many factors such as, the operating conditions expected, length of exposure, labour, material costs and manufacturing process.

Parylene C[2], Styrene-butadiene[1], Kapton[27] and Apiezon[20] has been used several times in literature to protect sensors, but long term effects are not characterized. Furthermore, mechanical interactions from the cell or manufacturing stresses may cause the coating to fail over time[2].

The use of Parylene-C(*poly(p-xylylene)*) [58] which has been used within literature for protecting sensors in harsh environments[59] and offering significant protection against solvents[60]. However, experimental work conducted within lithium-ion cells has shown to fail[2]. This could be possible due to an improper coating procedure or miss-handling of the sensors during embedding, neither was clear within the research publication.

Parylene is deposited using chemical vapor deposition (CVD). CVD is a three-step process process, the raw material, in this case Parylene-C is deposited onto a target material. First, the parylene is heated within a furnace to a high temperature (~150 °C), until vaporization occurs. The gas from the first stage material is then passed into

a furnace (~690 °C), where, the gas is split into a single monomer vapor. Finally, the monomer is passed into the target chamber. The monomers in the target chamber attach to nearly every surface, forming a clear, uniform and thin layer.

The manufacturing process advantage is that the target material is never above room temperature meaning no thermal damage could occur to a device, that may impact future performance of an instrument. However, the production costs per batch can be significant due to the amount of time required to service the machine after consecutive runs. This due to that Parylene bonds with all material in the target chamber stage of the process and subsequent runs of the machine would create a build-up of unwanted material

3.3.3 Instrumentation of Lithium-ion cells

Few publications involving sensors that are designed specifically for in-operando measurement of temperature exist. Nora Martiny[2,27] published two papers developing a multi-point thermocouple array by sputtering copper (Cu) and nickel (Ni) onto a polyimide substrate[2,27] .The formation of the two elements Cu and Ni provide an apparent sensitivity of 22.4 µV/°C according to the author's calculations. After calibration it was demonstrated that 18.5 µV/°C was the measured sensitivity. The reported explanation as to why the calculated and measured did not agree was not explored by the author, they also failed to note the transition between the spring contact and the connection to the data acquisition system, which may consequently cause a further thermocouple reference, and thus off-set the measurement voltage.

A connection of dissimilar metal effectively forms a second thermocouple junction. The transition can cause a voltage drop which should have been accounted for but it did not seem it was. Additionally, it is not clear how the cold-junction compensation is implemented or if they have simply measured the voltage on the terminals. The measurement method needed further analysis and validation and for this reason the results of testing could be confusing and false.

The author's experimental setup and source of thermal calibration are questionable; the author described attaching a thermocouple using an adhesive close to the sensor and heats the device using an element which is not described in detail. The sensor

printed circuit board (PCB) traces could have also been picking up stray electromagnetic noise from the cycling equipment. The noise could superimpose as a voltage on the trace. Electromagnetic pickup should be a concern with sub micro-levels of voltage and long lengths of track, that could act as a receiver. Figure 6 shows the calibration curve, highlighted in red is a considerable degree of noise can be seen in the voltage signal. The marked area could be mains pickup from the table the experiment conducted on and/or interference from the connected data acquisition unit (DAQ). To verify this phenomenon, the system can be subjected to varied electromagnetic (EM) fields at different distances/frequency and measure if a signal is superimposed upon the tracks. Once identified a suitable EMC reducing method can be applied in software or hardware. A spectrum analysis would also identify the frequency components of the noise.

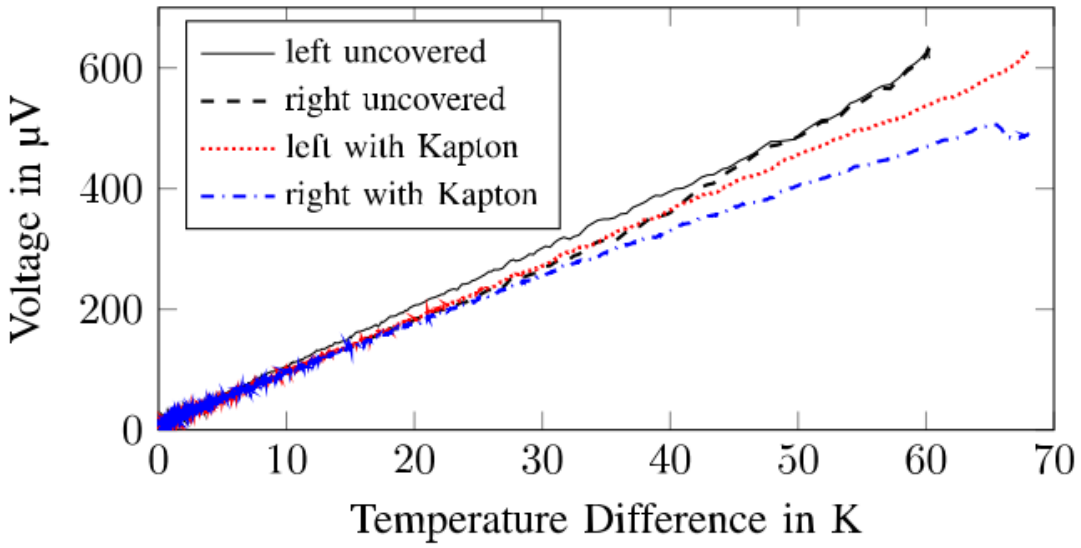

Figure 6 Calibration response of sensor proposed by Martiny[27] *et al*. A clear signal noise is apparent within the origin of the data.

The long-term implications of the sensor are not explored with only a limited number of cycles performed. A post-mortem analysis should have been undertaken, which could have highlighted any damaging/corrosive effects of the sensing element. The chemical resistance method of placing the sensor into electrolyte for an arbitrary period and measuring the weight, mass and density is a half measure of validation.

The method will not be able to take into account side reactions that could occur within the battery that might attack the sensing substrate.

Santosh *et al* development an 8-point thermocouple[31] array and embedded into a self-made laminated cell as shown in Figure 7. The authors had many of the experimental design errors, as described previously[2,27] in Nora Martiny *et al*. One improvement is the added cold junction references that are in close proximity to the battery tabs and measurement point. Using a one-to-one topology means 8 points need to be maintained at a constant temperature as the thermocouple can only measure relative temperatures. This will be difficult to achieve due to the varied heat generated from the battery tabs during discharge/charge periods and cooling method used in a battery stack. Electromagnetic coupling from the tabs onto the presumed silicon cold-junction would also be a concern. Sealing of the tabs was not described in detail either; this may leak after some time and should be explored to a greater degree.

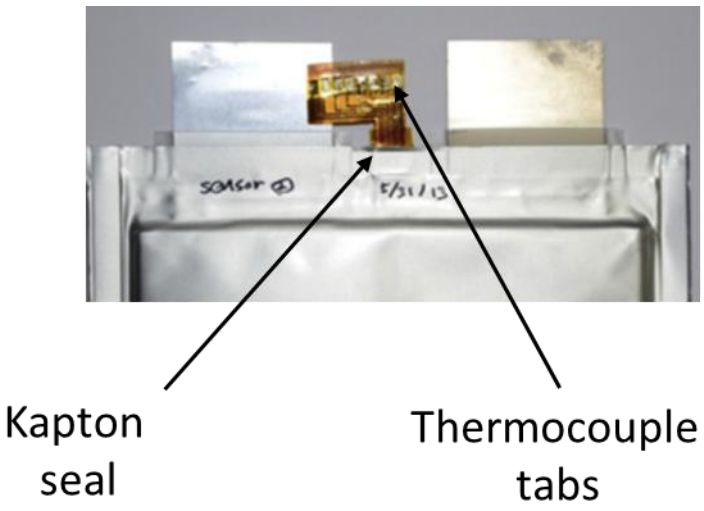

Figure 7 Thin-Film Thermocouple array and cold junction compensation[31]

Lee *et al* developed three-in-one sensors for measurement within a coin cell construction[23]. The sensing solution has considerable novelty however if the technology was to be adapted for a laminated cell it would need a degree of validation. Due to the construction topology of the resistance temperature detector

it can be affected by stress deformation introducing cross sensitivity to the element. The sensing element is also constructed of gold which adds considerable costs to each node. A maximum resistance range of 0.2 Ohms is extremely narrow, and sensitivity could become an issue. A limited bandwidth will require a high degree of instrumentation in order to read an accurate temperature.

Cylindrical *In-situ* temperature measurement

Measurement of temperature gradients within cylindrical cells has had several authors propose methods for modification, implanting and sensing technologies for in-situ measurement[9,10,18,22]. Zhang *et al* embedded[25] several 90µm thermocouples within the jelly roll of an 18650 cell during manufacturing. The method used for attaching the sensors to the layer was not described in detail. The sensors came insulated with an exposed tip. Parylene was applied to the element tip to protect the sensor from the electrolyte. No calibration of the effects of the coating were described; this would most certainly affect the measurement as shown in previous work[2]. Zhang *et al* compared the cell with an unmodified cell and noted a slight capacity loss during higher charge cycling, this was attributed to a possible higher resistance where the sensors are located. Not knowing the method that was used to attach the probes to the jelly roll could affect the local resistance. Furthermore, repeatability would also be a concern with this method due to the number of sensors that need embedding. If the data collected is position-critical then it is possible that they will drift during manufacture. Instrumented cell with thermocouples[9] embedded during a hand-made cylindrical cell.

Xinfan *et al* attempted to validate thermal modeling methods[33]. It would seem from the author's description that a custom cell was fabricated. It was not mentioned if the mandrel core was embedded during manufacturing or if a drill jig was used. The size of the thermocouple and whether or not it is in mechanical contact with the core is not described. The sensor may have had an air-gap between the element and jelly roll which could cause confusing errors. No calibration of the elements was conducted either which will add further measurement error.

A similar experiment conducted by Osswald *et al* embedded[20] several type-T thermocouples within the jelly roll of a cylindrical cell. Apiezon was used to coat the sensors from the electrolyte; no validation of the sensors was conducted after the conformal coating was applied. This could lead to confusing results. The long-term survivability is also not explored.

3.3.4 Reference electrode sensors

An electrode is one element in a system whose primary purpose is to conduct the flow of current. Understanding a lithium-ion battery's anode or cathode voltage potential[61–69] relative to that of Lithium can signify the current state of Health of the electrochemical system[62,64,66,70]. However, obtaining the specific potential of the electrode material is not possible with a standard arrangement of a cell, as a two-tab configuration. Therefore, meaningful measurements are only a relative potential difference, an absolute measurement of each anode and cathode potential is not possible.

Previous studies that involved the embedding of reference electrodes within a battery have used lithium references either embedded by modifying a commercial cell or the reference is connected externally via a conductive medium, which would be questionable as to how useful the data would be in a real-life system. Previous studies have investigated the in-situ embedding of a reference electrode into cylindrical cells[63,69,71–75]. A limited number of these have involved the fabrication of cells from scratch[69,73,74] or commerical[63,71,72,75] cells.

However, the methods of modification described have a high risk of damaging the devices in question and therefore, long-term reliability would be questionable. Furthermore, several research publications often added more electrolyte to the cell[75], consequently the characteristic internal resistance[76] are changed. Lastly, submerged an opened cylindrical cell and reference electrode[72] into a container of electrolyte, which not only adds to the previous issue, but also affects the accuracy of the measured potential profiles, due to the increased distance between the reference electrode and the jellyroll.

3.3.5 Sensor communication

The embedding of sensors within a cell requires electronic signals to be transmitted to the battery management system. Communicating with the sensing element through the cells' enclosure has several considerable challenges as the outer enclosure is constructed of a sealed metal, typically aluminium or steel.

Sensor communication methods

Signal communication can be divided into several categories including; hard-wired connections, capacitive, inductive, radio and power line. Each approach requires bespoke electronics, digital signal processing algorithms and fundamental different operational principles.

A wired solution is the most common method implemented in most situations. This is because electronic circuits are minimal, data and power can be transmitted over two wires (data/power and ground) and they are robust to interference. It was clear from previous research that a wired solution is the state-of-the art method for communication for *in-situ* sensors, however, wire-based sensors potentially have sealing issues as shown in literature[32,77]

Inductive communication uses the magnetic field as the dominant form of electromagnetic coupling. This method is often used within mobile phones for near field tags, pay point meters and vending machines. The technology requires a transmitter and receiver unit for communication. Each unit has an inductor which couples to the other unit when in near proximity, consequently data and power can be transmitted. One drawback with the technology is that objects between the device such as metal have a catastrophic effect upon the coupled electromagnetic field, thus essentially making the technology useless for communication though metal objects. However, this is not always the case, and with enough energy and high a frequency, data can be transmitted though metal[78–80]. The high frequencies, size of the inductor and operational temperature range make this choice un-suitable now for *in-situ* integration within a cell.

Capacitive communication uses the voltage field as the dominant form of communication. Two plates are coupled and the free-space or object between to communicate though acts as a capacitor. Therefore, an AC waveform can pass through objects. However, this approach has the drawback of needing exact alignment with a receiver unit, that also needs to be near proximity. This method has the advantage of being able to communicate through thin sheets of metal, which inductive communication would struggle to achieve in tightly constrained area such as a pouch cell.

A study showing the feasibility of capacitive communication through a pouch cell enclosure was proposed by Martiny[81,82] *et al*, using the aluminium laminate as one plate of the capacitor. The solution has promise but a full system integration would require the implementation of an application specific integrated circuit circuit and this has yet to be explored. Furthermore, several issues arise with the electronics required within the cell for communication such as temperature effects, aging, reliability and manufacturability.

Radio could be used if the battery can cell was turned into a radio antenna. Familiar protocols such as Zigbee®, Wi-Fi® and Bluetooth® could also be implemented. However, matching circuits, filtering and power requirements would be significant, but if range of less than a meter is required, then efficient tuning is negligible. Further issues with power requirements to drive the antenna changing as the load impedance changes with the cells state of health and charge. This being said, it could be possible to modify a cylindrical cell, so the centre can is a separate connection or radio antenna.

Module communication

Several Publications have focused on the development of capacitive communication methods at a module level[83]. The communication circuit, intelligence and the active circuitry are not embedded within the cell. However, capacitive communication through a battery enclosure of a pouch cell has been attempted [81,82] this method, adds significant circuitry, weight, and further wiring harness to a pouch cell assembly.

No work has focused on *in-situ* power line-communication for 18650 cells. However, power line communication is attempted frequently at a module cell level[84,85]. Limited information within the literature[32,77] has focused on the development of wireless solutions for *in-situ* sensors within a battery.

3.4 Optical fibre sensors

Originally designed for use in the communication industry fibre technology offers several advantages over traditional silicon/copper materials[86]. Fibres have a high tolerance to the effects of electromagnetic interference, no power supply required, single wire multiplexing for the capability to perform distributed sensing, small construction and corrosion resistant, with an appropriate recoat.

The technology has several limitations, including a cross sensitivity to temperature and strain, meaning differentiating between the two is challenging. Furthermore, fibres in their bare form are extremely brittle and prone to failure if handled incorrectly. Finally, inherent mechanical restrictions of the fibre due to reliance on light propagating through the fibre mean mechanical bending and compression can cause signal loss and inaccurate results if not prevented. These effects must be kept in mind when designing optical sensing elements and resolved before application.

Fibre Bragg gratings

A Fibre Bragg Gratings (FBG) sensor is a discrete and distributed location on a single mode fibre.

The raw fibres refractive index is significantly modified at discrete locations. Consequently, causing a known light frequency to be reflected while others can pass, effectively forming a band-stop filter. The etching pitch defines the Bragg wavelength of choice and many sensors can be incorporated on a single fibre. If the Bragg grating is subject to thermal or mechanical stress, the refractive index of the device shifts.[87].

The shift is directly correlated to a scalable factor and therefore, high accuracy measurements are possible. In essence, the grating zone is effectively acting as a filter for a particular wavelength, passing all light except the tuned frequency of the

grating[86]. Figure 8 shows the working principle of the sensor topology. It must also be noted that several sensor zones can be incorporated into a single fibre.

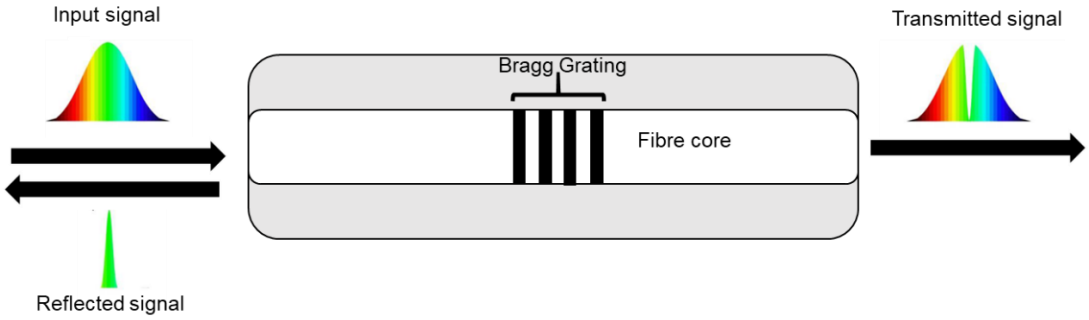

Figure 8 FBG sensing principle - black lines related to sensing zones[86]

One of the main issues with FBG technology is overcoming the inherent susceptibility to temperature and stress. This is a fundamental limitation with the technology meaning the external instrumentation cannot determine the true source of the wave shift alone. Therefore, it is critically important to understand the type of environment the sensors are going into and the type of measurement required, either stress or strain.

One method to overcome the cross sensitivity is to bond the FBG onto a substrate[88] reducing tension, compression, or torsion forces as shown in Figure 9. This method would allow for temperature measurements alone. However, the substrate could impose mechanical constriction upon the battery stack, possibly causing separator piercing.

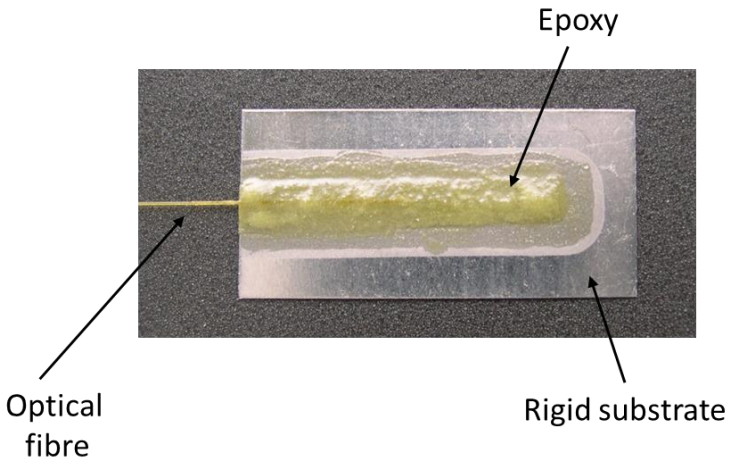

Figure 9 Strain resistant FBG assembly[88]

3.4.1 *In-situ* optical fibre sensors

Fibre sensors are becoming an interesting area for studying cells[1,30,97–104,89–96] and where traditional sensing technology could fail[105,106]. However little literature is available regarding the subject.

Summer[95,96,99] *et al* has published several papers regarding the subject. Summer's paper on in-operando measurement of electrode strain deformation had several experimental and instrumentation areas for further research. The measurement technique used to overcome the cross sensitivity to infer electrode by measuring skin temperature could be prone to a high degree of error. The publication suggests that the attached sensor on the outside of the skin will have little strain effect placed upon it which would be untrue due to the collective strain of the cell expanding during charging. A reference strain gauge should be placed close as possible to characters and calibrate out strain effects. The pouch cell was described as being loosely held together by the outer bag, whereas commercial cells will come tightly packed, which could cause issues using the method described by the author.

The research does not detail if any damage occurred to the fibre during manufacturing. The thermal sealing of the pouch material and compressive force used to achieve the seal could cause the fibre cable to break. An additional concern is the effect of the Styrene-Butadiene Rubber (SBR) thermal expansion over an entire operating temperature range of the cell; SBR has an extremely high thermal expantion (500-600 10-6/K). This would affect the response of the optical sensor by applying strain which would be inferred as temperature.

A further method used to measure in-situ strain in previous literature[1,95–97] uses a second FBG. The FBG is mounted to the outside of the pouch material in order to offset the temperature effects. This method would seem unreliable due to thermal delays from core the temperature reaching the outside of the cell.

Chang-Jun[1] *et al* has taken the research further by embedding the FBG directly within the electrode slurry during manufacturing. The method used for reducing the cross sensitivity is not entirely described but he is part of the same group who use an

externally mounted FBG to correct the wave shift. No apparent re-coat of the sensor was described in this paper which in the long-term would alter the sensitivity.

Meyer[98] *et al* used a two-sensor approach to counter-act cross sensitive issues. The sensors were not embedded within the stack but rather on the outside of the bag. This method would not enable a distributed view of the cell due to the minimum spacing required between each FBG. Whilst the response matches the thermistor to a good degree, what is noticeable is the noise pickup upon the thermistor trace. The author suggests this could be removed by introducing EMI-reducing components, but this would add a cost to the system. However, the cost would be minimal if the noise was removed in the firmware. The EMI is a minor issue in comparison with the higher complexity, cost and integration issues with the FBG technology.

4 Hypotheses

4.1 Introduction

This chapter describes the key gaps within the literature that is researched and developed as part of this thesis. A description of the justification for each hypothesis statement is given followed by a hypothesis statement.

4.2 Hypothesis one

Few publications exist that evaluate sensors designed specifically for *in-situ* distributed measurement of temperature[107,108], additionally little validation regarding the impact of the device upon the electromechanical system has been published and the effects upon the sensor itself.

Several researchers[2,27,31] have previously worked with thermocouples and resistance temperature detectors (RTDs). The publications focus on the development of the *in-situ* sensor, lacking any critical data regarding the impact and long-term reproducibility of the lithium-ion cells. While thermocouple and RTDs are well suited for high temperature measurement, they suffer from low sensitivity[109] - reference junction requirement and increased instrumentation.

Several research questions need to be addressed in order to understand the system consequences of embedding foreign elements within the electrochemical device, including: the correct method of manufacturing cells with instrumented elements, the implications of inserted elements upon the battery material and development of conformal coatings against harsh environmental conditions.

Lastly, previous studies have investigated the incorporation of a reference electrode into cylindrical cells[63,69,71–75]. Some have involved adding reference electrodes to commercial cells [63,71,72,75] and laboratory[69,73,74] fabricated cells. However, the invasive and highly likely damaging nature of the insertion approach risks damaging the cell or changing its performance characteristics.

Statement

In-situ sensors monitoring cell performance are a superior and significant improvement for cell characterisation provided they cause no lasting effect on cell performance.

4.3 Hypothesis two

The use of within the core of a cell of thermistors offer an interesting alternative yet were up to this point unexplored for suitability of cell in-situ temperature profiling. A method for internal temperature measurement of a cell using a thermistor as the sensing element is proposed. Furthermore, miniature surface mount technology is unexplored for suitability of cell *in-situ* temperature profiling. This is due to the fact it is presumed in literature that the sensor would damage the electrode material due to having a lumped mechanical profile.

A thermistor offers a high degree of sensitivity, low cost, point sensing, absolute measurement and strain resistant. Furthermore, the high sensitivity of thermistor compared with thermocouples and resistance temperature detectors may minimize the system resources required for reducing electromagnetic interference as shown in previous work[99]. Lastly, a high sensitivity is beneficial as small changes in temperature give rise to a large output signal change, meaning if an array of sensors is correctly calibrated minute changes in temperature can be observed. Thus, providing an unprecedented insight into cell dynamics. In addition, Lithium-ion cells are constrained to limited operating temperature ranges, according to the cell's assembly – most modern lithium-ion chemistries work properly under a maximum operating temperature of 60 °C[110–112] , therefore the benefits of a high temperature range sensors are negligible for such an applications.

Statement

In-situ thermistor arrays are a superior and updated method for identifying internal characteristics and safety limits of pouch and cylindrical cells.

4.4 Hypothesis three

The use of optical fibres are becoming an area of interest for monitoring lithium-ion cells[1,30,97–99,101,102,89–96], where traditional sensing technology could fail[113]. However, currently available literature regarding instrumentation of cylindrical cells using fibres and the effects upon the electrochemical devices are limited.

In-situ measurement for various Lithium-ion cell form factors are available, including pouch [1,91,93,102] and coin[89], but none have attempted to embed optical fibres within cylindrical cells. Here, significant engineering challenges need to be considered compared to pouch cells, due to internal structure differences, assembly materials and manufacturing methods, leading to substantially different observations. Several issues arise with using a "bare" silica fibre. The fibre Bragg grating sensor element is sensitive to both temperature and strain, thus introducing cross sensitivity to the measurement if unforeseen strain effects occur, such as vibration, mechanical impact and electrode expansion.

Furthermore, little attention has been devoted to the impact of cyclic behaviour, *in-situ* inspection and post-mortem analysis, which remains undocumented in literature. Consequently, given the lack of critical attention paid to instrumented cells, this work will present unprecedent experimental data concerning the characteristic behaviour of a cell compared with a standard virgin cells.

Statement

Optical sensors are a superior technique for characterising cylindrical lithium-ion cells' in-situ thermodynamics and offer insights for advanced charging protocols, which is not possible using external sensors alone.

5 Experimental setup, materials and equipment

5.1 Introduction

This chapter describes the experimental setup, instruments, methods and testing regimes for in-situ sensors of lithium-ion cells. The work is categorised into three distinct areas as follows:

- distributed In-situ thermal sensing using high accuracy nickel oxide thermistors
- distributed In-situ thermal sensing using optical fibre sensors
- electro-thermal instrumentation.

A description of the experimental description and devices under test is given followed by the analysis methodology used.

5.2 *In-situ* sensors for Lithium-ion cylindrical and pouch cells

5.2.1 Devices under test

The devices under test are Lithium-ion pouch cells constructed at Warwick Manufacturing Group's cell scale-up line. The cells evaluated for the *in-situ* sensors were constructe from 15-layers with a nominal capacity of 5.5Ah, consisting of a lithium cobalt oxide ($LiCoO_2$) cathode, graphite anode and a $LiPF_6$ electrolyte solution. The specification for the cell are shown below in Table 2.

Table 2 WMG pouch cell production capacity specifications

Type	Pouch
Weight (g)	48
Nominal capacity (Ah)	5.5
Nominal voltage (V)	3.6
Standard charge	1 C CC to 4.2V at C/10
Standard discharge	1 C to 2.6 V
Electrolyte (A)	EC:EMC 3:7 (salt) 1 mol/L LiPF6

The cylindrical cells evaluated were commercial 3Ah high-energy cells consisting of a lithium nickel cobalt aluminum oxide (NCA) cathode, graphite anode and a $LiPF_6$ electrolyte (B) solution. The specification for the cells are given in Table 3.

Table 3 BD 18650 characteristics

Type	18650
Weight (g)	49.5
Nominal capacity (Ah)	2.98
Nominal voltage (V)	3.6
Standard charge	0.3 C CC to 4.2V at C/10
Standard discharge	2 C to 2.5 V
Electrolyte (B)	unknown

5.2.2 Experimental descriptions

Sensors are to be designed and constructed that are capable of being embedded within a pouch cell. The sensor assembly will be validated versus calibrated reference sensors in a temperature-controlled environment. And further sent to a calibration house for a final verification. Lastly, a conformal coating will be employed to protect the sensor assemblies from the environment within the cell.

To validate the conformal coating, the sensor will be placed in raw electrolyte (A) at room temperature, for a sustained period. The sensor is then removed and inspected using high a resolution microscope. The sensors sensitivity is also validated.

Next, the sensor assembly is calibrated and inserted into a cell, the cells state shall be left at room temperature with no cycling and a second test will involve the cell being cycled within the manufactures recommended limits. This testing regime should give a clear indication of which conformal coatings are compatible with the electrochemical environment.

For pouch cell assemblies, several mechanical high-pressure events occur during manufacturing. Consequently, could this could be harmful to the sensor assemblies. Sensors will be placed within the bag sealing bars to understand if they can withstand the high pressures of the manufacturing process. Furthermore, the sealing around the sensor entry will be validated by weighing the cells to identify any loss of electrolyte and further testing in a vacuum chamber. These tests will produce a clear indication if the sealing methodology has worked in the first instance.

An in-situ inspection of the sensor assemblies within the cells could give a clear indication of in-situ hazards, optimum placement and any damage which occurred during manufacturing or modification. Therefore, the instrumented cells are inspected using x-ray tomography imaging technology. The cells are x-rayed directly after being modified within a glovebox or produced within the manufacturing assembly line. The aim of this exercise is to understand the impact of the sensor upon cells assembly materials and further optimise placement within the cell.

Once the sensor assemblies, manufacturing and sealing stability have been validated then the complete system can begin to be validated. Cells are cycled within the manufacturers recommended limits, therefore, significant data comparisons can be made versus virgin cells and datasheet information. Further rapid discharging protocols will be tested to the recommended limits of the battery. Additionally, the pouch cells were placed under pressure (2850 N/m^2) during formation and cycling, consequently, simulating real-life conditions expected in large scale battery systems.

Loss of electrolyte, cell damage and other parasitic effects encountered during the modification procedure may not appear in time domain analysis conducted in the previous section. Therefore, three cells were evaluated using Electrochemical Impedance Spectroposy at 100% and 0% SoC before and after modification

The excitation current was selected to be a relatively low amount of energy being injected into the system (C/20 for the devices under test), minimising the amount of Joule heating which would alter the impedance response[114] while keeping the electrochemical system within a linear region of response, as per Butler-Volmer relation.

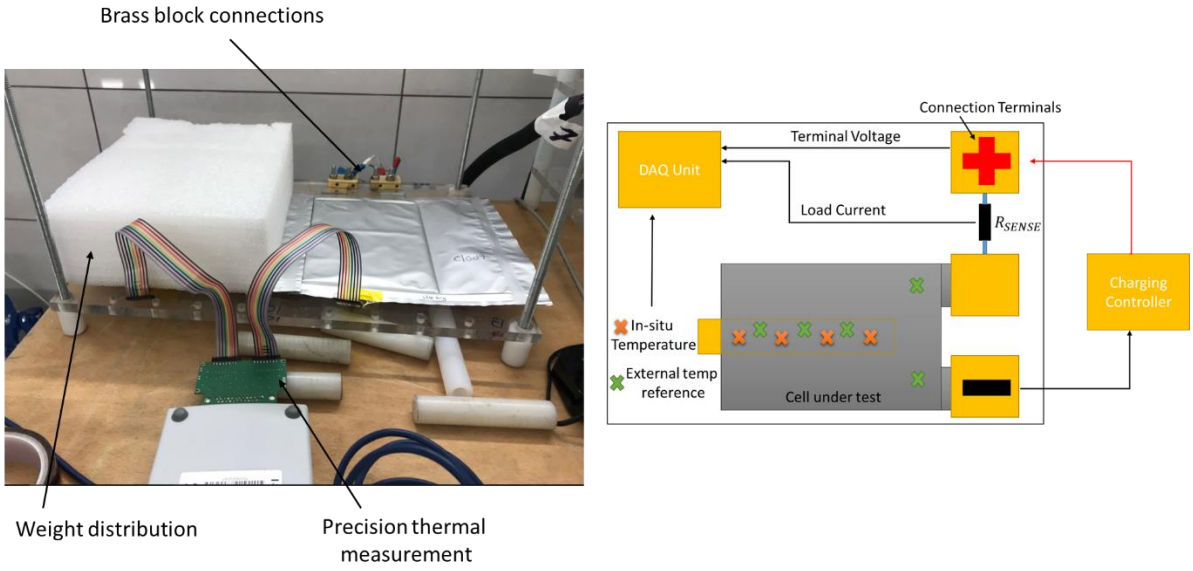

Figure 10 Illustration of the pouch cell instrumented experimental cell setup

5.3 Fibre optic sensors for cylindrical Lithium-ion cells

5.3.1 Devices under test

The cylindrical cells evaluated for *in-situ* sensors applications were commercial 3Ah high-energy cells consisting of a lithium nickel cobalt aluminum oxide (NCA) cathode, graphite anode and a $LiPF_6$ electrolyte solution.

Table 4 LG INR18650 HG2 18650 characteristics

Type	18650
Weight (g)	47
Nominal capacity (Ah)	3
Nominal voltage (V)	3.6
Standard charge	1.5A CC to 4.2 V at 50 mA
Standard discharge	600 mA 2.5 V
Fast charge	4.0 A CC to 4.2 V at 100 mA
Fast discharge	10 A to 2.5 V / 20 A to 2.5 V

5.3.2 Experimental descriptions

Raw fibres are extremely sensitive to handling which could cause significant measurement error, which may not be apparent with a single point calibration or appear for some-time after manufacturing. Furthermore, as the fibre alone is not suited for embedding into any form of electrochemical cell significant modifications are necessary. Several elements are explored for suitability for in-situ measurement which are used to construct an enclosure around the fibre.

It is possible that the characteristics of the sensor are altered from the modifications to the fibre and the embedding processes. The sensor assembly is validated versus a calibrated sensor element, in a temperature-controlled environment.

Once a sensor assembly has been validated that can withstand the environment within the battery from a theoretical approach, a modification method for embedding the fibres into commercially available cells is explored. This is achieved by disassembling cells in an argon glovebox. The cells are then sealed using an appropriate method, which is further validated via weighing of the cell and further cyclic aging.

An *in-situ* inspection using XCT of the fibre and battery cell assembly is undertaken, the purpose is to understand the effect that the fibre may have upon the unit and the construction reliability of the sensor assembly.

Once an appropriate sealing method and sensor assembly is verified cyclic aging of the cells is undertaken. The devices are cycled within the manufactures recommended limits and unmodified cells are also cycled alongside instrumented units for a comparison as a reference. Lastly, Electrochemical Impedance Spectroposy of modified and unmodified cells is explored at various state of health.

5.4 Analysis methodology

5.4.1 Test bench

To understand a cells characteristic response a Potentiostat *(Bio-Logic Science Instruments® VMP3*) is used. The device is capable of high accuracy cyclic aging and Electrochemical Impedance Spectroscopy (EIS). The device is controlled via computer software, where additionally, the battery cyclic data is stored. The unit has ability to measure external sensor inputs, but is limited to one channel, consequently meaning further data acquisition technology are required.

To log multiple sensor data a multichannel data acquisition (DAQ) PicoLog 1216 (PicoTechnology*®)* is employed. The unit has 16 general purpose analogue to digital inputs and up to 4 units can be combined for use on a single computer. The external sensors require an interface board to connect into the logging device.

For a low resistance, high current carrying conductors and a connection into the battery cycling equipment a brass block is employed, the block is connected to the anode and cathode of a cell and are clamped into place with a mechanical fixing. An acrylic sheet is used as the substrate for the cells under test and brass block connecters. A diagram of the equipment is shown below.

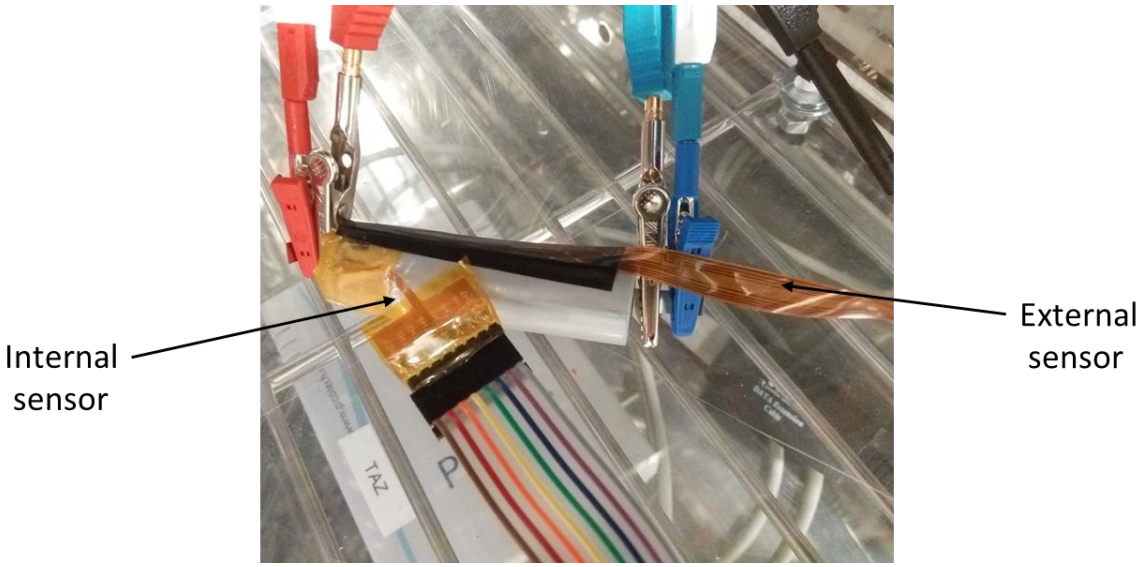

Figure 11 Illustration of an instrumented 18650 experimental setup

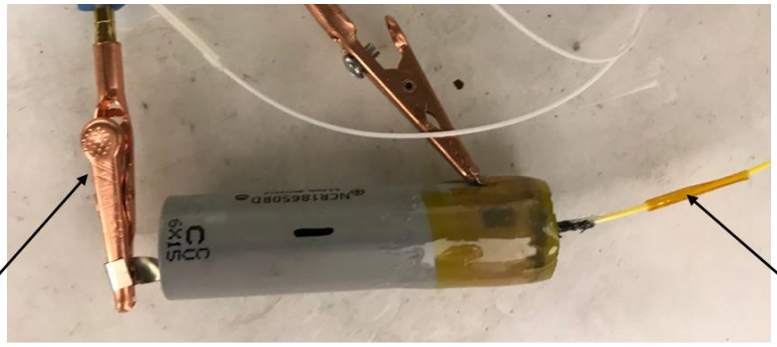

Figure 12 Illustration of an optical instrumented 18650 cell experimental setup

5.4.2 Optical sensor instrumentation

5.4.2.1 2-in-1 Optical sensor instrumentation

A spectrum analyser, broadband laser source (1530 – 1590 nm) and an optical circulator (Thor Labs) was used to interrogate an Bragg grating element. The spectrum analyser supports several measuring modes depending upon the required speed and accuracy of measurement the slowest and highest accurate method which provided 1 pM accurate was chosen. However, the measurement frequency is approximately at 1 second internals. With the need for a relatively low measurement frequency needed to characterize the cell temperature change, the compromise was acceptable. The spectrum analyser was connected via RS-232 to USB and the data was logged using terminal software, on a computer in real time. Figure 13 shows the block diagram of the optical sensor equipment setup.

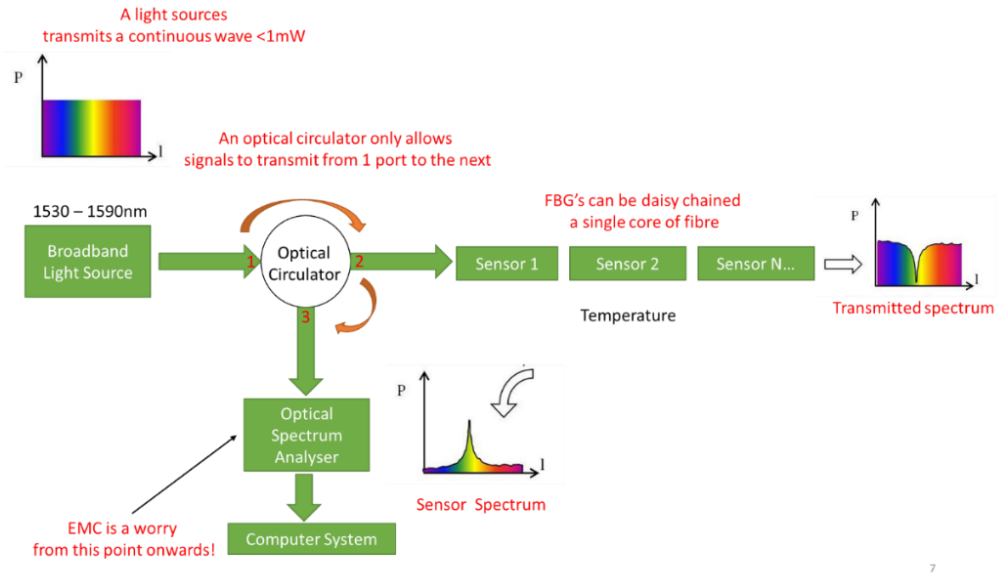

Figure 13 Optical System setup for interrogating FBG sensor arrays using an optical circulator, broadband laser source and an optical spectrum analyser

5.4.2.2 Distributed FBG interrogator

A fibre optical interrogator (Smart Fibres) is a device that is capable of interrogating multiple Bragg grating elements at the same time, meaning distributed sensor profiling is possible within a battery. To validate the response of the sensor in initial testing a thermocouple (Type-K) and a calibrated logging device (PicoLog 1216).

5.4.3 Cycling

For all experimental work described previously. The protocol involves a constant current (CC) until the terminal voltage reaches the maximum cell voltage. Which is defined by the manufacture. followed by a constant voltage phase (CV), where the current delivered to the devices is monitored, until reaching a cut-off threshold defined by the manufacturer.

5.4.4 Electrochemical impedance spectroscopy

To understand a cells frequency domain characteristic response a potentiostat (Bio-Logic Science Instruments® VMP3) is used for Electrochemical Impedance Spectroscopy (EIS). The hardware sweeps the device under test with a known frequency and applied current, the phase response is calculated from the response

given. EIS can be used to help determine several parameters of an electrochemical system including; State of charge, state of health, fault diagnoses[114,115] and temperature[116]. However, this data is open to interpretation and is often measured under extremely controlled environments in a lab-based setup. The configuration used for EIS is shown below in Table 5. EIS was measured at 100% and 0% SoC due to the highly non-linear response of the system.

Table 5 GEIS configuration for instrumented cell research

Mode	**Single Sine**
Start Frequency (mHz)	10
End frequency (kHz)	20
I amplitude (mA)	200
Range (A)	1

5.4.5 Post-mortem glovebox tear down

The cell was discharged to the minimum voltage of 2.5 V as stated on the manufacturer's specification sheet before being transferred into an argon glove box with atmospheric O_2 and H_2O concentrations of <1 ppm

5.4.6 Microscope inspection

A digital microscope from VHX-6000 Series (*Keyence*) is used to inspect the sensors after *in-situ* embedding with the cell.

5.4.7 X-ray tomography

X-ray tomography scans were performance in house at WMG with the help of Remy Guillaume. Tomography uses x-rays and computer software to construct a 3D cross sectional images of objects under test. The parameters used for each cell type is given in Table 6.

Table 6 Metris X-TEK XTH 320 LC XCT configuration

	18650	**pouch cell**	**18650 flexibles**
Software	X-ray Controller Inspect-X CT Pro Version XT 2.2 Service Pack 1a		
Exposure Voltage	215 kV	200 kV	200 kV
Exposure Power	18.92 W	51.8 W	30 W
Exposure Time	0.708 msec	1000 msec	0.708 msec
Duration of Test	37 mins	44 mins	37 mins
Filters	Tin	Tin	Tin
Thickness	0.1 mm	0.5 mm	0.25 mm
Voxel size	13.16 um	47.68 µm	33.4 µm

The material density as well as geometry of the pouch and cylindrical cell are significantly different, thus requiring a greater degree of exposure time for penetrating the cell material. A cylindrical cell has a diameter of 18mm while a pouch cell is much greater in one direction, roughly 180mm, while also being anisotropic.

5.4.8 Environmental control

A high accuracy thermal chamber (*Binder®)* is incorporated into all experimental work to maintain a constant, stable and reliable ambient thermal dynamic environment. The thermal chamber can hold temperatures of -20 °C to 155 °C with an accuracy of 0.1 °C. The unit will also to some degree limit the possibility of electromagnetic interference. A high accuracy calibrated temperature reference sensor Pt100 (Pico Technology®) is used as a source of reference for the experimental procedure.

All experiments were conducted in an environmental chamber maintaining a temperature of 25 °C (+/- 0.1 °C). Calibration of all sensing equipment was conducted where possible near the time of the experiment. Additionally, all equipment was warmed up for 4 hours before experimentation to reduce the effects of analogue measurement error due to temperature variations.

6 Instrumentation of pouch cells

6.1 Introduction

This chapter describes the experimental work and results undertaken for thermal-instrumentation of pouch cells using distributed thermistor elements'. The development, validation and testing of the instrumentation is described, followed by the validation of the instrumented electrochemical system. The cells evaluated for the *in-situ* sensors application were 15-layer pouches built in house at WMG with a nominal capacity of 5.5 Ah. Consisting of a lithium cobalt oxide ($LiCoO_2$) cathode, graphite anode and a LiPF6 electrolyte solution.

6.2 Research and development

6.2.1 Sensor design and validation

A raw NTC thermistor element (Murata©) was selected due to a high precision, near linear beta curve, wide availability and a temperature range of -20℃ to 125℃[117]. A high precision means the temperature sensors output response has a high degree of reproducibility. The complete sensors assemblies are shown in Figure 22 and the specification is given in Table 7.

Table 7 Murata NCP03WF104F05RL NTC thermistor element characteristics[117]

Size (L x W) (mm)	0.6 x 0.3
Operating range (°C)	-20 to 120
Tolerance (%)	1
Resistance at 25°C (Ohm)	100k
B-Constant (25-50°C) (K) +/- 1%	4250
Maximum operating current (25°C) (mA)	0.032
Maximum voltage (V)	5

The thermistor sensor in question, offers a near linear region using the beta coefficient as given by the manufacture (4250). The temperature region interest for this research will not exceed 80°C and a lower limit of 25°C. Therefore, this thermistor was selected as suitable choice.

Lastly, it must be noted that he is heating of the sensor element could be caused by the instrumentation injecting current into the device. The datasheets for each thermistor provide a maximum current limit before self-heating becomes an issue. In the case of my thermistors it was 0.032 mA. A well-designed sensor instrument should not cause self-heating issues, my instrument was limited to 3 uA. The 3 uA effectively amounts to a 90 uW power dissipation within the thermistor.

A 25µm flexible Kapton© tape was used as a substrate for the thermistor elements, selected for its mechanical, chemical and thermal conductivity properties. Additionally, the material is readily available in a standard manufacturing setup. Furthermore, it is possible to bond Kapton together, which may negate the need for expensive and time-consuming conformal coating.

The raw thermistor elements were bonded onto the polyamide substrate using standard reflow soldering technology. The substrates were designed in an Electronics PCB and Schematic software (*Easy-PC*). Due to the thermistor elements being exposed a lead-free solder is employed to bond the elements onto the substrate - therefore, cross contamination between the battery's assembly material is possible. Consequently, a conformal coating was required to encapsulate the sensor elements and substrate.

For initial testing a conformal coating of Polyvinyl Fluoride (PVDF) applied, due to its regular usage within battery assembly technology. The coating was applied by hand and cured using a hot air gun at a low temperature. A second layer was applied in order to maximize the barrier thickness. The sensors were embedded in two pouch cells for one week. However, several elements failed once cycling had occurred. This was concluded to be a manufacturing issue rather than the coating having no effect at protecting the sensors.

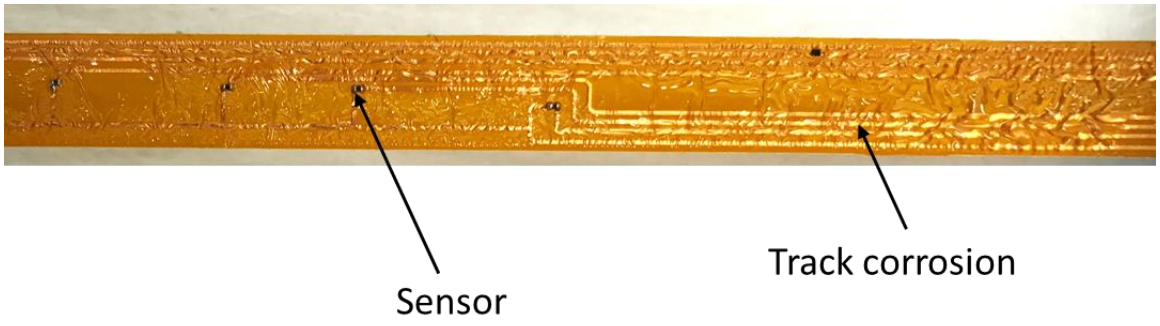

Figure 14 Failed conformal coating showing clear track corrosion and delamination

Further investigation for protecting the sensing elements and the materials tested are outlined below.

Parylene – This material was selected due to its mass use in harsh environments for protecting circuits and sensor elements. The coating is applied at room temperature and provides a clear, thin, flexible and corrosion resistant barrier.

PTFE: Another common and highly non-reactive polymer, this material is also used within the battery manufacturing. However, the grade of PTFE remained an industry secret therefore, further research is required.

PVDF: Is used a binder material in cell assemblies. It can provide a barrier from electrolyte solution

Polyuretheane: An off-the shelf conformal coating used extensivity within the electronics industry. This was selected due to the availability of the material and low productions costs.

Acrylic: An off-the shelf conformal coating used extensivity within the electronics industry.

FEP/PET: Used as a heat-shrink material for protecting fibre cores from corrosive solutions.

Kapton: Used extensively inside manufactured cells. Furthermore, previous literature regarding instrumented cells have used Kapton as a substrate for sensor elements and protecting the sensors assemblies from electrolyte corrosion.

Table 8 Conformal coating testing results for pouch and cylindrical cell formations

Coating	Thickness	Cell Type	State	Notes
Parylene-C	1um	Pouch	Success	Success
Parylene -C	1um	Cylindrical	Failed	Electrolyte fail
PTFE	1um	Pouch	Failed	Failed to fully encapsulate
PVDF	2um	Pouch	Failed	Success
Polyurethane	< 1 um	Pouch	Failed	Electrolyte fail
Acrylic	< 1 um	Pouch	Failed	Electrolyte fail
FEP	1mm	Cylindrical	Success	Success

PET	1mm	Cylindrical	Success	Success

To verify the mechanical failure and exclude human error a conformal 1µm coating of Parylene was deposited over the sensor assembly using a PDS 2010 Labcoter® 2 (*Specialty Coating Systems*). The result was a uniform non-porous layer, protecting the sensor from electrical, chemical and mechanical interactions. The sensors were embedded within a battery and cycled 15 times. The cycle number was selected to show the feasibility of the sensing topology that no abnormal responses were apparent in the cells response, such as a sudden capacity loss or catastrophic failure.

The sensors remained intact with a meaningful temperature reading in accordance with the controlled thermal chamber environment.

It is important that both the cell and the sensors suffer no negative impact due to the integration of the sensor and the measurement process. The sensors stability was evaluated by comparing the readings of a coated and an uncoated sensor as shown in Figure 16. It is clear from that the measurement produced by the uncoated sensor (broken line) become erratic after 100 minutes only, compared the coated sensor that is stable for over 10 hours. The results are confirmed by the corrosion observed on the tracks of a cells as shown in Figure 14.

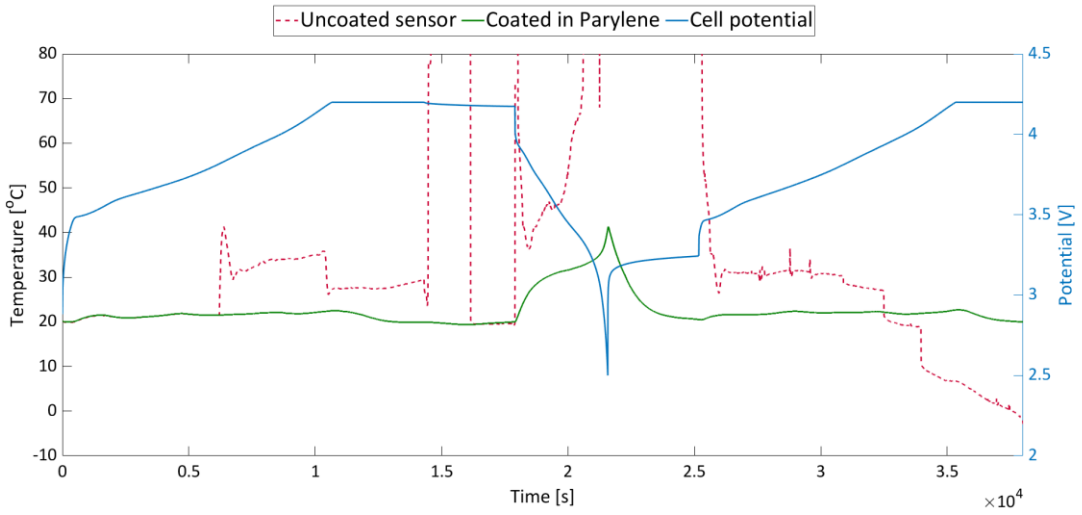

Figure 16 Failed sensor versus a coasted sensor embedded into a pouch cell during a CC/CV cycling phase

Furthermore, conformal coatings could affect the sensitivity, thermal response and characteristic curve of sensor elements. Therefore, a batch of sensors was sent to an accredited test house (*Taylor Instrument services*) for validation versus raw thermistor elements. No abnormal response was observed with the maximum tolerance well within manufactured stated limits. This was achieved using a thermal chamber and a high accuracy platinum resistance temperature detector (RTD) PT100 (*Pico®*) calibrated in a United Kingdom Accreditation Service test facility.

Several iterations of the sensors were fabricated, and after considerable development it also become clear that not a single mechanical format was suited for both cylindrical and pouch formations. Figure 17 shows the sensor revisions. The electrical connectors proved to be extremely brittle due to the sensitive nature of flexible-PCBS. The connector in question is a surface mount device and on a flexible substrate printed circuit boards often have a stiffer on the backside to reduce risk of track delamination through bending and repeated mechanical handling. The sensor design in question did not have this feature present, as we often found moving the connector and applying pressure would bring the sensor elements back to life. This would lead to confusing results and irregularities. Therefore, future design iterations used a flat profile connector.

A low-profile connector means that suitable instrumentation needed to be in close proximity with the sensor strip, while a push type connector would allow extension wires as in versions A,B and C, such as ribbon cables.

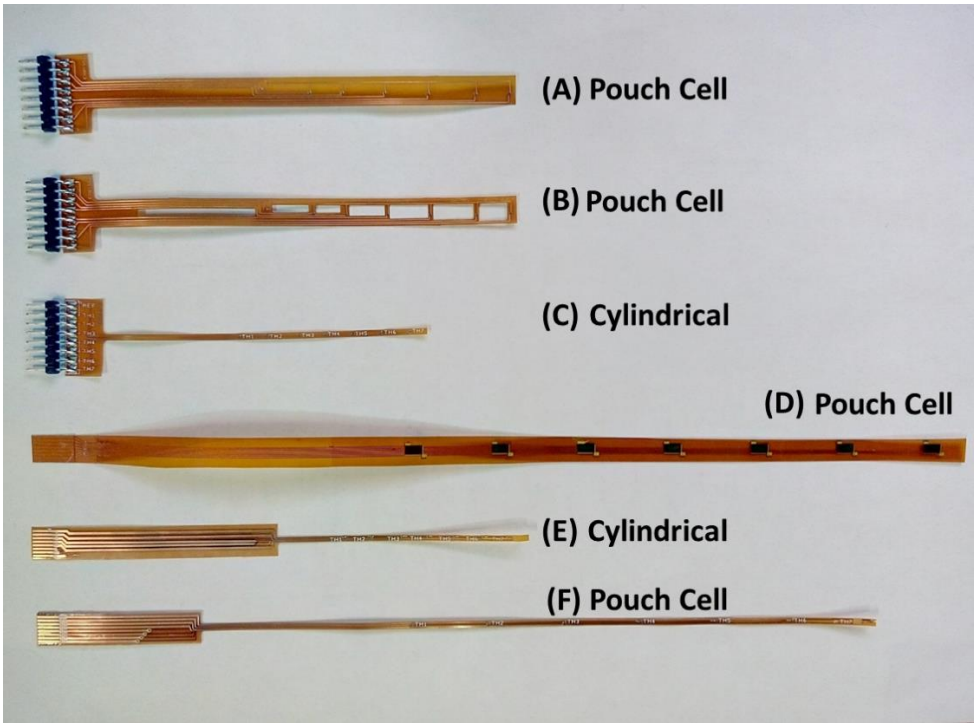

Figure 17 Distributed thermal sensors (A),(B),(D) and (F) for pouch cell constructions and (C) and (E) for cylindrical cells

Calibration

Calibration of the sensors built this way is of high importance because measurement error can lead to distorted data, false results and repeatability issues. The thermistor devices in question have an operating range of -20 °C to 120 °C and the manufacturer stated beta coefficients are evaluated over several discrete temperature spans. Each element on the substrate requires an individual calibration curve plotting over the operating span of the sensor. The data from the test house showed a maximum deviation of 0.15%, which is within the characteristic response.

6.2.2 Instrumentation

Thermistors have several engineering design challenges that need to be addressed, including a non-linear response and self-heating. For this reason, an absolute minimum amount of analogue circuitry was added to the design of the system. Each

thermistor node is arranged in series with a 0.1% precision resistor and a 0.1% voltage excitation source, effectively forming a voltage divider circuit. The voltage is measured between the two resistive elements. Figure 18 displays the instrumentation circuit described previously. C1 is a transient voltage capacitor and V1 is a precision voltage source.

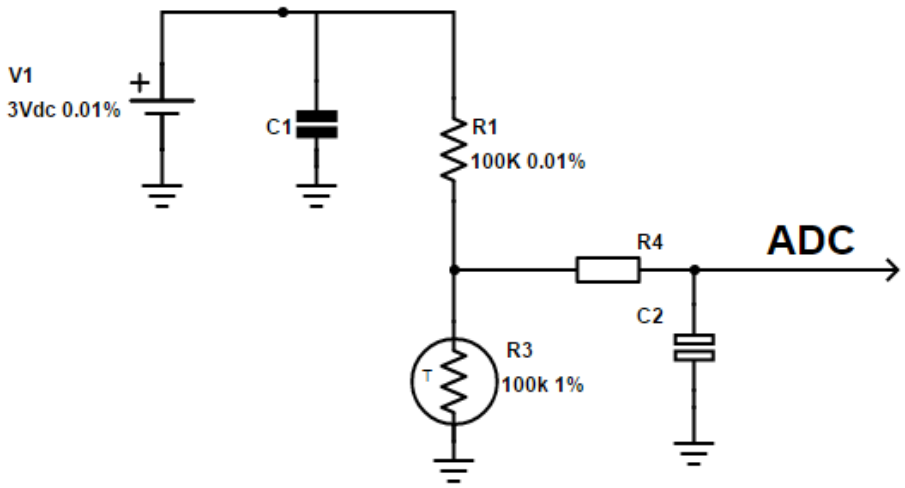

Figure 18 Thermistor instrumentation circuit conditioning

The voltage input into the analogue to digital converter (ADC) is given below in Equation 1, this is then converter into a voltage using the Steinhart equation.

$$V_{ADC} = V_1 * \frac{R_3}{R_1 + R_3}$$

Equation 1 ADC voltage input transfer function from thermistor instrumentation

The instrumentation configuration has the advantage of a minimum self-heating, an inherent resistance to voltage converter and signal linearisation. The voltage measurement is converted to temperature using the Steinhart-Hart equation shown in Equation 2. The obvious limitation is the increased processing required to calculate the temperature, this is due to the complex functions within the equation. However, modern BMS systems have high speed processing units, capable of handling complex equations using be-spoke DSP processors.

$$T = \frac{B}{In(\frac{R_{Thermistor}}{R_0 * e^{\frac{-B}{T_0}}})}$$

Equation 2 Steinhart-Hart equation used for converting thermistor resistance to temperature

Where B is the beta coefficient of thermistor element, R_0 is nominal resistance at room temperature, T_0 = temperature at R_0 and $R_{Thermistor}$ is measured resistance

The instrumentation PCB plays an important role in maintain a reliable data reading. For this reason, significant engineering and thought of the design was undertaken. Firstly, a large hatched ground plane on both the top and bottom of the circuit board have been added. The hatched copper pour helps reduce the effects of high frequency electromagnetic interference. Furthermore, each trace for the sensor has a ground connection on both sides, which elements the possibly of cross talk between conductive traces.

Pouch cell production

The reliability of the pouch cell assembly materials was found to be critically important. Significant effort for producing high quality electrode material were undertaken by visually inspecting each electrode before cell stacking. Table 3 data shows how inconsistencies, electrode damage and poor manufacturing have a serious effect on battery performance. The initial formation (C/20 charge to 4.2V and then C/10 discharge to 2.5V) showed a significant difference between the production theoretical capacity and experimental data. Furthermore, during formation. Manufacturing errors included un-even electrode depositing, clumps of electrode material forming grain like regions. This was a particular issue during cell quality checking, as shown in Figure 19.

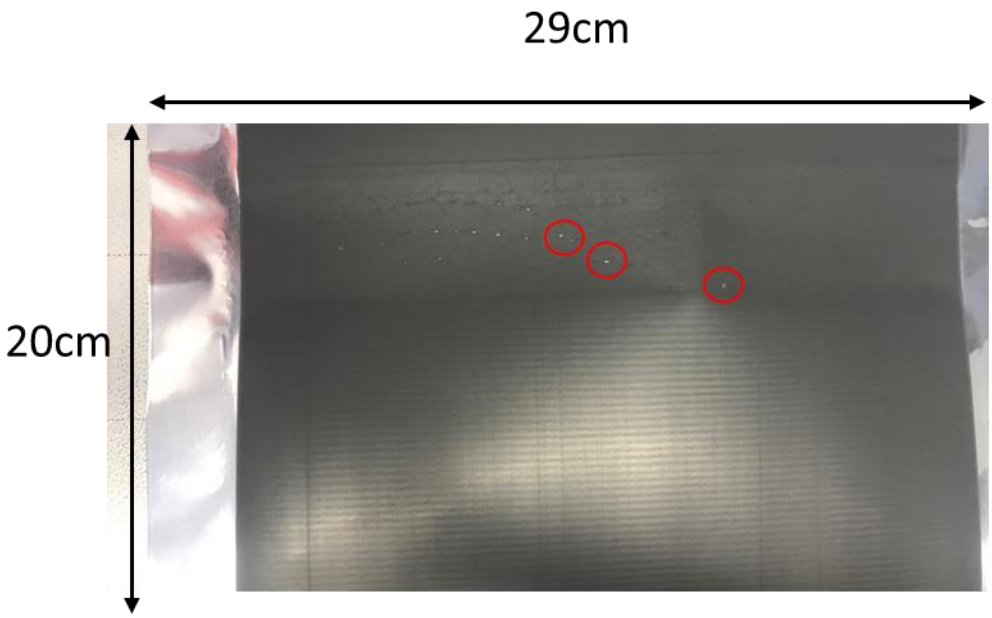

Figure 19 Illustration of poor electrode coating.

The instrumentation showed to have a minimal percentage differences compared with an instrumented cell, even with significant assembly faults present.

Table 9 Cyclic data of poor production quality cells during formation

Cell	Embedded Sensor	Theoretical Capacity	Experimental Discharge	Capacity Loss
1	No	5.5	4.22	23.27%
2	Yes	5.5	4.28	22.18%
3	Yes	5.5	4.12	25.09%

Table 10 Cyclic data of poor production quality cells over 10 cycles

Cell	Embedded Sensor	Capacity (C/2)	Capacity (1C)	Theoretical Capacity
1	No	5.5	4.95	5.5
2	Yes	5.5	4.85	5.5
3	Yes	5.5	4.66	5.5

Therefore, for consistent quality the electrode material for the anode an cathode were produced and weight for consistency. The weight of the cells' electrode

material has a correlation for usable capacity. Furthermore, it was important to monitor the cell weight throughout the manufacturing and cycling aging process. Figure 20 show the mass variation from the production of 40 cells. The data presented no more than 0.6% deviation from the calculated weight of electrode material, which means capacity retention would be close to each other.

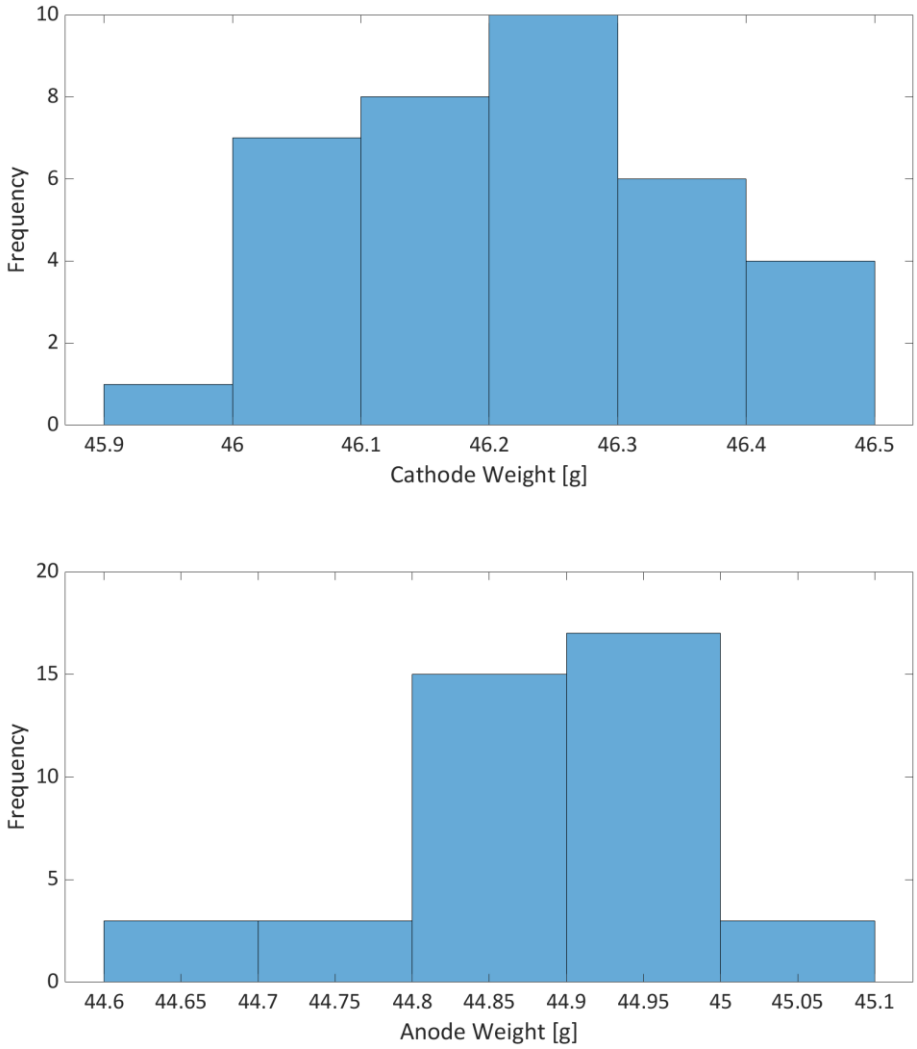

Figure 20 Anode and cathode mass variations during manufacturing for instrumented cell production units showing a maximum of 0.4% variation from the target mass

Table 11 Instrumented pouch cell cycling aging after 35 cycles at C/10

Cell	Embedded	Theoretical	Experimental	Capacity

	sensor	capacity	capacity	loss
1	No	5.2	5.02	1.09%
2	Yes	5.2	5.01	1.13%
3	Yes	5.2	5.1	-0.65%
4	Yes	5.2	5.15	-1.58%

Figure 21 displays the cyclic data extracted from the cells in question. The data clearly displays a capacity increase over time. This is due to the cells' being manufactured and filled with electrolyte. The electrolyte solution spreads within the cell causing an increase of capacity as more electrode material becomes activated.

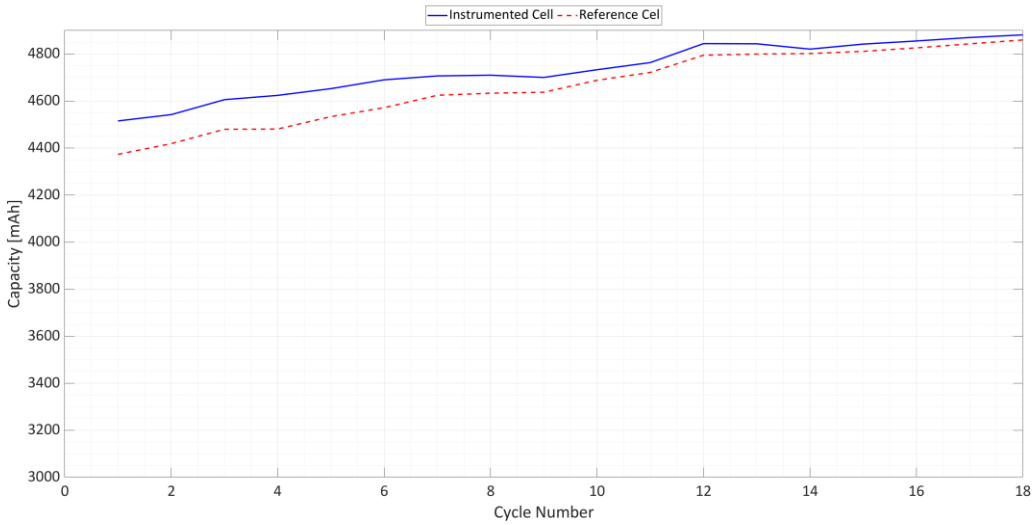

Figure 21 Cycling aging of a reference vs an instrumented cell at C/10 for a Lithium-ion pouch cell showing negligible aging versus a non-instrumented cell

6.2.3 Cell modification procedure

The entry point into the cell required modifying the manufacturing process, this was achieved by examining the entire process and identifying where would cause minimal damage, to the electrode and separator material from the sensor.

After the electrode materials are stacked into appropriate number of layers, the cell is placed into one half of the outer bag material, which is later sealed using high mechanical and thermal pressures. The sensor was tested several times in its

uncoated form to know if it can withstand the mechanical pressures that it would be under during sealing of the bag material. The test proved that no effect upon the sensor track occurred which was a real concern as the tracks are only 0.15mm wide and 1um thick.

Before the stack was sealed it was pried open and the sensor slipped between the middle layers as shown in Figure 22. A double layer of hot melt adhesive (polymer tape) was added to both sides of the sensor to form a complete seal. The modification procedure creates the possibility of electrolyte leakage and further leakage may occur in case of inadequate sealing around the entry hole of flexi-sensor. Several iterations of the sensors were put under vacuum to test the sealing, no effect was noticeable.

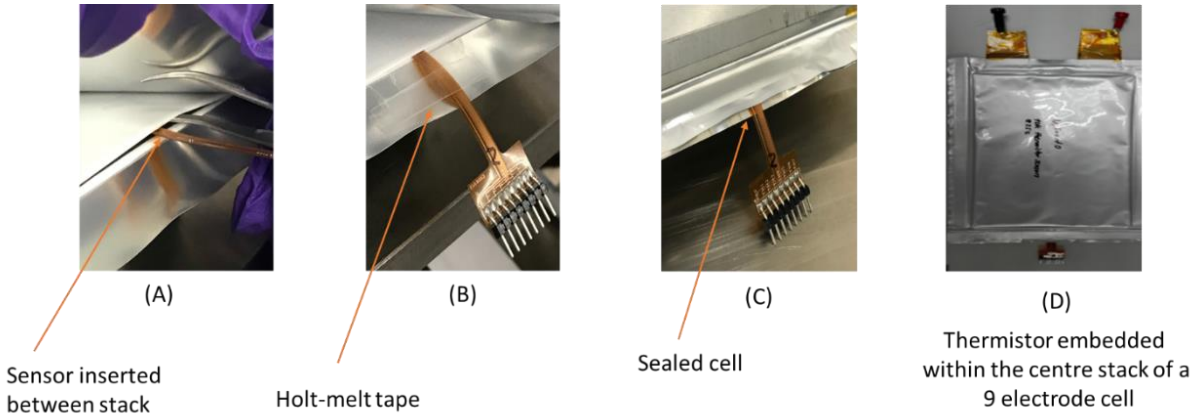

Figure 22 *in-situ* Thermistor embedding and testing procedure for a Lithium-ion pouch cell (a) Sensor insertion (b) Hot melt tape applied (C) Unit sealed using heat bars and (D) Complete instrumented cell

6.2.4 Time domain analysis

The response of a three-point *in-situ* sensor within the center stack during a CC/CV charge and CC discharge phase is shown in Figure 23. The placement of the sensor in the pouch cell is shown in Figure 29. The thermal sensors observed temperature shift which is closely related to the charge/discharge phase of the battery and the external thermocouple measurements. This validates that the elements are responding with no visible lag and providing accurate thermal data.

The data presented indicates a clear and significant temperature correlation between the core and skin of the cell, thus underlining that the surface measurements do reflect the temperature of a cell for pouch cell formations in the through plane direction.

Temperature spikes observed during the cell cycling are tightly correlating with the constant current/constant voltage charge phases. The high temperature rise and asymmetric behaviour of the charge and discharge phase can be explained with the internal resistance increasing as the cell reaches minimum charge. As the cells reach maximum charge the ionic resistance increases due to the limited holes available in the positive electrode. Therefore, increasing the total internal resistance of the cell in question and thus generating significant ohmic heating under constant load compared with a charge cycle where the internal resistance is low and thus generates less heat.

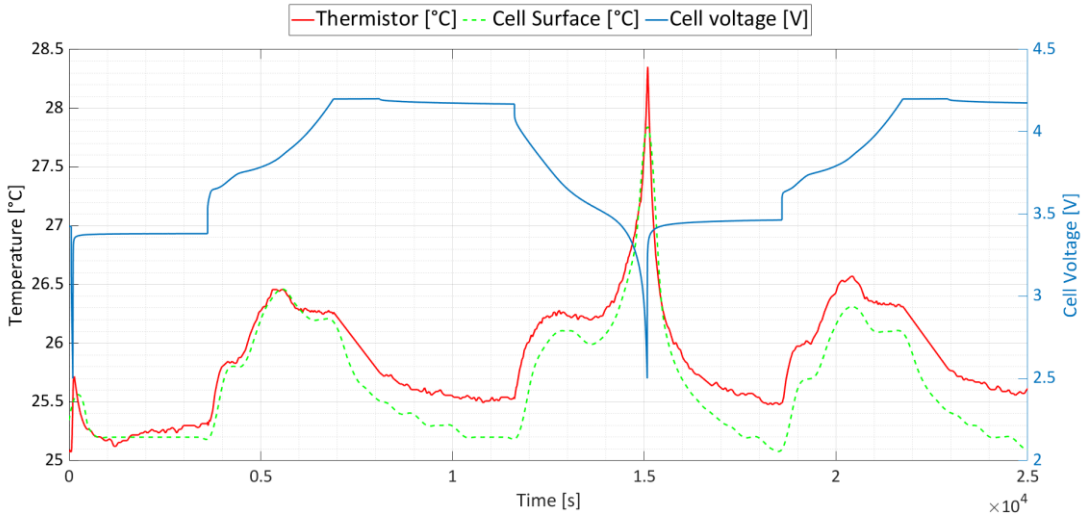

Figure 23 In-situ temperature response of Lithium-ion cell 1-C rate

The data presented in Figure 24 shows a snap shot of the distributed thermal behaviour, a slight change of less than 0.3°C in the temperature is apparent where the sensors are in near proximity with the battery tabs, where, significant thermal heating occurs. Furthermore, it shows after considerable cycling and resting between the embedding of the sensor and the x-ray inspection, no corrosion of the traces is apparent

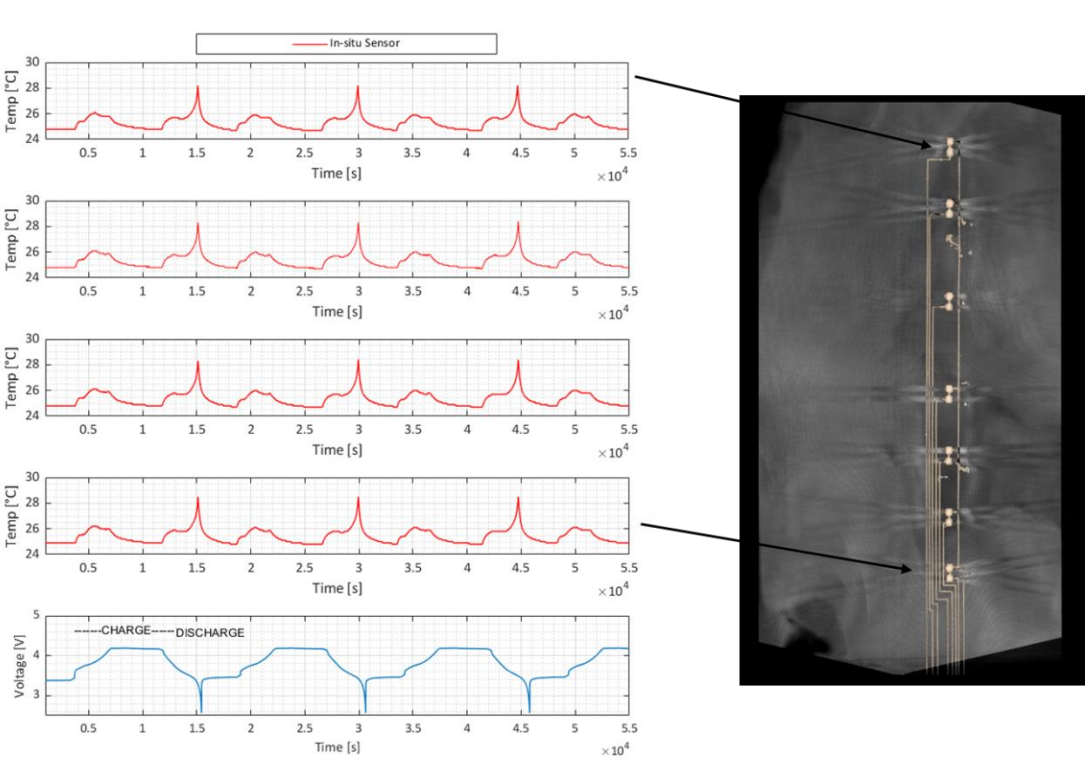

Figure 24 *In-situ* thermal response of a pouch cell using distributed thermistor elements and corresponding x-ray tomography image

The capacity comparison of a cell before and after modification is shown in Figure 25. The evaluated cells were cycled at a rate of C/10 during formation. The data recorded shows a complete match between the cell discharge profile before and after modification. Due to the cells being constructed in house an understanding of capacity fade, batch tolerance and manufacturing errors are known from previous non-instrumented builds. The data presented clearly suggests that any loss of electrolyte due to failures in the ceiling method or cell material damage incurred during cell manufacturing and modification is negligible and has no observable effect on the electrochemical system even during the cell formation.

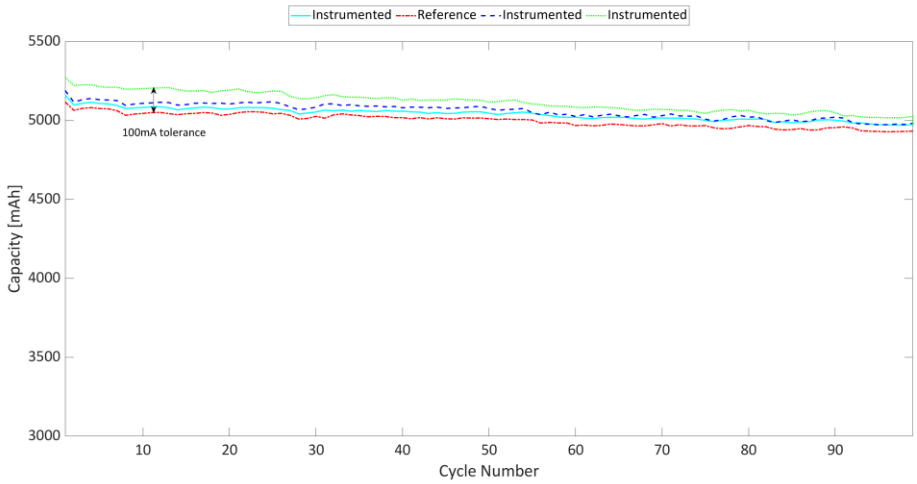

Figure 25 Illustration of a 100-cycle capacity extract of instrumented pouch cells vs none instrumented at a rate of C/10 using a CC/CV charge and CC discharge.

6.2.5 Frequency domain analysis

As the adverse effects on the cells, including electrolyte loss or electrode damage, are possible during the modification procedure, may not appear in time domain analysis conducted in the previous section, the cells evaluated were analysed using Electrochemical Impedance Spectroscopy (EIS) at 100% and 0% SoC for pristine cells and modified cells - data obtained is shown in Figure 26. The sensitive nature of EIS measurements means that even minimal electromagnetic interference or connectors change can cause measurement errors - to nullify the external connectors' influence the series resistance element of the Nyquist plot was zeroed, enabling us to focus the analysis on the internal cell changes.

In case of pouch cells EIS profile some shift in mid-frequency region corresponding to the charge transfer is apparent. The shift can be explained with the surface impedance increase due to the sensor covering some electrode area within the cell. This effect can be minimised by further optimising the sensors layout and substrate footprint reduction. None of these effects observed here are visible in the cell cycling data as they are of negligible scale.

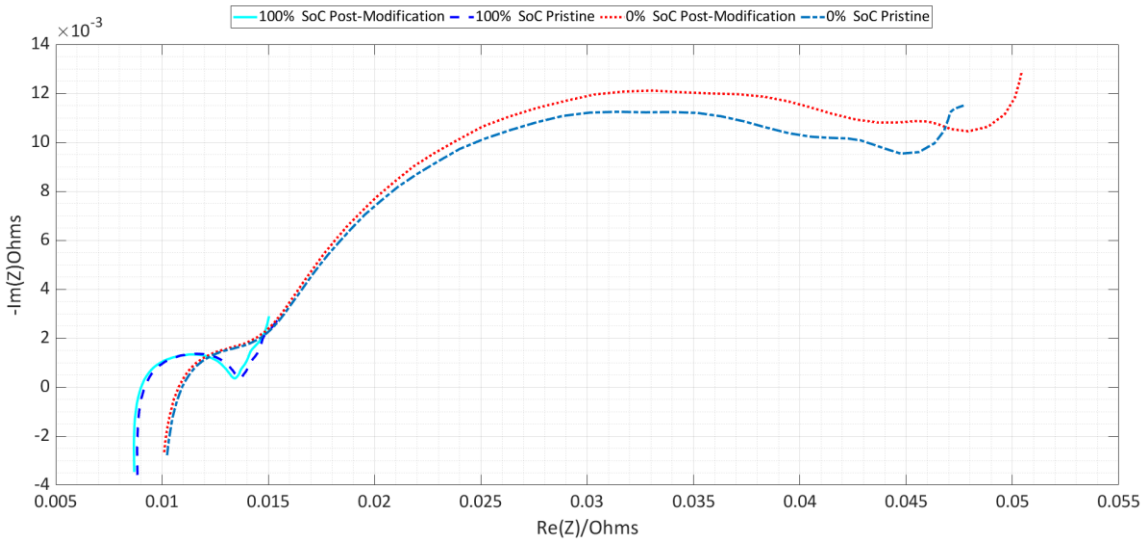

Figure 26 Illustration of Electrochemical Impedance Spectroscopy (EIS) at 100% and 0% SoC for pristine cells and modified cells

6.2.6 Electrode and sensor inspection

Figure 27 shows the *in-situ* sensor(a), anode collector(b) and separator material(c) that were in close proximity to the sensor. The sensor substrate had a dark substance deposited onto the substrate, which is coming from the electrode material that has delaminated from the current collector. The area exposed to the sensor would have increased the surface impedance and limit the ionic flow, leading to capacity loss, however this was found to be negligible as shown previously in Figure 25. Despite the increased mechanical profile compared with printed technology utilising thermocouples[27] and resistance temperature detectors[35] sensor topologies. The temperature range of the sensor is limited when compared to other temperature sensing methodologies, but this is not a concern as the maximum temperatures that a battery can survive is currently limited by several inherent material properties of the electrochemical assembly. Post-mortem active material delamination would also be expected with other solutions which utilise any form of substrate to support sensing elements inserted between electrodes stacks.

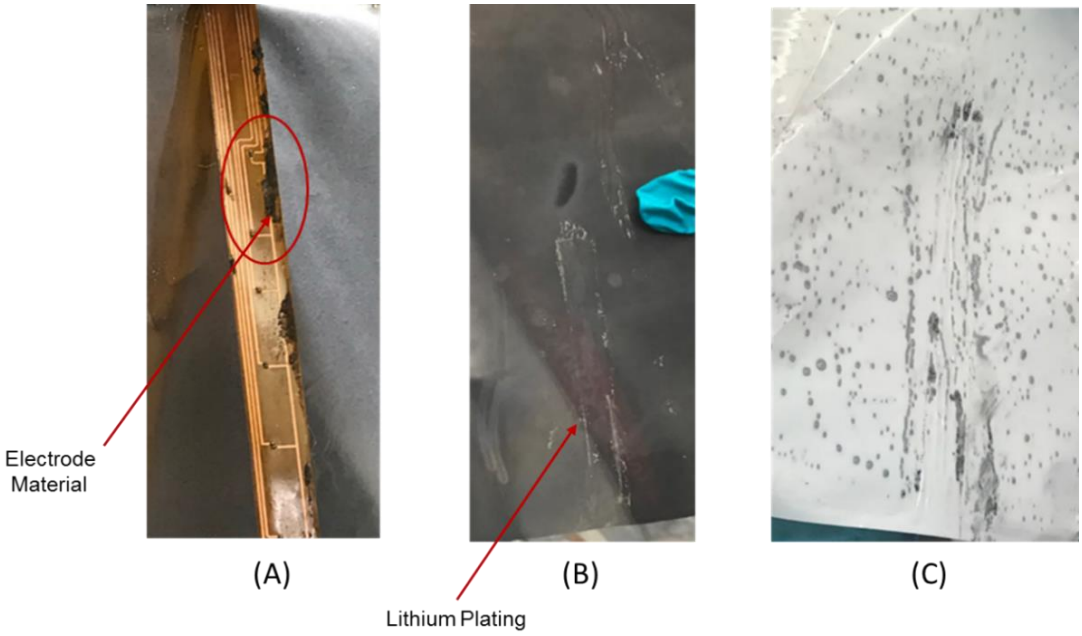

Figure 27 (A) sensor removed from pouch (B) Anode material (C) separator material

Figure 28 shows the sensors before and after cycling within a cell for a three-month period. The sensor coating and track both remain intact and show no signs of delamination or tracking corrosion. Further validating that the coating of choice and thickness are appropriate for pouch cell constructions.

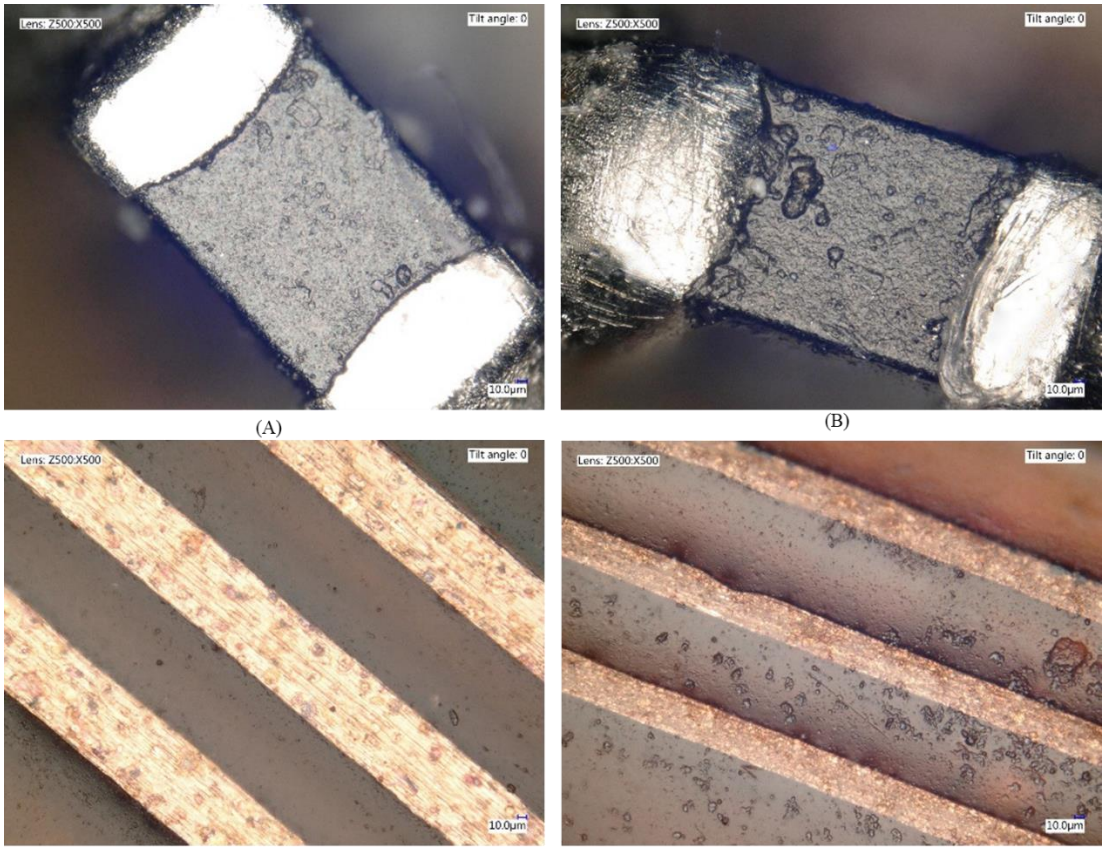

Figure 28 Illustration of sensors removed from an instrumented cell before and after cycling

6.2.7 *In-situ* inspection

To assess possible failure of the polymer sealing method and any subsequent loss of electrolyte solution, the pouch cells were weighed directly after the manufacturing procedure and later after cycling. No difference in mass was observed -. this proves that the sealing method applied is an effective solution for securing the modified cells, preventing exposure to air or electrolyte leaks.

The exact position of the thermistor sensor within the cell core and the element's impact upon the electrode material was evaluated using X-ray Computed Tomography (X-TEK XTH 320 LC, *Metris*), the results of which are shown in Figure 30. As can be expected from the lumped elements a slight bump occurs where the MEM's devices are located, yet no damage had occurred to the layers in near proximity, which could otherwise lead to a short circuit event. Figure 29 illustrates the steps for the modification and inserting the sensor into a pouch cell ready for *in-situ* inspection

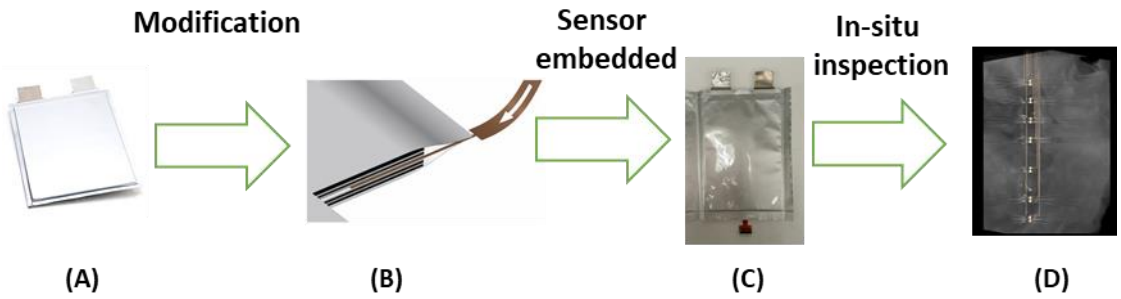

Figure 29 Instrumented pouch cell construction showing modification procedure

The embedding procedure for an *in-situ* sensor is extremely harsh compared with an 18650 design. During manufacturing significant pressure is placed upon the sensor substrate. Therefore, it was necessary to conduct an *in-situ* image of the entire system, as shown in Figure 30. It can be clearly seen that the sensor traces remain intact and no obvious damage to the electrode material is apparent. Which could be of concern due to the lumped nature of the sensor element. This means significant engineering time and resources are reduced compared with low profile ink formulations or metallic deposits used in other forms of thermal monitoring

techniques. Lastly, the sensor elements are mass produced in many other applications, meaning capital costs for design changes are negligible.

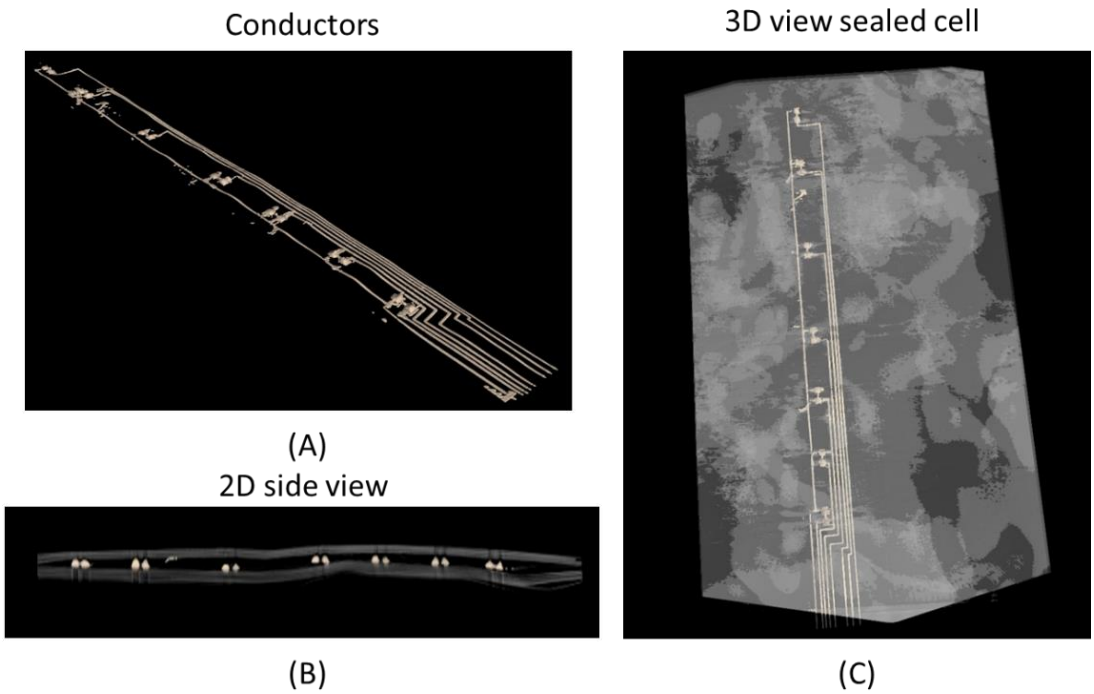

Figure 30 *In-situ* inspection of an instrumented pouch cell (A) top view of sensor (B) side view of pouch cell and (C) top view of pouch cell

6.3 Chapter conclusions

Research conducted for instrumented cells have focused on the development of sensor elements. Little attention has been devoted to the impact of cyclic behaviour, *in-situ* inspection and post-mortem analysis, which remains undocumented in literature. Consequently, given the lack of critical attention paid to instrumented cells, this work has presented unprecedent experimental data concerning the characteristic behaviour of a cell compared with a standard virgin cell. Furthermore, previous research efforts have modified commercial units, this work addressed a deeper understanding of the industrial process required for manufacturing a smart cell within a production facility. Where consistency between the control units and modified units are maintained though out all experimental data.

This work has shown the development of novel flexible sensor arrays that can be inserted into the electrode stack of a pouch cells. The sensors can be embedded in commercial units or be added during the manufacturing of new units on a production line as shown in this work. The conformal coating used on the sensors has also shown to survive the electrolyte solution and mechanical stress encountered during production. The impact of the sensor battery stack has also shown to increase localised dendritic growth around the edges of the sensor. This could be minimised with an improved sensor design, minimising the surface area impact on the cells electrodes.

The impact of the sensors upon the cells performance has also been shown to be negligible, with over 100 cycles conducted, versus unmodified cells. This was validated using time and frequency domain analysis. Additionally, the cells were placed under a considerable amount of pressure during the entire cycling regime. Thus, emulating real-life battery module conditions.

In-situ sensors devices published in literature for instrumented cells have used resistance temperature detecotrs or thermocouples, which are inherently a low sensitivity device, consequently, accuracy is limited. The thermistor sensor methodology presented in this work is a significant improvement on previous

research efforts in terms of distributed sensing, low cost instrumentation, high accuracy and sensitivity. This work has further showed that lumped thermistor elements have no effect upon the substrate, where previously all known literature has stated that such devices would not be suitable for *in-situ* measurements due to the increased mechanical profiles.

7 Instrumentation of cylindrical cells

7.1 Introduction

This chapter describes the experimental work and results undertaken for thermal-instrumentation of cylindrical cells using distributed thermistor elements'. The development, validation and testing of the instrumentation is described, followed by the validation of the instrumented electrochemical system. The cylindrical cells evaluated for *in-situ* sensors applications were commercial 3Ah high-energy cells consisting of a lithium nickel cobalt aluminium oxide (NCA) cathode, graphite anode and a $LiPF_6$ electrolyte solution.

7.2 Research and development

7.2.1 Sensor design and validation

The previous chapter explored the fundamental sensor topology of using thermistors and validated the conformal coating procedure and element reliability. Figure 31 displays how the *in-situ* sensors fit within the mandrel core of a battery. However, Chapter 6 had focused on the development of a conformal coating into an environment a known electrolyte solution and substantially different form factor cell. Therefore, it was necessary to understand if the coating and the sensors did not affect the new type of cells under investigation.

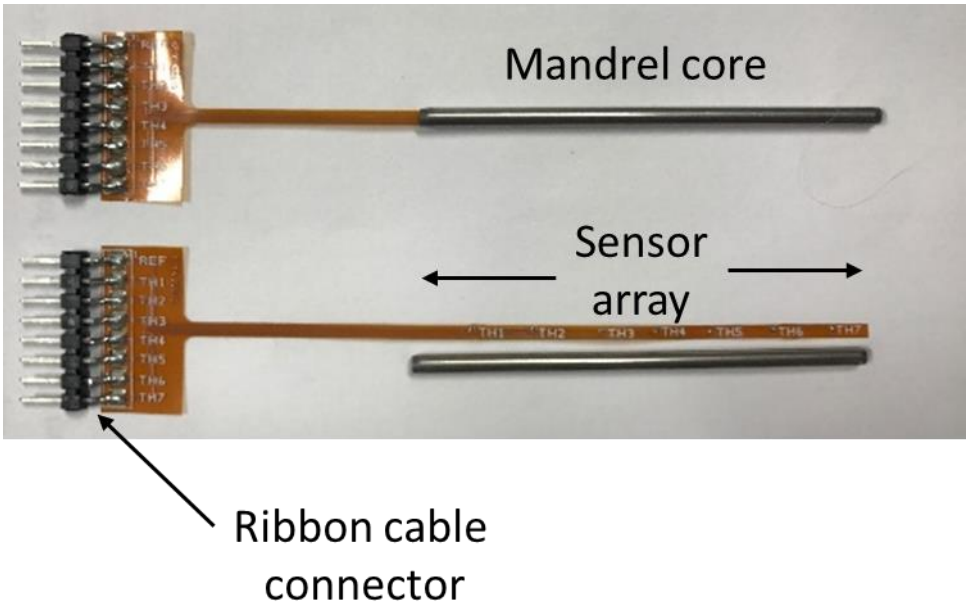

Figure 31 Core temperature sensor for a cylindrical cell. The 7-point sensor covers the entire core length

Initial testing showed the conformal coating of parylence C proved to be ineffective alone in protecting the sensor from the mechanical influences within the cell as shown in . This issue was overcome by increasing the conformal coating thickness and adding a second coverlay protection during manufacturing. This approach does increase the mechanical thickness however. But, this is not of a concern with cylindrical cells as considerable room is available within the core. Lastly, the weighted

connectors proved to be a serious flaw in the engineering design, later iteration of the sensors were upgraded to include a flat profile connector.

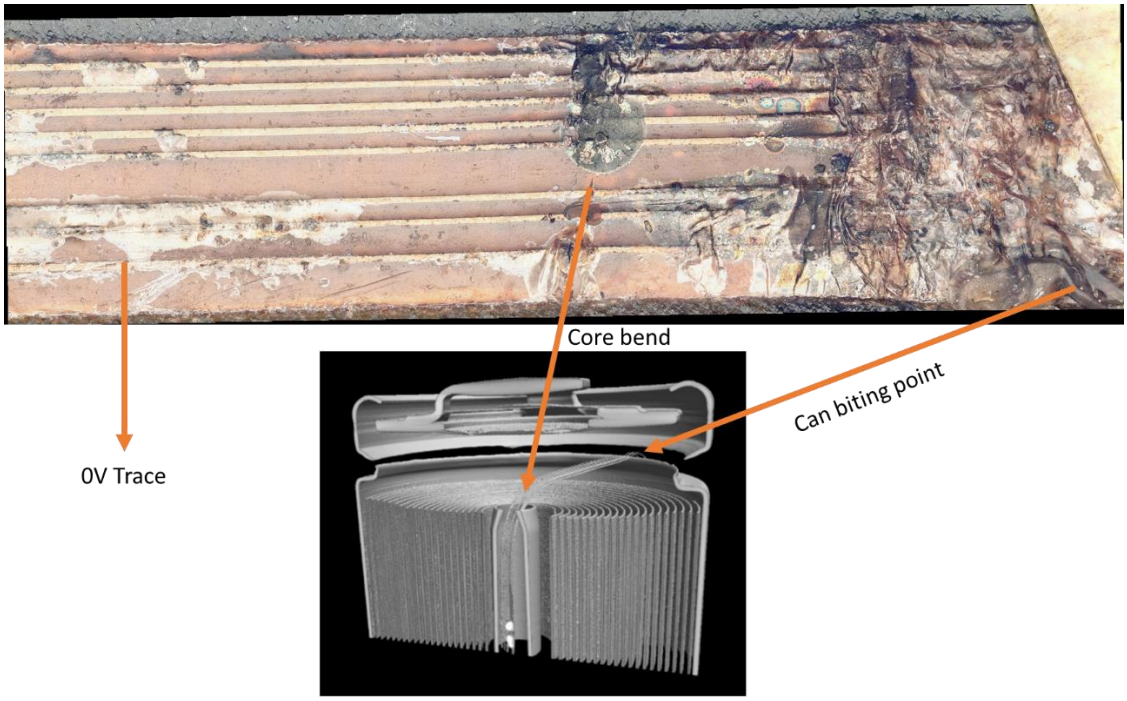

Figure 32 Failed Sensor removed from the core a of an 18650 cell

7.2.2 Cell modification procedure

The modification procedure can be achieved in two ways as shown below in Figure 34, (A) shows how the sensor is placed through the cap of the battery and (b). A non-conductive pipe cutter was used to remove the cathode cap, after which the internal cathode current collector was slung over the side of the cell can. The thermistor sensor assembly was then carefully fed into the core, the attached cathode cap held in place using Kapton tape around the rim and an external application of a fast-setting epoxy resin, ensuring gas-tightness. Modifying the cell to the degree described here would not be necessary in an industrial application as a custom design could be implemented

(A) (B)

Figure 34 Instrumented 18650 Cells. (A) shows the top cap drilled through and (B) top cap left intact

The response of the sensor remains stable for far beyond 100 cycles, concluding that long-term effects are negligible compared with an unmodified cell. This confirms the data and sensor methodology provides an invaluable tool for monitoring the core temperature of a battery, thus, a reliable understanding of core thermal dynamics is possible. The difference in thermal energy generated are significantly different during the two distinct phases of operation, charge and discharge. The mechanisms behind this is due to the internal electrochemical processes with the cell. The cells' maximum resistance occurs during the discharge of the cell and minimal resistance during charging; hence the Joule heating is significantly different during the two distinct phases. This effect is due to the ionic mobility. As the cells reaches maximum charge the ionic resistance increases due to the limited holes available in the positive electrode. Thus, adding to the total internal resistance therefore, generating significant ohmic heating under constant load compared with a charge cycle where the internal resistance is low and thus generates less heat

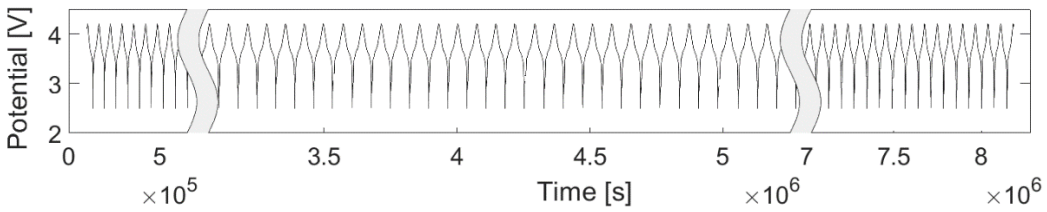

Figure 35 Long-term 0-100% SoC cycling of an instrumented cell. Data collected over 100 cycles, with axis breaks to improve readability. Consistent and stable cycling behaviour is clearly visible[104,107,108]

7.2.3 Time domain analysis

A constant-current (CC) followed by constant-voltage (CV) charge is the standard charging methodology for lithium-ion chemistry. However, advanced pulsed or variable-current cycling techniques are increasingly applied to enable rapid-charging of cells[54,108]. Such modes are applied to the cells evaluated in this study to show conditions which a battery could encounter during its operation.

The thermal sensors observed temperature shift is closely related to the charge/discharge phase of the battery and in agreement with the external thermocouple measurements. This validates that the elements are responding with no visible lag and provide accurate thermal data. Furthermore, the temperature spikes observed during the cell cycling are shown to be tightly correlating with the constant current/constant voltage charge phases. The internal and external temperature readings from the flexible thermistors array is shown in Figure 36.

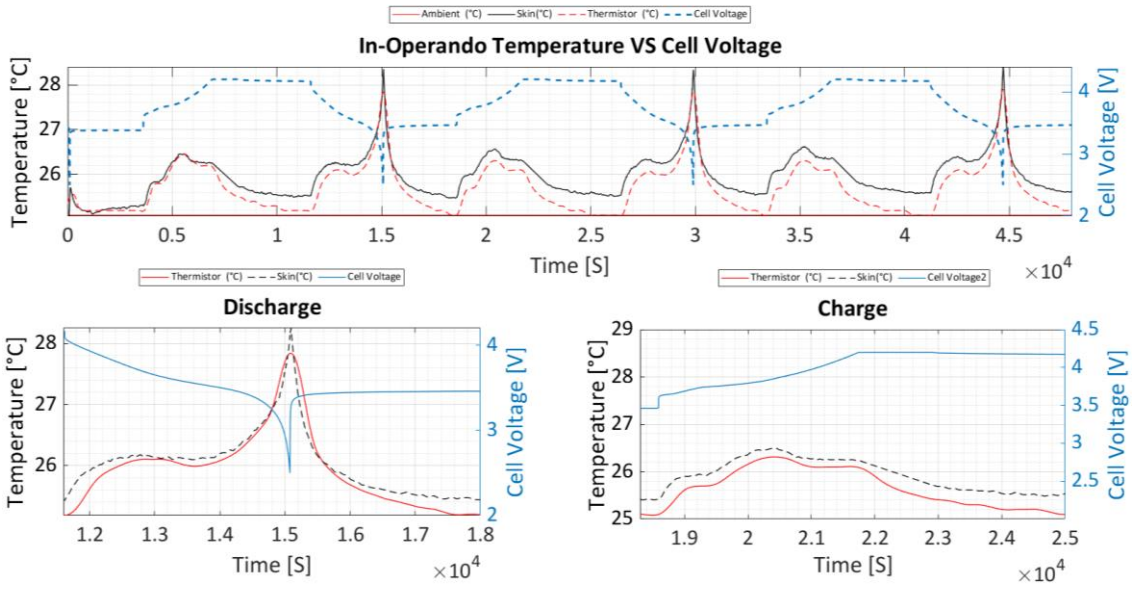

Figure 36 *In-situ* temperature profile of an 18650 cell during a CC/CV charge and CC discharge cycle.

***In-situ* rapid discharging**

The data collected in Figure 37 shows a significant temperature difference between the core and skin of the battery. The battery is charged significantly faster than the manufacturers rating of C/3 and yet the internal temperature remains below the recommended safety limits, dictated by the stability of the electrolyte[45,108].

This suggests the cells can be pushed past the recommended input energy levels without internal temperature reaching beyond safety limits – no cooling was applied to the cells in this experimental set-up. If the safety temperature limits were breached, as the cell heats up the reaction rates for the decomposition of the electrolyte and electrode materials increase, which can lead to the materials breakdown and gas formation, resulting in pressure build-up in the cell[46].

This creates a very high risk of the cell undergoing thermal runaway[45] and explosion or a sharp cycle life shortening if the cells repeatedly operate above very specific temperature limits - usually between 10°C and 60°C[118]. If a thermal run-away triggering event occurs, an exothermic reaction arises, causing temperature to increase uncontrollably. The high temperatures can cause the separator to melt and

cause a short circuit between electrodes. Once thermal run-away has started the reaction can become self-sustaining. Consequently, resulting in pressure build-up within the device in question, that can lead to explosive failure[119,120].

However, this study shows that, with the help of appropriate *in-situ* measurement tools certain cells can be pushed significantly beyond the limits suggested by the manufacturer, without compromising thermal safety limits. This concept is extremely useful for rapid charging protocols and high energy applications and could be integrated within the operating characteristics of battery management systems.

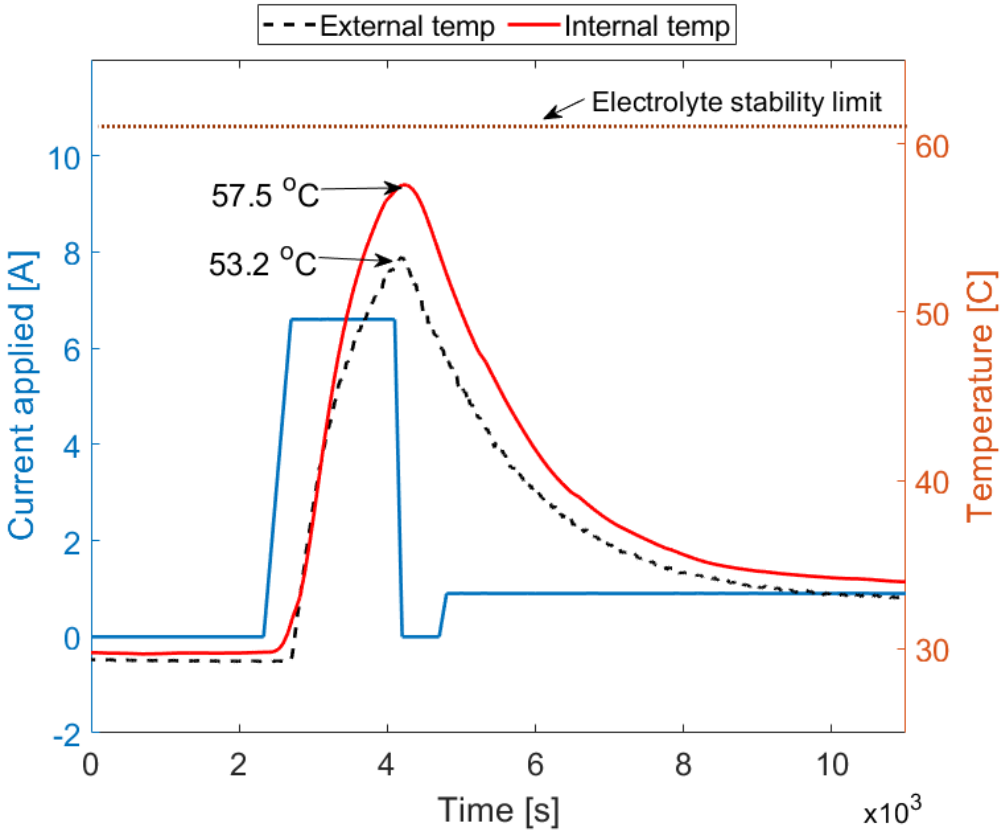

Figure 37 Lithium-ion battery core and *in-situ* temperature under a high constant current load (2C). Clear difference between the internal and the external cell temperature is visible. The core temperature is significantly higher yet still below the safety limit.

Rapid pulse discharge profile is represented in Figure 38. As high-energy Lithium-ion cells suffer from high internal resistances[121,122], heavy electric current loads result in significant temperature increases - the *in-situ* data temperature is again showing a significant differential compared with the skin of the battery. More importantly, the safety limits of the cell operation have been breached after 50% of the time the unit is in discharge, with the total core temperature reaching 72.5°C, meaning damage to the electrolyte is highly likely.

Such internal damage is almost impossible to detect for a standard battery management system and can lead to a catastrophic event if experienced repeatedly[45]. Ability to closely observe of the cell's internal temperatures is paramount in solving these issues. The instrumentation devised offers a solution by enabling unprecedented view of the internal cell thermodynamics, enabling assessment of real thermal performance and safety limitations[107].

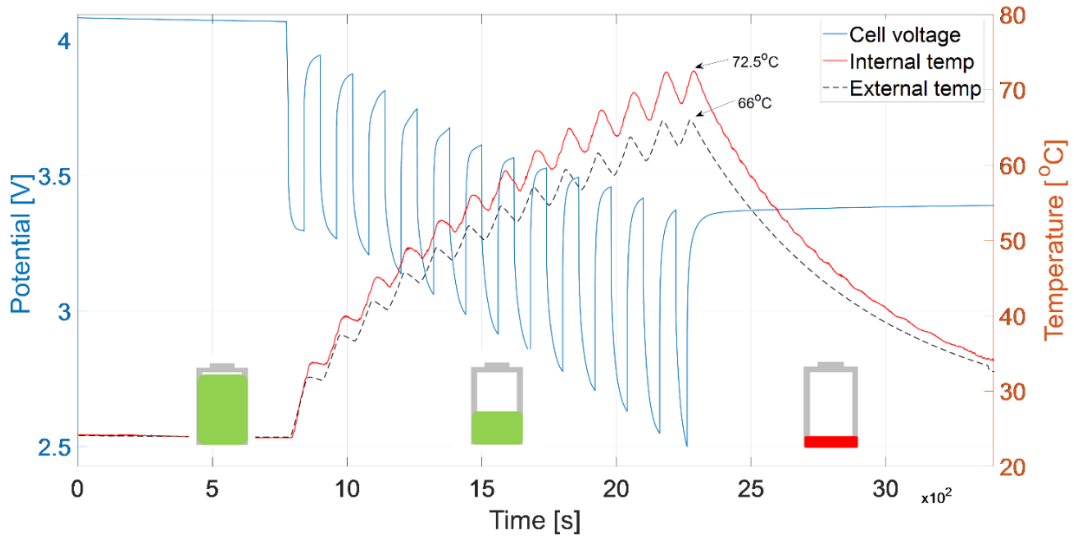

Figure 38 Pulsed power rapid discharge of an instrumented 18650 cylindrical cell. Clear and increasing difference between the external and internal temperature is shown.

7.2.4 Frequency domain analysis

As the adverse effects on the cells, including electrolyte loss or electrode damage, are possible during the modification procedure may not appear in time domain analysis conducted in the previous section, the cells evaluated were analysed using Electrochemical Impedance Spectroscopy (EIS) at 100% and 0% SoC for pristine cells and modified cells - data obtained is shown in Figure 39. The sensitive nature of EIS measurements means that even minimal electromagnetic interference or connectors change can cause measurement errors - to nullify the external connectors' influence the series resistance element of the Nyquist plot was zeroed, enabling us to focus the analysis on the internal cell changes.

The data describing 18650 cell characteristics shows some change within diffusion region of the data. This can be explained by the pressure relief caused by opening the cell after the formation cycles. In case of pouch cells EIS profile some shift in mid-frequency region corresponding to the charge transfer is apparent. Cylindrical cells are not normally de-gassed after formation [123], which results in increased internal pressure. Opening the cell releases this over-pressure and subsequently unblocks pores in the electrode active material enabling easier access to their surface. While of positive effect - reducing the diffusion and charge transfer resistances - such changes have negligible impact on the cell .

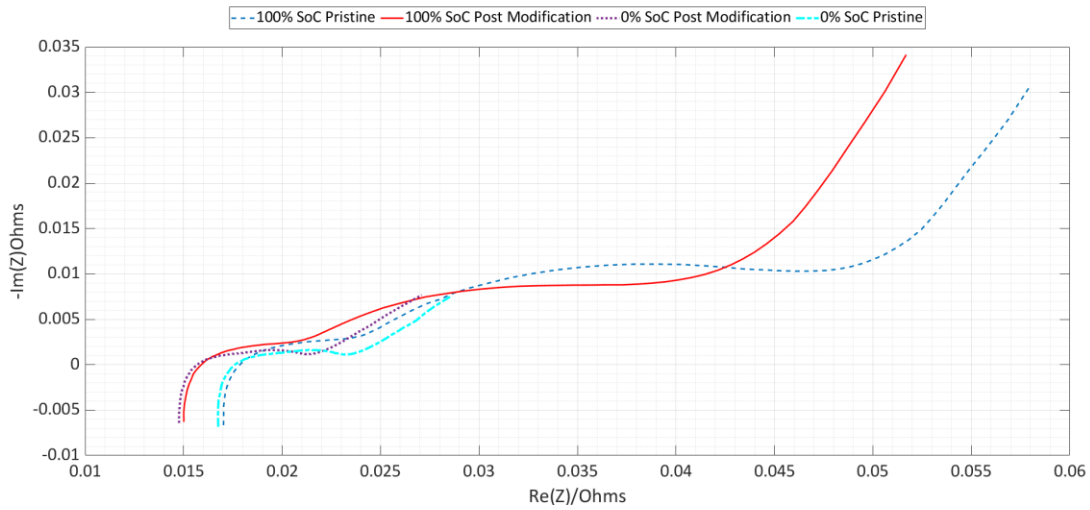

Figure 39 Illustration of Electrochemical Impedance Spectroscopy (EIS) at 100% and 0% SoC for pristine cells and modified cells

7.2.5 *In-situ* inspection

An *in-situ* view of an instrumented battery in given below in Figure 41 and the procedure in Figure 40. It can be seen that the sensor covers the entire length of the battery, thus meaning, the method presented is an indicator of temperature gradients and hot spots if they become apparent during operation.

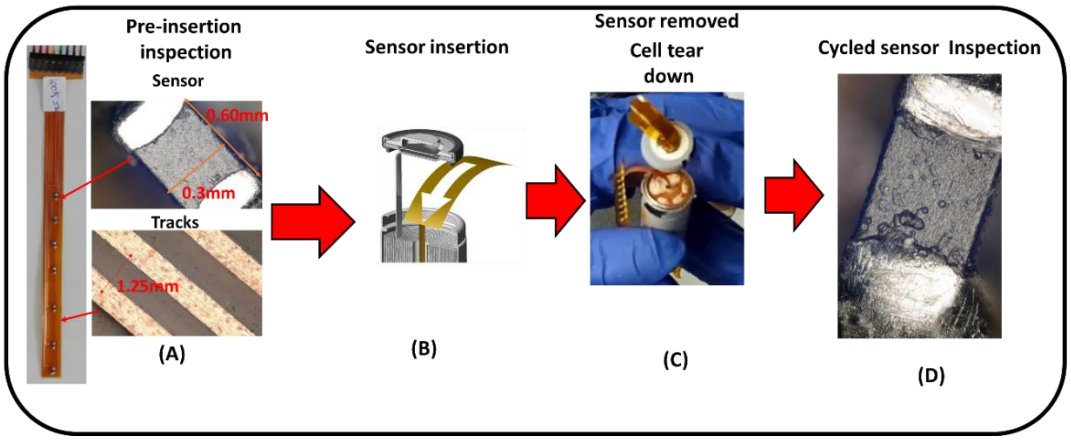

Figure 40 *In-situ* inspection of instrumented cells showing the assembly procedure, sensor methodology and resulting effects on the sensor extracted

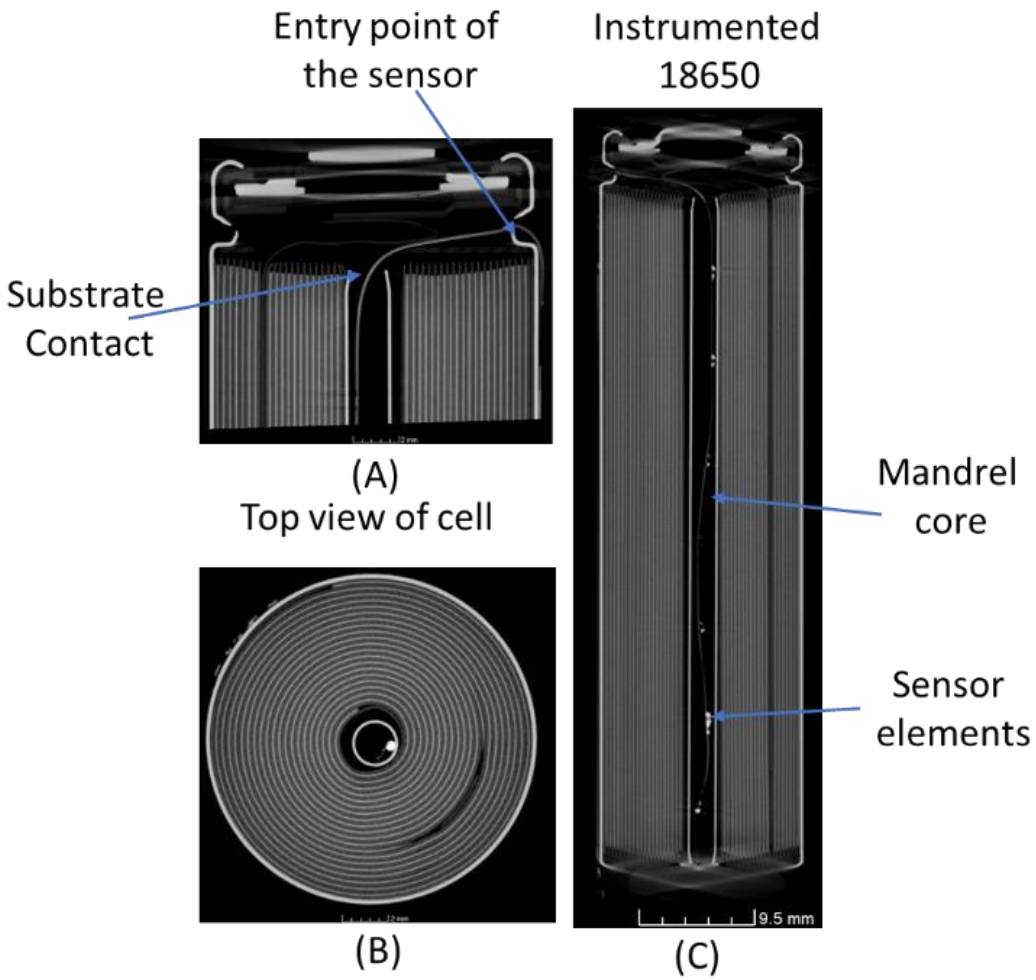

Figure 41 XCT 2D scans of an instrumented 18650 cell after the modification procedure

7.3 Chapter conclusions

Previous research conducted for instrumented cells have focused on the development of sensor elements. However, little attention has been devoted to the impact of cyclic behaviour, *in-situ* inspection and post-mortem analysis, which remains undocumented in literature. Consequently, given the lack of critical attention paid to instrumented cells, this work has presented unprecedent experimental data concerning the characteristic behaviour of a cell compared with a standard virgin cell.

Furthermore, this work has shown the development of novel flexible sensor arrays that can be inserted into the core of a cylindrical battery and the engineering required to modify a cell for the sensors in question. The sensors can be embedded in commercial cells or be added during the manufacturing of new cells on a production line.

The impact upon the cells performance has also been shown to be negligible, with over 100 cycles conducted, versus unmodified cells. This was validated using time and frequency domain analysis. Furthermore, with the help of herein proposed *in-situ* measurement tools, certain cells can be further optimised without compromising thermal safety limits, while under particular scenarios safety limits can be breached earlier than the external sensors would indicate, showing how paramount *in-situ* thermal data is to the operational safety.

The thermal data gathered with the use of the smart cells represents a vital source of information key for the battery management systems to maintain a most optimal performance and an up-to-date understanding of the cells State of Health during deployment in real-life scenarios. The sensing methodology developed here will support the design, research and rapid prototyping of new cells and smart battery modules, enabling considerably greater performance to be safely harnessed from these increasingly prevalent Lithium-ion energy storage systems.

8 Optical instrumentation of cylindrical cells

8.1 Introduction

This chapter describes the experimental work and results undertaken for optical instrumentation of cylindrical cells'. The development, validation and testing of the instrumentation is described, followed by the validation of the instrumented electrochemical system. The cylindrical cells evaluated for *in-situ* sensors applications were commercial 3Ah high-energy cells consisting of a lithium nickel cobalt aluminium oxide (NCA) cathode, graphite anode and a $LiPF_6$ electrolyte solution.

8.2 Research and development

8.2.1 Sensor cell design and validation

The base sensor element is a single-mode SMF-28, 9/125 µm fibre with four 8 mm FBGs evenly spaced and a polyamide recoat. Each FBG element has an approximate sensitivity factor of 11 pm/°C and a -270 °C to +300 °C temperature range. However, due to the sensitive nature of silica fibre and the cell's core environment, further sensor modifications were necessary.

Table 12 Raw FBG sensor specification

Centre Wavelength (nm)	1528 - 1608
Operating range (°C)	-270 to 330
Temperature Sensitivity (pm/°C)	11
Temperature Resolution (°C)	0.05
FBG Length (mm)	8

Research conducted within our group has shown sensors have some capacity for movement while inside a battery, which can lead to the FBG sensor being susceptible to strain effects and would produce misleading data or regular re-calibration of the units would be necessary. Figure 42 shows an x-ray *in-situ* image of an instrumented 18650 battery. The figure clearly shows considerable room for manoeuvre is apparent. Therefore, it is important to maintain a vibration and strain free sensor methodology.

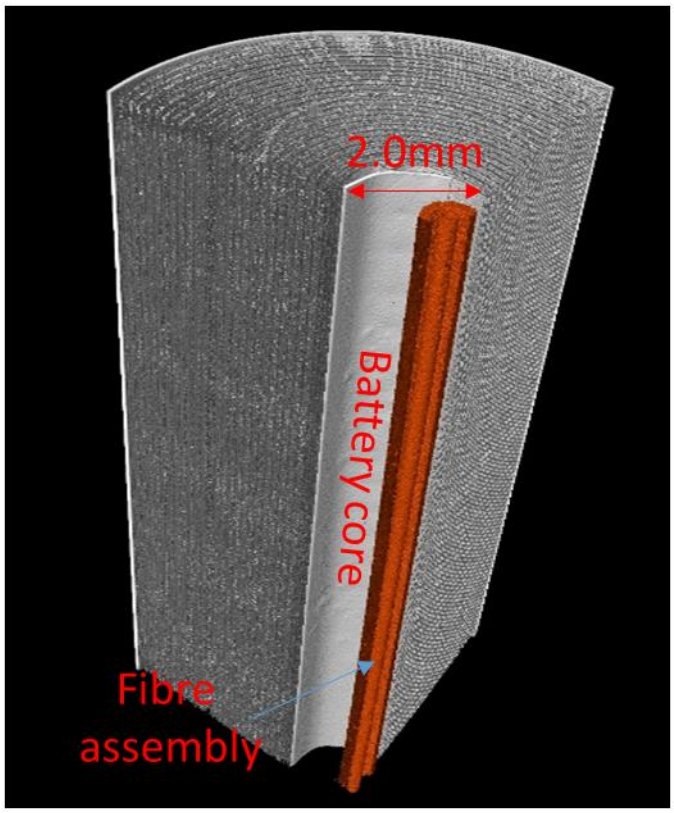

Figure 42 *In-situ* x-ray of an instrumented 18650 cell showing room for manoeuvre within the core

To cope with the conditions expected within the battery. The fibre was threaded through a bespoke aluminium tube, to provide strain relief. An outer skin of Fluorinated Ethylene Propylene (FEP), was applied over the aluminium tube, thus holding the strain relief tubing in place and providing protection from environmental interaction with the electrolyte. The strain relief tubing has the added benefit of protecting the element from mechanical influence during manufacturing, lifetime operating disturbances and thermal expansion from the FEP material.

The FEP resistance to the electrolyte was evaluated by immersing a section of FEP tubing in commercial Lithium-ion electrolyte solution (LP30, *BASF*) for 1 month, which revealed no noticeable degradation of the material. Parylene[2], SBR[1], Kapton[27] and Apiezon[20] have been successfully used by other researchers for coating various *in-situ* sensing elements. However, they were less desirable in this instance due to the requirement of the additional strain relief housing, availability of materials and increased manufacturing costs.

To overcome the reduced flexibility and high element failure risk, an outer skin of Hytrel™ Furcation Tubing, was applied to the tail end of the fibres. Figure 43 (a) shows the complete instrument design for the FBG sensor and Figure 45 (b) presents the complete instrumented cell setup.

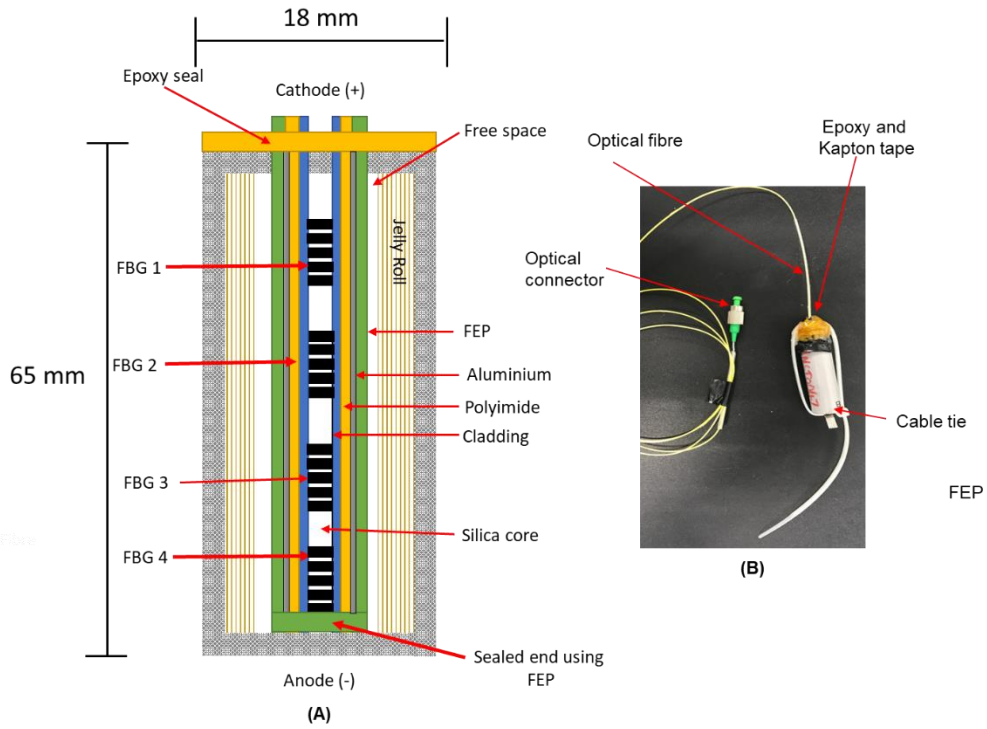

Figure 43 - (A) assembly detail for instrumented cell and (B) complete system

Furthermore, any conformal coating upon the fibre would affect the thermal sensitivity of the element and strain effects upon the fibre from thermal expansion of the coating, possibly causing false temperature readings. Additionally, after sensor fabrication and embedding within the cell, any mechanical deformation imposed during the process will affect the response of the element. Therefore, a single point calibration was necessary. This was achieved using a thermal chamber and a high accuracy platinum resistance temperature detector (RTD) PT100 (*Pico®*) with a UKAS accredit test certificate. In the long term, mechanical drift arising from abuse conditions such as vibration and shock could cause the Bragg wavelength to shift from the ambient temperature wavelength. As such, occasional recalibrations are advised for measurement certainty over a long period of time.

8.2.2 Cell modification procedure

In terms of mechanical placement several issues arise; Safety mechanisms on the positive side of the cell disallow for such embedding of a sensor therefore the negative side is the next possible choice. However, this has several challenges of how to remove the terminal cap end without damaging the jelly roll and causing short circuits from the external can. This approach is explored first as entering the positive terminal would require removing the in-built safety mechanisms

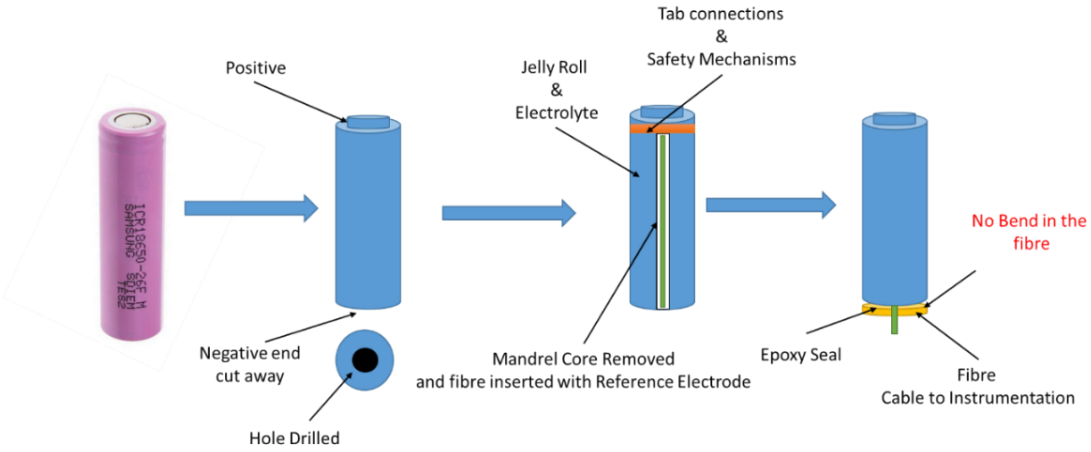

Figure 44 failed sensor insertion techniques using the negative entry side of the cell.

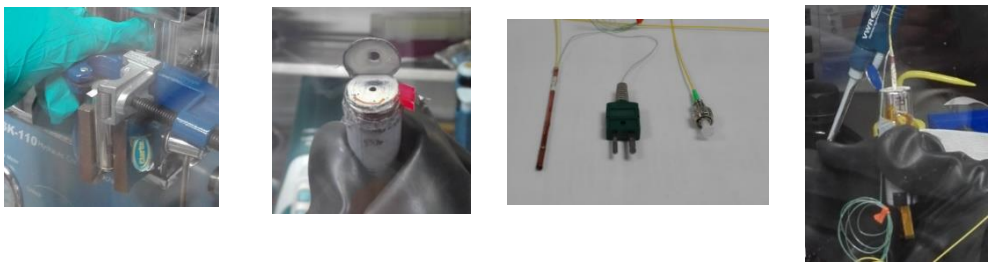

Figure 45 *In-situ* sensor consutrction. (A) Sensor removed using a pipe cutter (B) Cap and entry hole exposed (C) Two in one sensor construction (d) complete instrumented cell

The cell was discharged to the minimum voltage of 2.5 V as stated on the manufacturer's specification sheet before being transferred into an argon glove box, $LiPF_6$-based electrolyte solutions are used within this study. However, traces of water and moisture can react with the decomposition components of electrolyte and small amounts of hydrofluoric acid can arise[27], therefore the glove box was necessary to

minimise this possibility by enabling atmospheric O_2 and H_2O concentrations of <1 ppm.

The optical sensor assembly was prepared in advance and fed through a pre-drilled cell cathode cap for easier assembly. A non-conductive pipe cutter was used to remove the cathode cap, after which the internal cathode current collector was slung over the side of the cell can.

The FBG sensor assembly was then carefully fed into the core, the attached cathode cap held in place using Kapton tape around the rim and an external application of a fast-setting epoxy resin, ensuring gas-tightness. Modifying the cell to the degree described here would not be necessary in an industrial application as a custom design could be implemented

8.2.3 System testing and validation

Lastly, it is important to consider that optical sensors may indeed appear to work during first calibration. displays how the *in-situ* elements failed and produced a temperature variation of 3°C at the end of the temperature cycling. This error was concluded to be that the sensor failed due to poor manufacturing procedures. It must be noted however that the electrochemical response of the sensor remains stable throughout the entire procedure, further re-enforcing the fact that the modifying procedure has little effect upon performance.

Furthermore, Figure 46 shows the reliability of a failed sensor, the data clearly indicates that the sensor response range is out of calibraiton completely. This again was attributed to damage during manufacturing of the instrumentation. It was concluded that strain was been imposed onto the fibre from the epoxy used. To verify the problem the sensor was cycled through a high and low temperature range to deduce that the effect was perminant and none-recoverable.

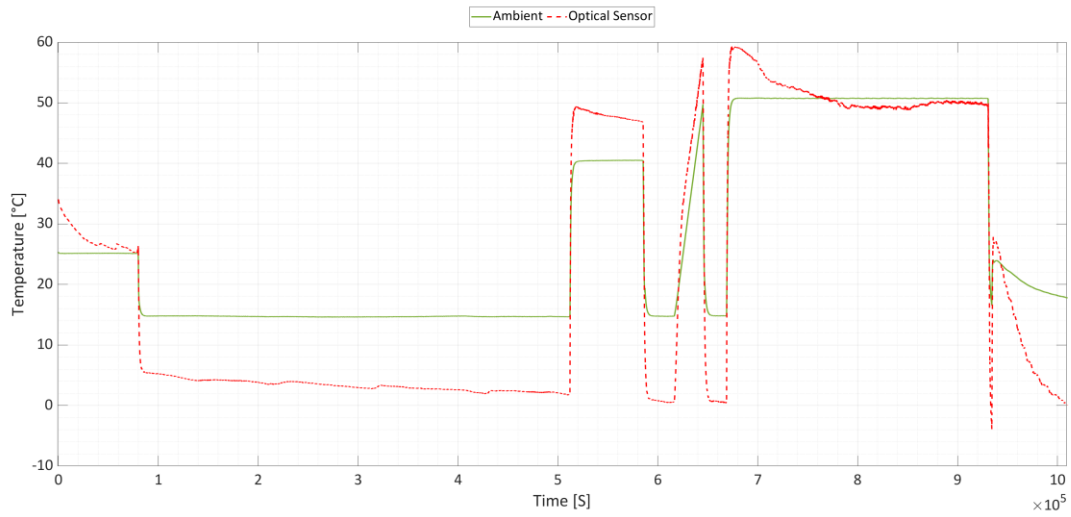

Figure 46 Illustration of the failed FBG sensor calibration at various temperatures

The correct response of the FBG sensor assembly is shown below in Figure 47 and long-term cycling aging in Figure 48

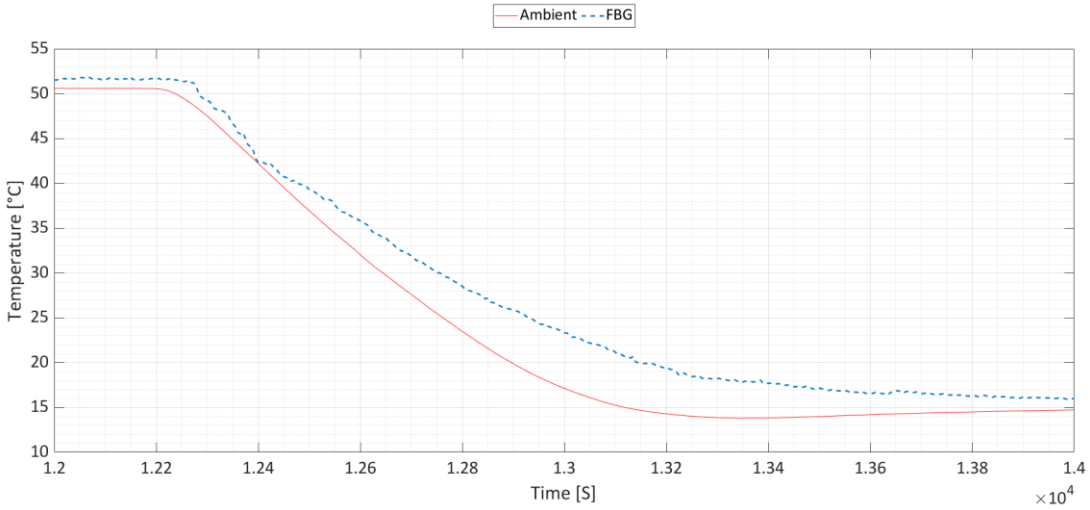

Figure 47 Illustration of the FBG two-point calibration and long-term stability of the instrument

The response of the sensor over a sustained period is shown below in Figure 48. The data presented clearly displays that the electrochemical system and sensor remain stable. Furthermore, unlike previous experimental work as shown in the sensor does not encounter drift over time. The drift effect means the sensor reading has not offset from the original calibrated state, a detailed view of the data presented in Figure 48

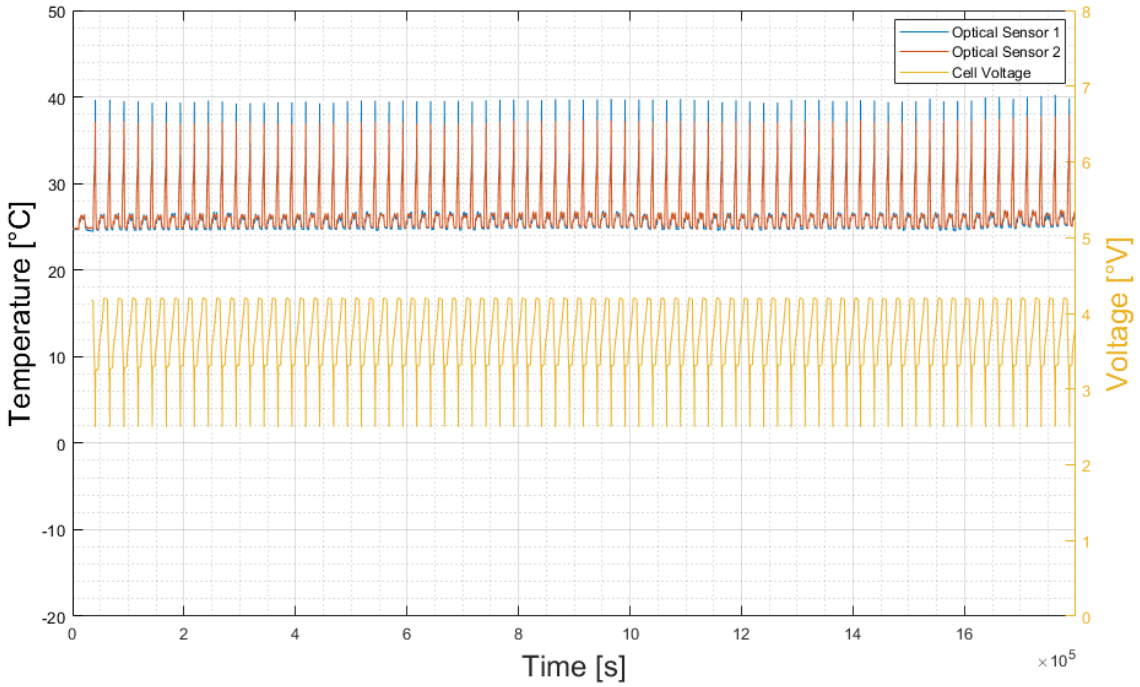

Figure 48 100 Cycle extract for a stable sensor construction of an 18650 cell

The results of adding extra protection to the raw sensor to cope with the conditions with the battery have led to a significant decrease in operating temperature. However, this is not of concern as the maximum temperature required would be limited to less than 60°C. Lastly, the sensitivity of the device has also decreased by 0.2pm/°C, this can be accounted for using the correct calibration techniques.

Table 13 Modified FBG assembly specification

Modified FBG specification	
Centre wavelength (nm)	1528 - 1608
Operating range (°C)	-270 to 250
Temperature sensitivity (pm/°C)	11.2
Temperature resolution (°C)	0.05
FBG length (mm)	1
FBG quantity	4

8.2.4 Time domain analysis

The response of the internal and external sensor data during a CC/CV charge and CC discharge cycling is shown in Figure 49 (a). Additionally, one peak charge and discharge period is extracted from the cycling procedure for temperature analysis, shown in Figure 50 and Figure 51 respectively. It can be seen that the recorded optical sensors wave shift response is closely related to the charge/discharge phase of the battery. This validates that the elements are responding with no visible lag and providing accurate thermal data.

The data presented indicates a clear and significant temperature difference between the core and can of the cell of up to 5 °C during discharge and 3 °C during charge, thus underlining that the surface measurements do not reflect the real temperature of a cell. Temperature spikes observed during the cell cycling are correlated to the constant current/constant voltage charge phase. The high temperature rise can be explained by the internal resistance increasing as the cell reaches maximum charge [124], thus generating more heat under constant load. The high temperature rise can be explained by the internal resistance increasing as the cell reaches maximum charge, thus generating more heat under constant load. The high temperature rises and asymmetric behaviour of the charge and discharge phase can be explained with the internal resistance increasing as the cell reaches minimum charge. This effect is due to the ionic mobility. As the cells reaches maximum charge the ionic resistance increases due to the limited holes available in the positive electrode. Thus, adding to the total internal resistance therefore, generating significant ohmic heating under constant load compared with a charge cycle where the internal resistance is low and thus generates less heat. Finally, previous work[18,25] has not measured axial temperature differences within the cell core, with this work clearly displaying temperature gradients depending on the cell cycling phase.

It was discovered that, during charge, the core closer to the positive end of the cylindrical cell presented higher temperatures, while the opposite was observed during discharge - a clear 1 °C temperature gradient was observed. Anode *vs.* cathode temperature disparity can be caused by differences in heat generation,

observation of which is possible due to the anisotropic heat conduction inside the cell and the preferential heat conduction path being the current collector, resulting in local heat zones. Differences in the heat generated on the electrodes during charge/discharge can be correlated to the electrode reactions and the subsequent entropy changes, quantifiable by the per-electrode voltage differences, however it is not the topic of this research and is a subject of future work.

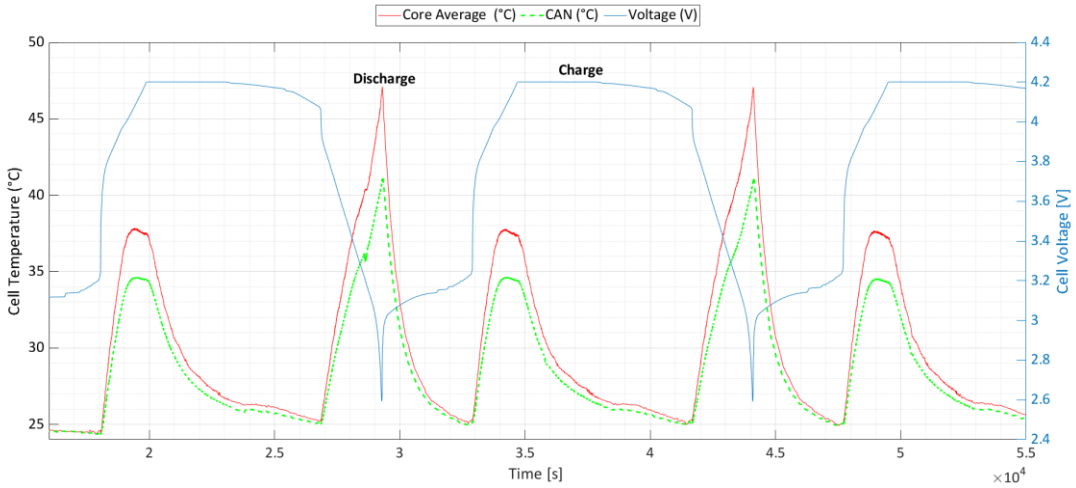

Figure 49 Average core temperature, can and drive voltage

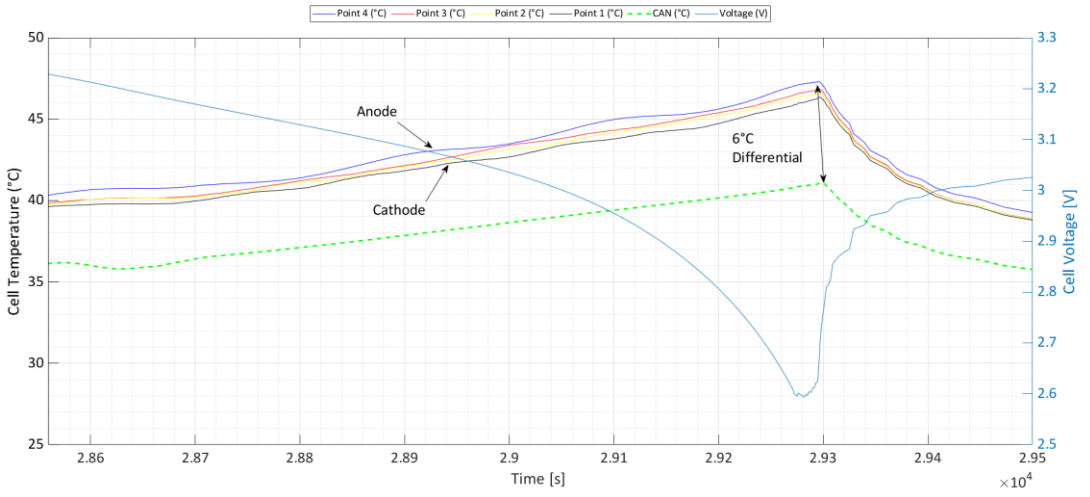

Figure 50 Thermal discharge characteristics extract from Figure 49

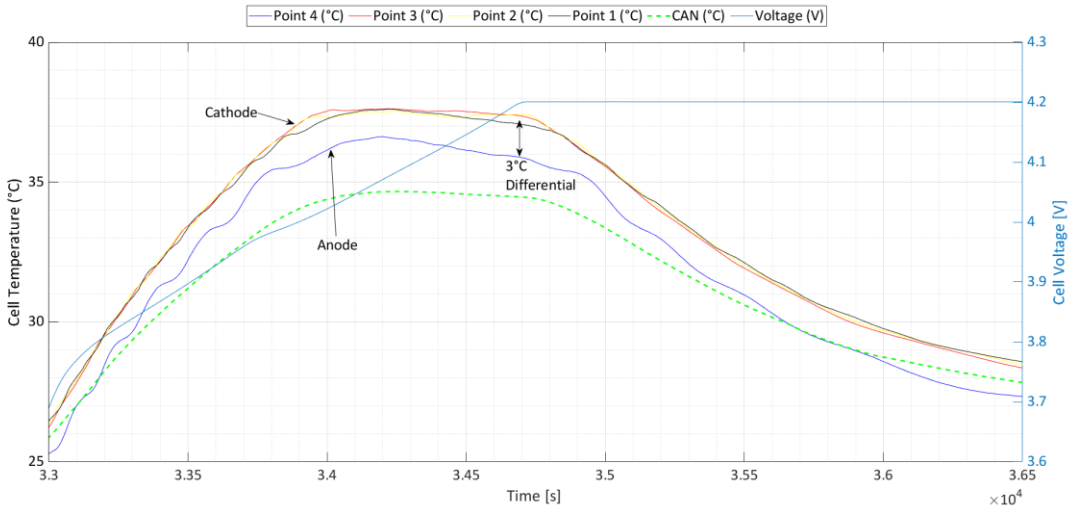

Figure 51 Thermal charging characteristic extract from Figure 49

Lastly, Figure 52 illustrates the location of the optical fibre within the cylindrical cell alongside a comparison of all the *in-situ* thermal data.

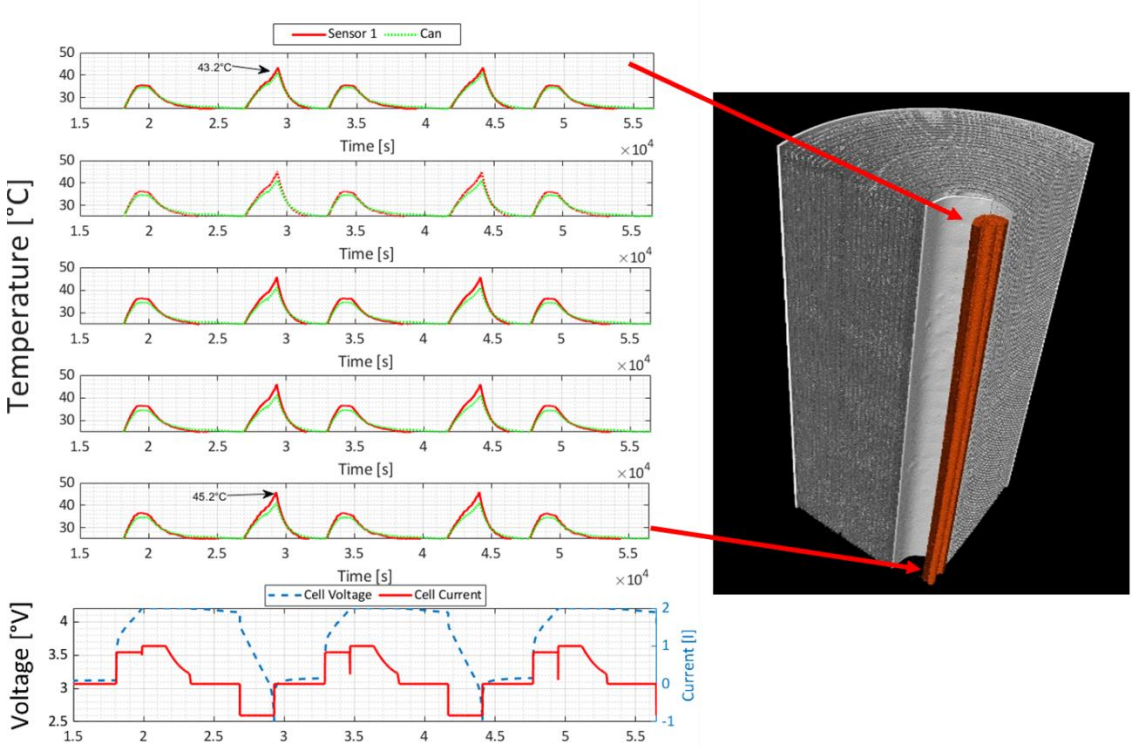

Figure 52 Illustration of the disturbed *in-situ* thermal data of 18650 cell

The capacity comparison of a cell before and after modification is shown in Figure 53. The evaluated cells were cycled at a rate of 1C. The data recorded shows a complete match between the cell discharge profile before and after modification. This suggests that any loss of electrolyte or cell material damage incurred during cell modification is negligible and has no observable effect on the electrochemical system in the short term. However, due to the cells being constructed by a third-party manufacturer, a true understanding of capacity fade and pre-cycling procedures can be difficult to quantify, as the exact cell chemistry, batch tolerance and manufacturing errors are unknown. Therefore, in our future work, cylindrical cells will be built from raw materials in an in-house production line with sensors embedded during production.

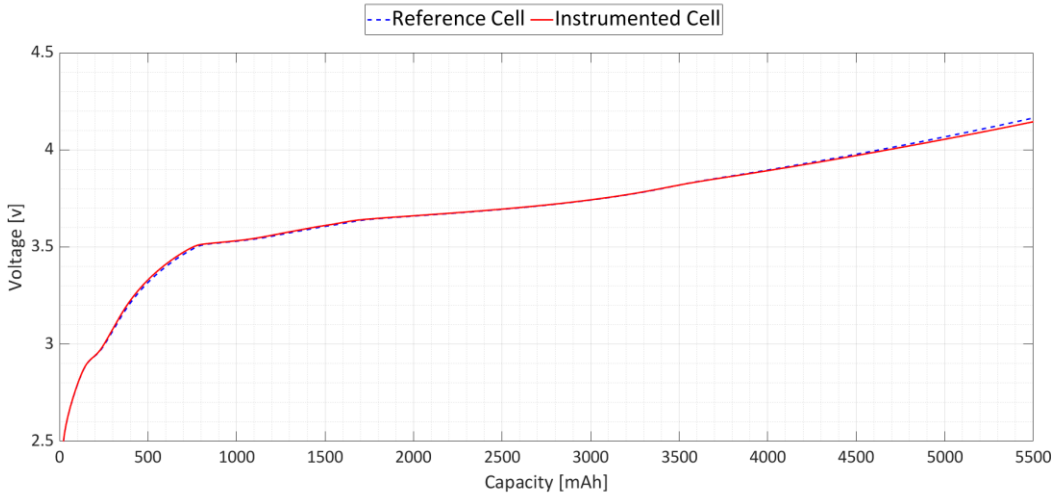

Figure 53 Discharge capacity comparison of an instrumented vs virgin pouch cell

8.2.5 Frequency domain analysis

Loss of electrolyte, cell damage and other parasitic effects encountered during the modification procedure may not appear in time domain analysis conducted in the previous section. Therefore, three cells were evaluated using EIS at 100% and 0% SoC before and after modification as shown in Figure 55. For modified cells, the now-exposed current collector had to be connected to the potentiostat using crocodile-clips instead of bulky but more consistent brass or copper blocks. The sensitive nature of Electrochemical Impedance Spectroscopy (EIS) measurements means that even minimal electromagnetic interference can cause data to be misleading. Therefore, the series resistance element of the Nyquist plot was zeroed to obtain characteristic features that are present in the data. This enabled us to focus the analysis on the internal cell changes.

Experimental data generated is presented in . A clear shift in the diffusion element of the EIS spectrum can be seen for 100% SoC, which is absent from the 0% SoC scan. This phenomenon can be explained by the possible pressure relief enabled during cell modification, as the pressure building up during cell formation cycles is never released in case of cylindrical cells manufacture procedures. This results in less overpressure experienced in fully charged state, slightly improving the cell performance. Such a difference would not be noticed during normal cell usage but is visible using methods of high precision such as EIS.

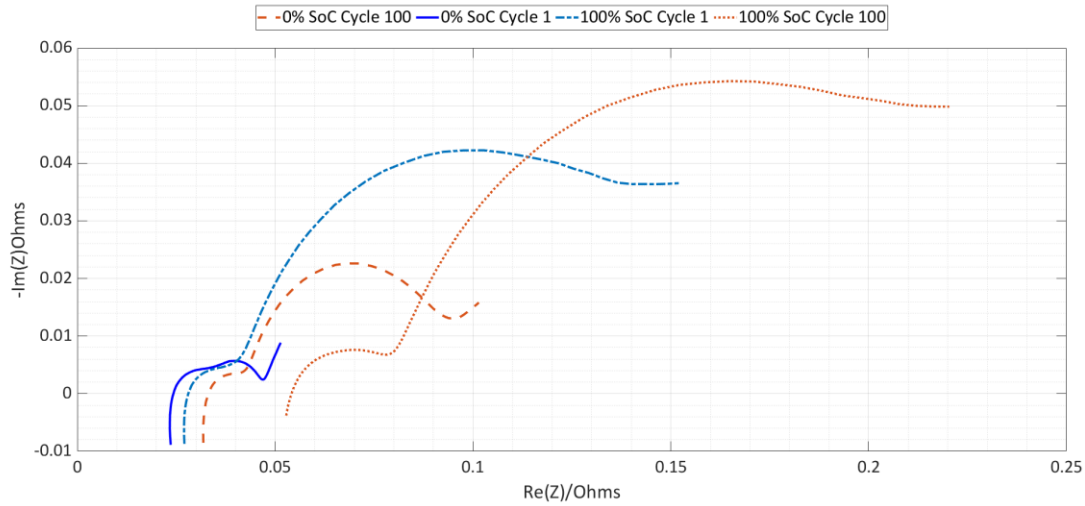

Figure 54 Illustration of Electrochemical Impedance Spectroscopy (EIS) at 100% and 0% SoC for pristine cells and modified cells at 1 and 100 cycles

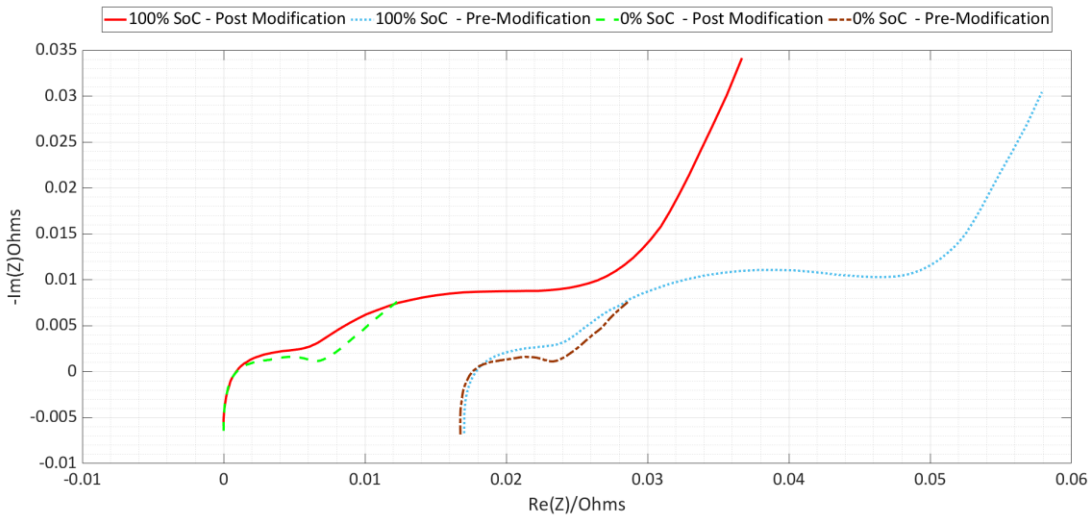

Figure 55 Illustration of Electrochemical Impedance Spectroscopy (EIS) at 100% and 0% SoC for pristine cells and modified cells

8.2.6 *In-situ* inspection

In order to assess possible failure of the epoxy sealing method and subsequent loss of the electrolyte solution, the 18650 cells were weighed directly after the modification procedure and later after cycling. No difference in mass was recorded over the period of time taken for cell cycling and evaluation. This proves that the epoxy resin applied is an effective solution for sealing the modified cells, preventing exposure to air or electrolyte leaks.

The exact position of the fibre sensor within the cell core and the element's construction was evaluated using X-ray Computed Tomography (X-TEK XTH 320 LC, *Metris*), the results of which are shown in Figure 56. As can be seen in Figure 4(D), the optical fibre is in near contact with the jelly roll, providing good thermal contact yet leaving considerable room available within the core. The scans also shows that certain fibre sections are likely to become in contact with the metallic tubing, leading to a strain effect imposed upon the fibre due to the thermal expansion of the surrounding material in case of higher temperature scenarios. However the presence of an air gap between the tubing and the fibre minimises this possibility.

When applied to a number of cylindrical cells or various models, the external sensor tubing may become in contact with and impose pressure on the jelly roll material, due to the variability of the cell core diameters and possible cell manufacturing inconsistencies. This could have a direct impact upon the cell performance, causing local impedances increase where the sensor has a physical connection with the active battery materials.

Therefore, cell geometry and space constraints must be considered before sensor application, and small adjustments might be required depending on the specific cell design. Alternative studies have measured radial [25] and axial [18] temperatures using multiple temperature sensors, adding complexity, potential failure points and considerable modification time, in which extended exposure of the cell active materials may result in cell degradation. The novel solution presented here provides distributed and high-accuracy insight into the temperature profile properties of cylindrical lithium-ion cells using a single-fibre solution, having a near negligible

impact upon the cell performance whilst providing highly relevant and complementary thermal data.

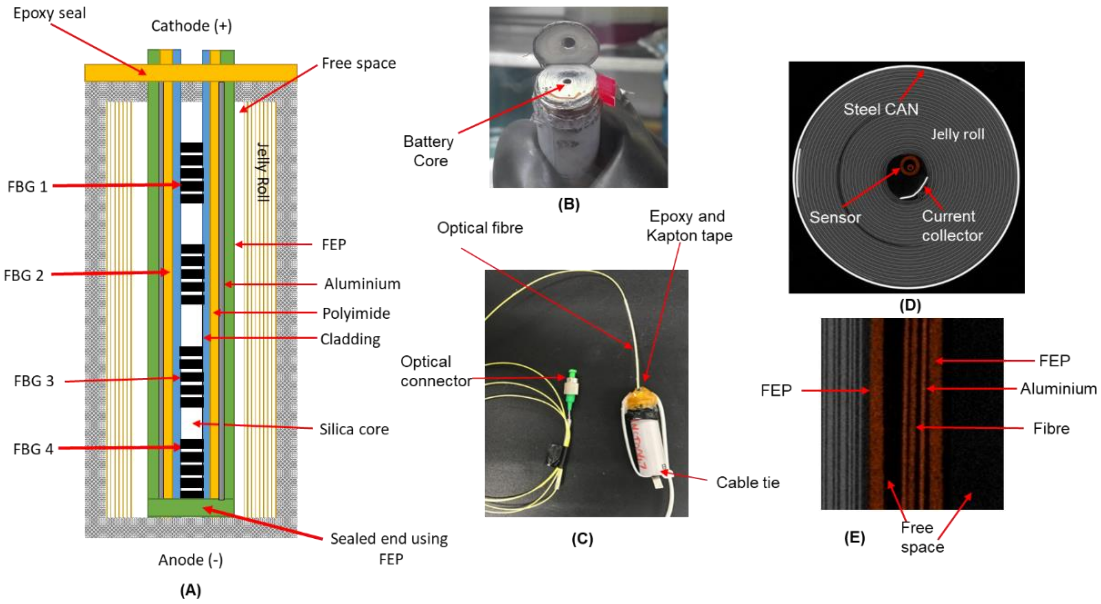

Figure 56 CT Scan of a modified cell - (A) instrumented cell assembly (B) top view of cell and entry hole (C) complete instrumented cell (D) top view XCT image and (E) *In-situ* view of optical sensor

8.3 Chapter conclusions

This work shows the development of a promising temperature sensor for *in-situ, in-operando* monitoring of live Lithium-ion cells. Utilising modified optical fibre sensors has been proven to be the optimal solution for Lithium-ion cells instrumentation due to their low profile and high resilience to the internal cell environment. The cell instrumentation method used also allows for easy sensor recovery and subsequent reuse, while being proven to have negligible impact on the cell's performance. A significant temperature difference was identified between the cell's core and can temperatures of up to 6 °C during discharge and 3 °C during charge phase. Therefore, underlining the necessity of real internal cell temperature measurements for thermal management and safety validation.

The observed axial temperature gradient can be a vital source of information about local overheating zones and anode/cathode temperature differences, supporting materials and electrochemical research. The knowledge gained from the instrumentation developed here can be used to significantly improve and support the design and prototyping of cells and battery modules for optimum charging profiles and greater safety and offers highly reliable validation for thermodynamic models and State of Health prediction mechanisms.

9 Thermo-electrochemical instrumentation of cylindrical cells

9.1 Introduction

This chapter describes the experimental work and results undertaken for thermo-electrochemical instrumentation of cylindrical cells'. The development, validation and testing of the instrumentation is described. Followed by the validation of the instrumented electrochemical system. The cells evaluated for *in-situ* sensors applications were commercial 3Ah high-energy cells consisting of a lithium nickel cobalt aluminium oxide (NCA) cathode, graphite anode and a $LiPF_6$ electrolyte solution.

9.2 Research and development

9.2.1 Sensor design and validation

For the design of a two in one electro-thermal sensor, several iterations were developed, with each one having various issues and problems. Which are described here after.

9.2.1.1 2-in-1 thermo-electrochemical optical sensor

Method 1: Lumped element sensor

In the first instance a copper tube was used to replace the mandrel core and allow for a vertical entry hole into the battery system for the optical sensor. A Polytetrafluoroethylene (PTFE) and a Fluorinated ethylene propylene (FEP) dual heat shrink was used to protect the fibres from electrolyte and add mechanical strength for manufacturing. The mechanical strength was important due to the reduced dexterity when manufacturing the instrumented cells in a glove box environment. Lastly, for chemical compatibility the PTFE and FEP was placed in electrolyte for seven days at room temperature, no issue was found.

The copper tube was plated using electroplating in a vial of electrolyte solution. Copper tube was the working electrode (WE), lithium metal was the counter electrode (CE) providing lithium ions. Lithium metal was then plated galvanostatically with a current density of 10 mA cm^{-2} for 30 minutes. The coated tube was then rinsed in DMC and vacuum dried**.**

However, once the copper tube had been constructed and plated with lithium the diameter of the copper increased. The increased diameter of the copper rod was found to work on some 18650 cells, however the core diameter varied between cell manufactures. Consequently, reducing the dimeter to 2mm and inner bore hole to 1.6mm solved the issue. However, the solution was now mechanically too small for the PTFE/FEP protection to fit inside the copper rod. To try and solve this issue a potting compound for the sensing elements was tested. The compound of choice must have a low viscosity, to fully encapsulate the fibre and flow to the bottom of

the copper tube. Lastly a low linear thermal expansion coefficient, as the stress imposed onto the sensing area would falsify the temperature data measurements.

Opti-tec 5001 epoxy from Adhere was selected as a suitable choice. The solution was mixed and injected into the copper tube and left to cure for 3 days. A reference thermocouple was also placed as validation for the optical sensing. A diagram of the complete sensor is shown below in Figure 57.

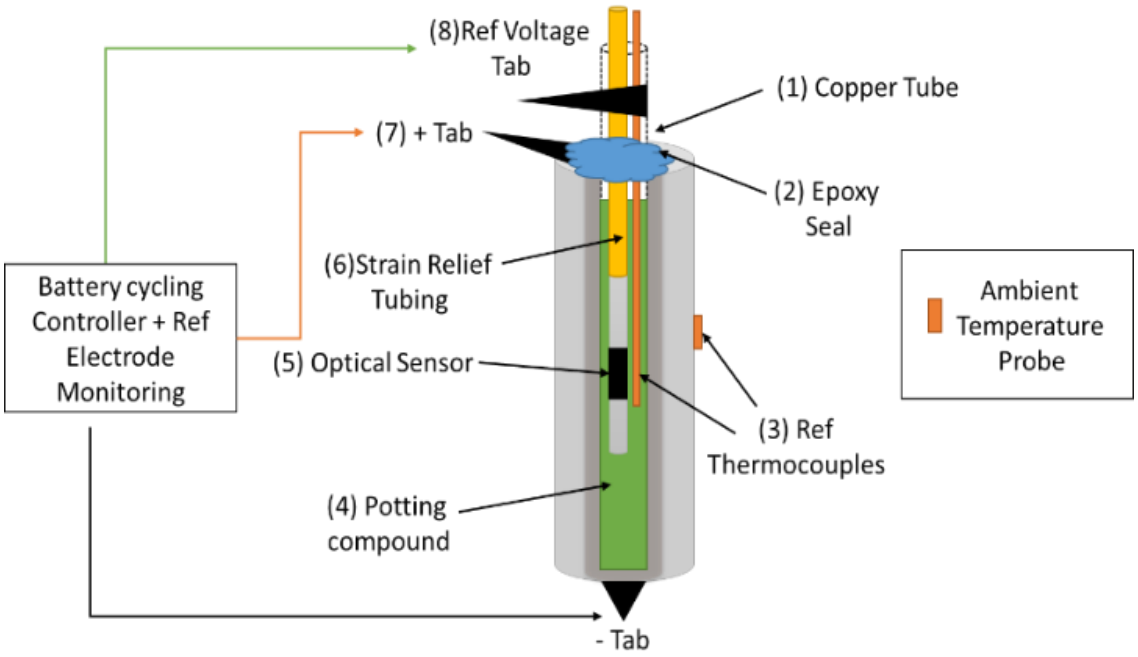

Figure 57 Failed experimental setup of a 2-in-1 thermo-electrochemical sensor, using a potting compound to form a complete mass

The potting compound linear thermal expansion during the initial testing showed to affect the response of the sensor. This is due to the temperature rise from the heat generated within the cell. Figure 58 shows the response of the failed sensor, it is clearly shown that the response is not what was expected concluding the potting compound indeed imposed a strain effect on the sensor.

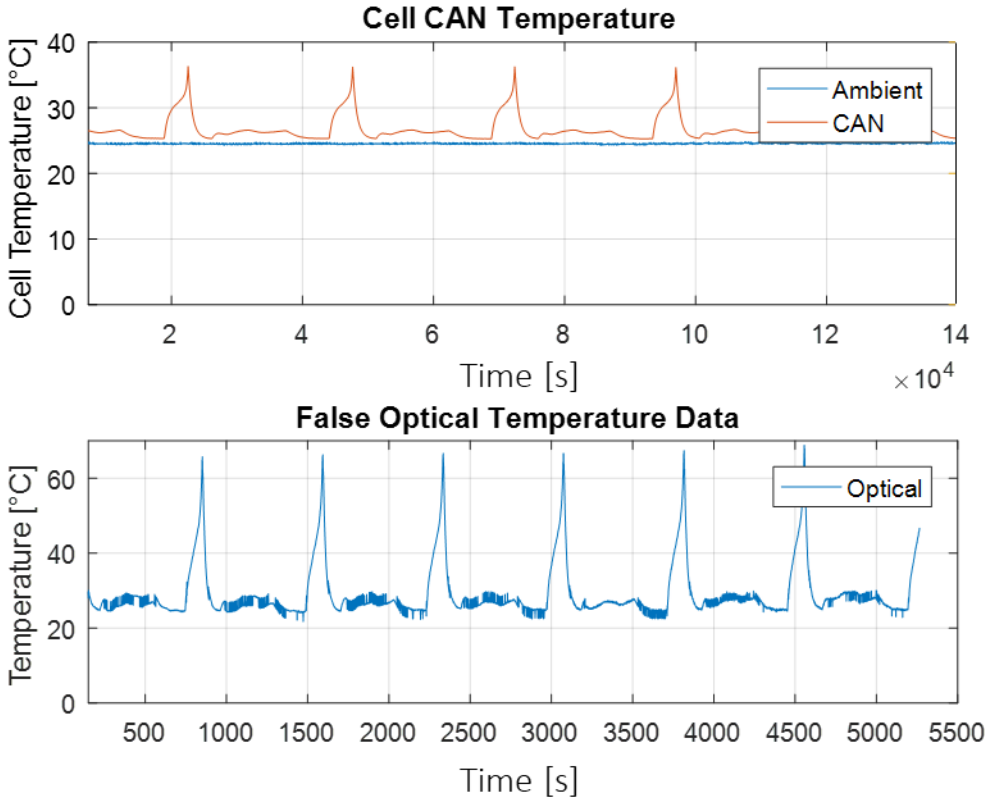

Figure 58 Illustration of a failed optical sensor assembly, clearly indicating a measurement cross sensitivity on the fibre

One solution to the cross sensitivity would be to calibrate out the stress applied by using the thermocouple as the reference but this would be unrealistic in a commercial scale setup a proposed solution would be to pass the FBG area through a steel tube attach each end using an epoxy, this would limit the strain applied during temperature rises in cycling.

Method 2: Rigid optical sensor

A further solution was required to measure only temperature within the copper tube. A hybrid sensor based on the above two instrumentation procedures was developed. This consisted of an FBG optical sensor, inserted into a 2mm diameter Li-electroplated copper tube. The internal cathode current collector was slung over the side of the cell can and the cathode cap was no longer used as a terminal. The section of copper tube that touched the cathode can upon exiting the cell was insulated with Polytetrafluoroethylene tape, leaving the protruding end of copper bare so that it

may be connected to the reference sense cable on the potentiostat. The new sensor concept is shown in Figure 59.

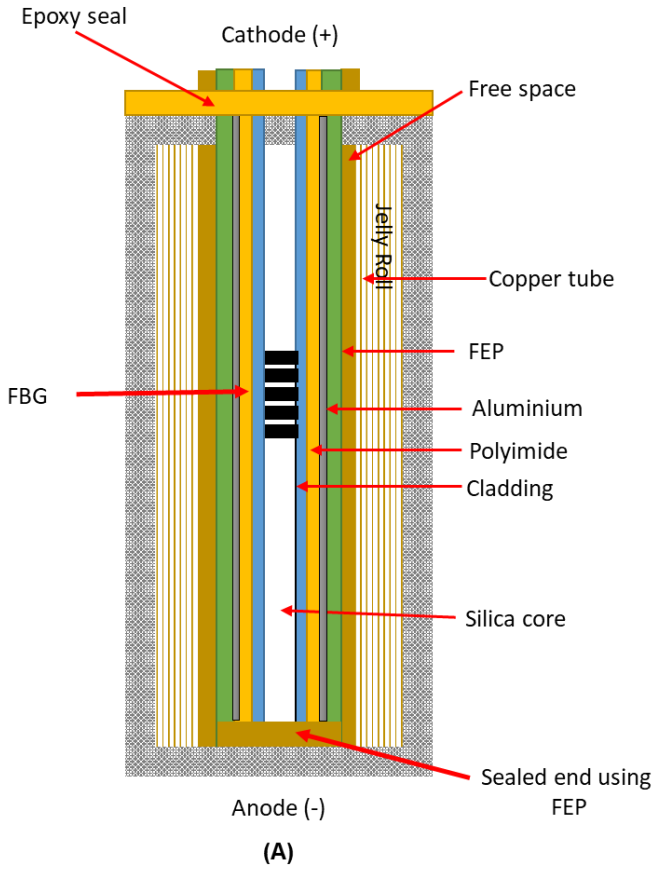

Figure 59 A two in one thermo-electrochemical sensor for smart cells'[107]

The new approach as was tested and validated using a reference thermocouple and an resistance temperature detector to calibrate both sensors prior to insertion. the response is clearly in-line with the response of the thermocouple and no strain effect has been imposed from the surrounding materials. Meaning the sensor is responding with accurate thermal measurements.

9.2.1.2 Single electrochemical sensor

Method 1: Lithium-plated copper wire reference electrode

For validation copper wire with a diameter 1mm was coated with lithium. This was then embedded into the cell as described previously in section 9.2.1.1.

Method 2: Platinum wire reference electrode

A platinum electrode was also used as a reference due to the high stability of the metal[125], thus minimising the risk of oxidation. The wire was wrapped in a separator material before insertion, which was held in place using Kapton tape. The cell was then sealed using epoxy and Kapton with the sensor exiting the unit.

The platinum reference electrode was used as in important reference for the reliability and repeatability of the lithium-ion reference electrode methodology.

Method 3: Lithium tongue reference electrode

A single piece of lithium was inserted into the cell with a copper connector attached to the material. The sensor assembly was then wrapped in Kapton to add mechanical strength to the joint and protect the sensor from short circuiting on the enclosure of the battery. Furthermore, a small section was wrapped in separator material, therefore ensuring electrochemical connectivity to the cell.

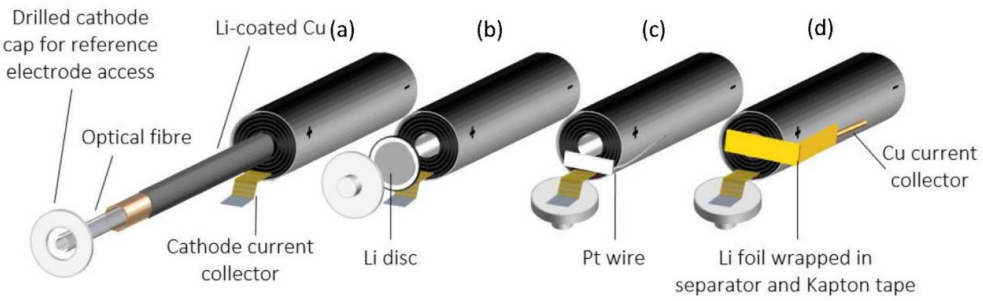

Figure 60 Illustration of the instrumentation methods used within this study[107]

9.2.2 Time domain analysis

Several iterations of reference electrode design were presented but with varying degree of success were achieved. The 2-in-1 thermo-electrochemical sensor was the first instrument to be considered in this study.

The response of the 2-in-1 optical *in-situ* assembly with a reference type-k thermocouple embedded alongside is presented in Figure 61. It is clearly shown the response of the thermocouple is in good agreement with the optical assembly. Concluding that the build procedure and modification techniques applied to the fibre are reliable and stable. Lastly, the modifications procedure upon the electrochemical system were previously validated in chapter 6,7 and 8.

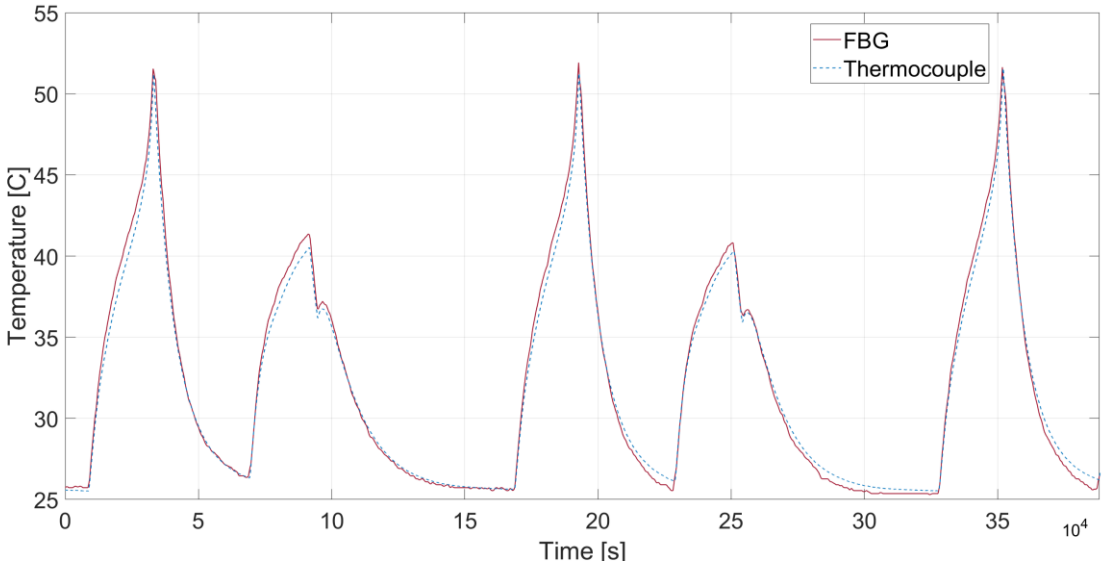

Figure 61 *In-situ* sensor validation of the two in one sensor using a reference thermocouple[107]

As can be seen in Figure 62 (a) the core and can temperature incur a differential of up to 5°C during cycling from 0% - 100% SoC. Furthermore, subsequently charging the call at 1.5C to a cell terminal potential of 4.2V, the rate chosen was specifically five times higher than stated by the manufactures. The data clearly presents the need for accurate *in-situ* instrumentation for thermal characterisation. The data can be used for decreased charge times and push safety limits past current standards, where

skin surface sensors alone would fail to identify before possible catastrophic failure occurred.

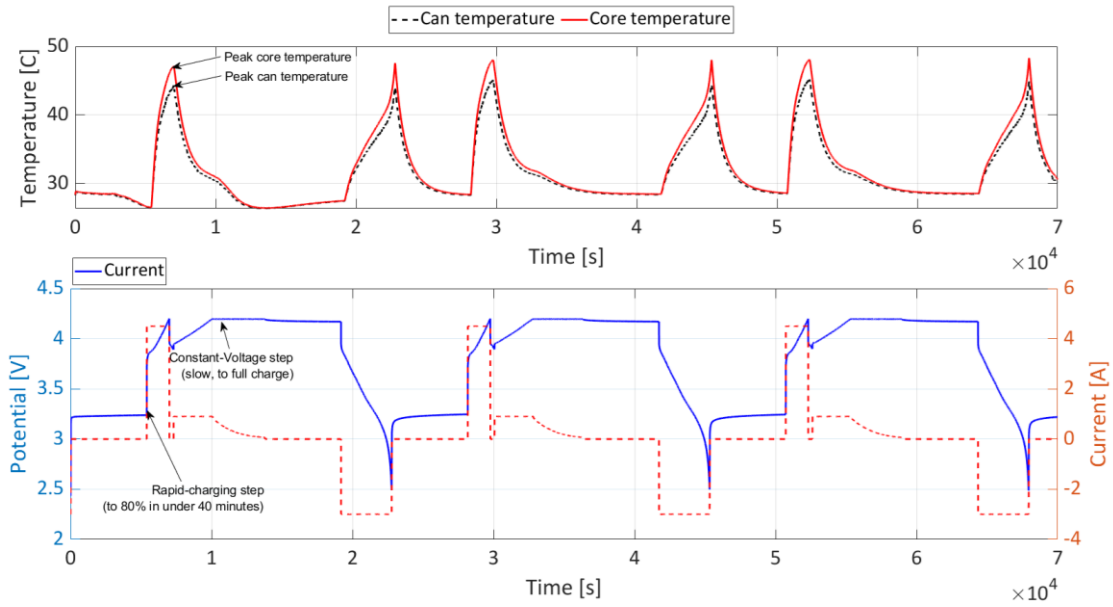

Figure 62 Rapid charging protocol and *in-situ* thermal response of an instrumented 18650 cell[107]

The amount of electrolyte within the commercial cell is limited and is soaked into the cell materials. The voltage potentials shown in Figure 63 a clear drift after cycling. This was found to be the sensor had poor ionic connectivity with the anode. Therefore, a new solution was explored, using a lithium-disc solution.

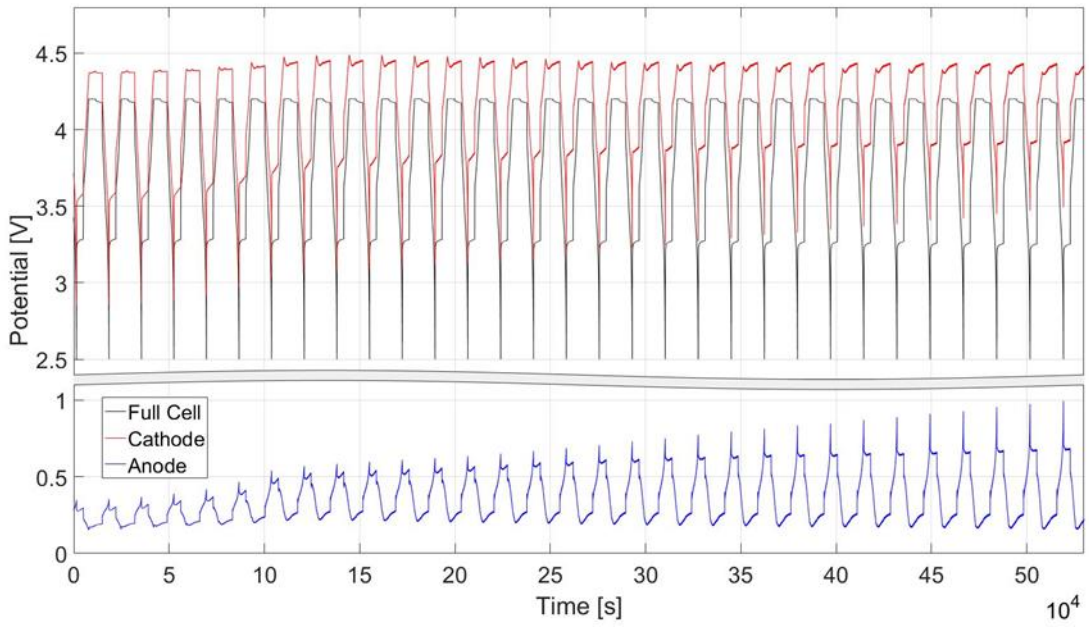

Figure 63 A failed 2-in-1 thermo-electrical sensor[107]

The construction of the sensor, specifically the usage of the PTFE material to hold the separator material into place failed. This was found to be the case after several post mortem tear-downs of the cell and sensor within a glovebox. The sensor separator material had become degraded, indicating that electrolyte exposure was causing damage. The adhesive material was changed to Kapton, a readily available material and used often within cell assemblies - replacing the Polytetrafluoroethylene fixing. However, drift still occurred, and it was concluded that electrolyte was penetrating the cap of the cell, which is currently acting as its own reference terminal after being disconnected from the cell.

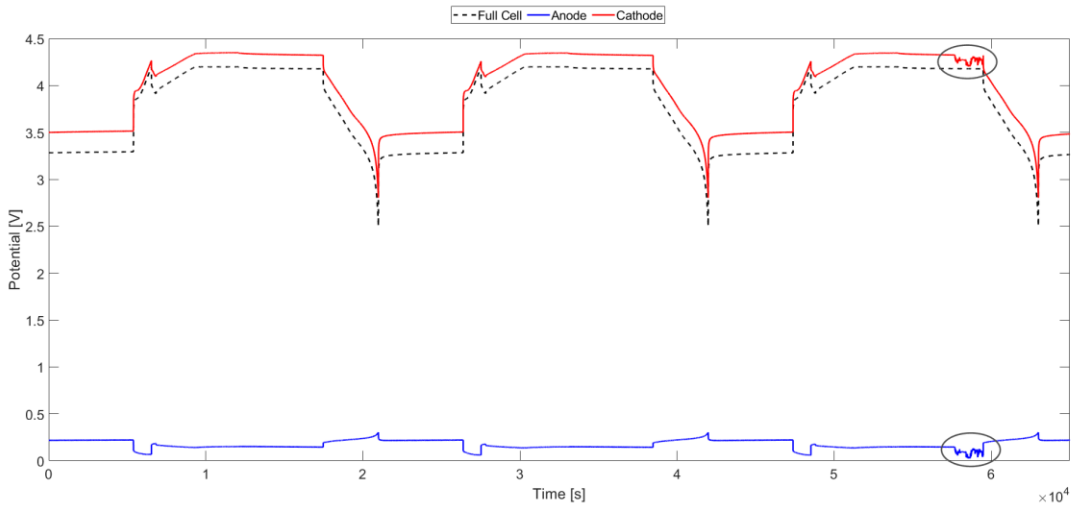

Figure 64 Illustration of the cell potentials of failed a lithium-disc reference electrode embedded into a cylindrical cell[107]

The anode, cathode and electrode potentials of a cell using a platinum wire is illustrated in Figure 65. After cycling for some time, a clear drift in the anode potential becomes apparent, despite the high stability of platinum metal. Some drift would be expected if the cell was fresh from the manufacturing facility, but this was not the case as previous studies have shown for pouch cell formations[62].

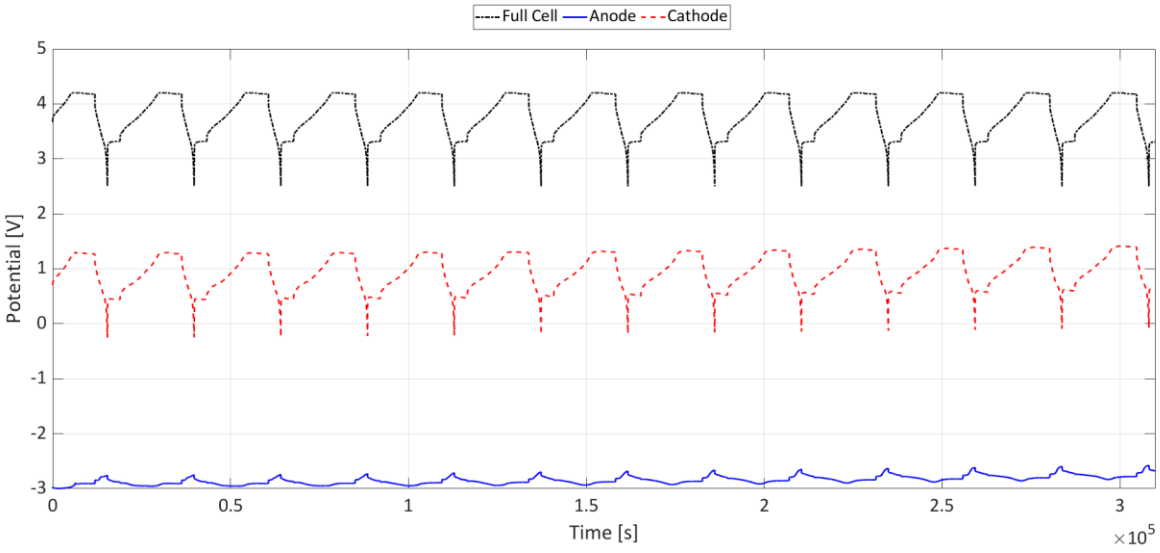

Figure 65 Illustration of a Platinum wire reference electrode drift failure over-time[107]

The previous sensor failures, a solution that only used lithium as the element exposed within the cell minimised the possibility of cross contamination, short circuits and electrolyte interference. Furthermore, adding a spacer within the top cap of the battery increased the certainty that the reference electrode had ionic contact with the cell. Figure 66 shows the response of a stable potential of the anode, cathode and reference, which clearly shows no noise, drift or unexpected result.

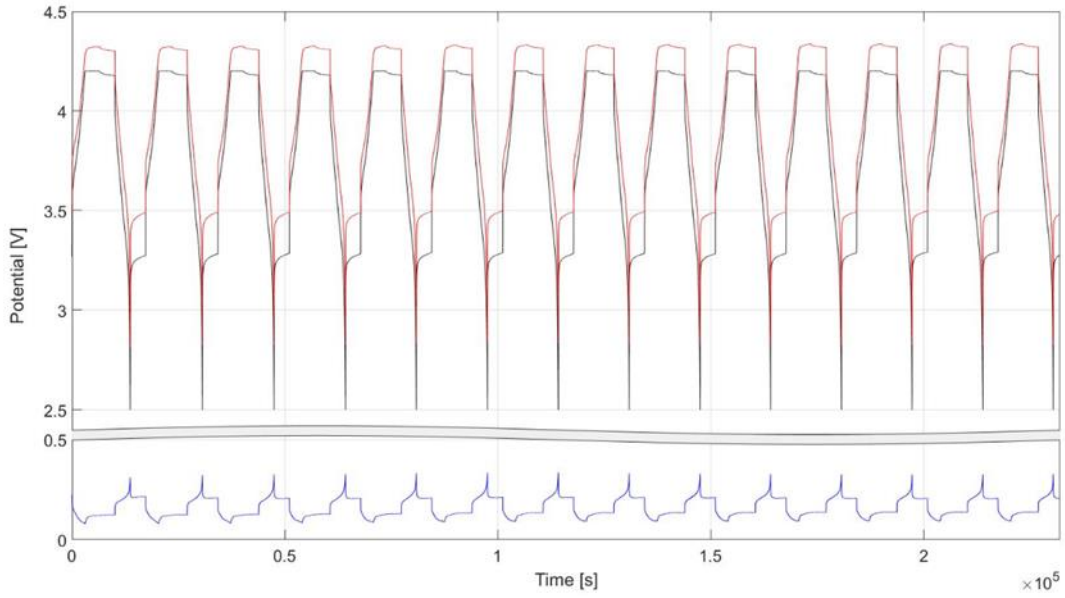

Figure 66 Illustration of stable reference electrode potentials using a lithium tongue instrumentation[107]

Loss of electrolyte, cell damage and other parasitic effects encountered during the modification procedure may not appear in time domain analysis conducted in the previous section. Therefore, three cells were evaluated using electrochemical impedance spectroscopy before and after modification.

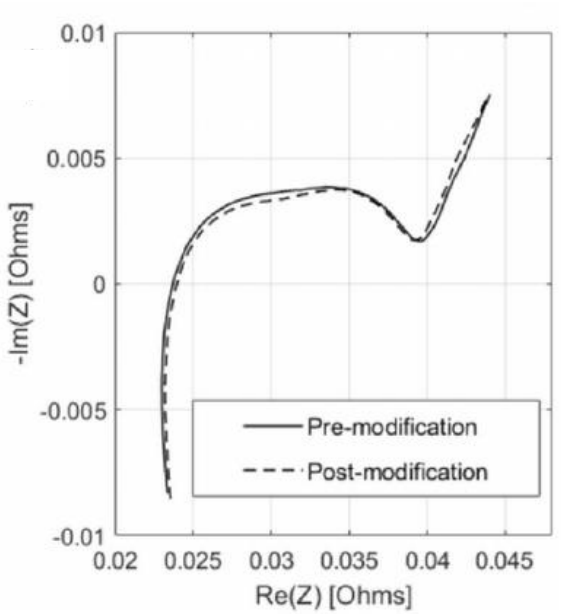

Figure 67 Impedance response of a modified versus virgin cell assembly[107]

9.3 Chapter conclusions

This work shows the development of a promising 2-in-1 temperature and electrode potential sensor for *in-situ, in-operando* monitoring of live Lithium-ion cells. Utilising modified optical fibre sensors alongside lithium metal reference has been proven to be an optimal solution for Lithium-ion cells instrumentation. Due to their low profile and high resilience to the internal cell environment.

Previous research conducted for instrumented cells have focused on the development of sensor single sensor elements However, little attention has been devoted to multi-purpose sensing elements and the impact of cyclic behaviour and post-mortem analysis, which remains undocumented in literature. Consequently, given the lack of critical attention, this work has presented unprecedent experimental data concerning the characteristic behaviour of a cell using multiple sensor topologies.

The cell instrumentation method used also allows for easy sensor recovery and subsequent reuse, while being proven to have negligible impact on the cell's performance. The data presented clearly highlights the safety and operational requirements can be pushed further post manufactures recommended limits. The impact upon the cells performance has also been shown to be negligible, with over several cycles conducted, versus unmodified cells. This was validated using time and frequency domain analysis.

10 Thesis conclusions

In-situ sensors developed here enable accurate monitoring paramount for the cells' safe operation and optimised performance, key for the battery management system to maintain an up-to-date understanding of the cells State of Health during deployment in real-life scenarios. Several in-depth characterisation studies were used to validate the sensors implementation - X-ray imaging was used to assess locations of the sensors and negligible mechanical impact upon the system. Electrochemical impedance spectroscopy and standard cycling over a sustained period was used to assess the cell's electrochemical performance and was concluded to be on-par with unmodified cells. A full cell tear-down and sensor inspection followed, proving the sensors resistance to the cell's harsh chemical environment which allows for long-term monitoring without the sensors degradation.

A lack of sound engineering and academic output regarding instrumentation of Lithium-ion cells is limited in literature. Consequently, this work has significantly improved the manufacturing knowledge to construct a reliable cell. And guarantees the long-term reliability of *in-situ* sensors for pouch and cylindrical formations. Furthermore, previous research efforts have modified commercial units, this work addressed a deeper understanding of the industrial process required for manufacturing a smart cell within a production facility. Where consistency between the control units and modified units are maintained though out all experimental data.

The sensing technique developed enable unprecedented high-precision *in-situ* and operando thermal monitoring of pouch and cylindrical format Lithium-ion cells. High-fidelity thermal responses from inside the cell were successfully monitored under various cycling conditions, while the sensor topology and the system modifications were proven to be durable and of no noticeable effect on the cells performance. The sensors successfully detected rapid temperature changes with no response lag – more importantly demonstrating a significant divergence between the core and skin cell temperatures, which leads to a false sense of security under the current skin-only sensor arrays commonly deployed in automotive batteries.

Data collected shows that, with the help of appropriate *in-situ* measurement tools certain cells can be further optimised without compromising thermal safety limits, while under scenarios safety limits are breached earlier than the external sensors would indicate. Consequently, the instrumentation technique evaluated and developed in this study enables insight into the cell's thermodynamic behaviour that can be used to significantly improve the cells performance and safety, health prediction and early failure detection.

Utilising modified optical fibre sensors has been proven to be a real solution for Lithium-ion cells instrumentation, due to their low profile and high resilience to the internal cell environment. The cell instrumentation method used also allows for easy sensor recovery and subsequent reuse, while being proven to have negligible impact on the cell's performance. A significant temperature difference was identified between the cell's core and can temperatures of up to 6 °C during discharge and 3 °C during charge phase. Therefore, underlining the necessity of real internal cell temperature measurements for thermal management and safety validation.

The thermal data gathered from these *in-situ* sensors represents a vital source of information about the cells actual thermodynamic responses, supporting materials, cells and battery module level research. This work can also support the design and rapid prototyping of new cells and battery modules, enabling considerably greater performance to be harnessed from these energy storage systems.

Lastly, the sensing methodologies and modification techniques developed in this work can be applied to all range of cells from small bespoke systems that are used within mobiles phones up to large scale battery modules and packs for electric vehicles and off-grid storage. The data collection enabled by these *in-situ* and operando sensors is invaluable for energy storage systems life-time prediction, performance fine-tuning and safety monitoring.

11 Further work

The use of conductive inks and printed sensors has had a rapid boom in recent years due to the demand for cheap diagnostic instrumentation, the internet of things revolution and the high availability of low cost manufacturing methods[126]. Many sensor types (can be fabricated using printed technology) such as but not limited to humidity, chemical[65], biosensors, capacitive, and temperature[127].

A number of these sensing elements can be combined onto a single substrate allowing an array of multiple sensing platform. There are several benefits to using printed technology such as the ability to have distributed sensing elements, low cost production and manufacturing onto plastic films, metals or polymers.[126,128]

The work presented within this thesis for electronic based sensors focused on using pre-manufactured thermistors, which are readily available in mass production volumes. The development of low-profile temperature sensors that could be manufactured to be embedded within the jelly roll of an 18650 would provide an invaluable insight of *in-situ* characteristics.

The ability to print onto the PP/PE/PP battery separator substrate of a battery could provide detailed information however no literature is present at the time of this publication regarding the stability and integration issues with the technology. The separator layer would the first choice as this can be rolled through out the battery stack providing a single substrate distributed throughout the battery.

Lastly, Optical fibres can be modified to sense a multitude of phenomena including chemical, stress, temperature and pressure. This gives rise to the possibility of monitoring multitude of inputs using a single optical fibre within a battery system, however, significant challenges exist with this approach.

12 Reference list

1. Bae, C.-J., Manandhar, A., Kiesel, P. & Raghavan, A. Monitoring the Strain Evolution of Lithium-Ion Battery Electrodes using an Optical Fiber Bragg Grating Sensor. *Energy Technol.* **831**, 1 – 6 (2016).

2. Martiny, N. *et al.* Development of a thin-film thermocouple matrix for in-situ temperature measurement in a lithium ion pouch cell. in *IEEE Sensors Journal* **14**, 3377–3384 (2014).

3. Saw, L. H. *et al.* Computational fluid dynamic and thermal analysis of Lithium-ion battery pack with air cooling. *Appl. Energy* **177**, 783–792 (2016).

4. Mikolajczak, C., Kahn, M., Kevin White & Long, R. T. Lithium-Ion Batteries Hazard and Use Assessment. *Analysis* 112 (2011). doi:10.1007/978-1-4614-3486-3

5. Balakrishnan, P. G., Ramesh, R. & Prem Kumar, T. Review: Safety mechanisms in lithium-ion batteries. *J. Power Sources* **155**, 401–414 (2006).

6. Shu, J. *et al.* Comparative study on surface behaviors of copper current collector in electrolyte for lithium-ion batteries. *Electrochim. Acta* **56**, 3006–3014 (2011).

7. Zhang, X., Winget, B., Doeff, M., Evans, J. W. & Devine, T. M. Corrosion of Aluminum Current Collectors in Lithium-Ion Batteries with Electrolytes Containing LiPF6. *J. Electrochem. Soc.* **152**, B448 (2006).

8. Huggins, R. A. *Advanced batteries: Materials science aspects*. *Advanced Batteries: Materials Science Aspects* (2009). doi:10.1007/978-0-387-76424-5

9. Spinner, N. S. *et al.* Novel 18650 lithium-ion battery surrogate cell design with anisotropic thermophysical properties for studying failure events. *J. Power Sources* **312**, 1–11 (2016).

10. Osswald, P. J. *et al.* Temperature dependency of state of charge

inhomogeneities and their equalization in cylindrical lithium-ion cells. *J. Power Sources* **329**, 546–552 (2016).

11. Wang, P. *et al.* Real-time monitoring of internal temperature evolution of the lithium-ion coin cell battery during the charge and discharge process. *Extrem. Mech. Lett.* **9**, 459–466 (2016).

12. Bohn, P., Liebig, G., Komsiyska, L. & Wittstock, G. Temperature propagation in prismatic lithium-ion-cells after short term thermal stress. *J. Power Sources* **313**, 30–36 (2016).

13. Panchal, S., Dincer, I., Agelin-Chaab, M., Fraser, R. & Fowler, M. Thermal modeling and validation of temperature distributions in a prismatic lithium-ion battery at different discharge rates and varying boundary conditions. *Appl. Therm. Eng.* **96**, 190–199 (2016).

14. Panchal, S., Dincer, I., Agelin-Chaab, M., Fraser, R. & Fowler, M. Experimental and theoretical investigation of temperature distributions in a prismatic lithium-ion battery. *Int. J. Therm. Sci.* **99**, 204–212 (2016).

15. Lee, C. Y. *et al.* Flexible micro sensor for in-situ monitoring temperature and voltage of coin cells. *Sensors Actuators, A Phys.* **232**, 214–222 (2015).

16. Yildiz, M., Karakoc, H. & Dincer, I. Thermal Modeling and Validation of Temperature Change in a Pouch Lithium-ion Battery at Various Discharge Rates. *Int. Commun. Heat Mass Transf.* 1–14 (2015). doi:10.1016/j.icheatmasstransfer.2016.03.009

17. Schwarz, R., Semmler, K., Wenger, M., Lorentz, V. R. H. & März, M. Sensorless Battery Cell Temperature Estimation Circuit for Enhanced Safety in Battery Systems. in *Ieee Iecon* (2015). doi:10.1109/IECON.2015.7392319

18. Waldmann, T. & Wohlfahrt-Mehrens, M. In-Operando Measurement of Temperature Gradients in Cylindrical Lithium-Ion Cells during High-Current Discharge. *ECS Electrochem. Lett.* **4**, A1–A3 (2015).

19. Spinner, N. S. *et al.* Physical and chemical analysis of lithium-ion battery cell-

to-cell failure events inside custom fire chamber. *J. Power Sources* **279**, 713–721 (2015).

20. Osswald, P. J., Erhard, S. V, Wilhelm, J., Hoster, H. E. & Jossen, A. Simulation and Measurement of Local Potentials of Modified Commercial Cylindrical Cells: I. Cell Preparation and Measurements. *J. Electrochem. Soc.* **162**, A2099–A2105 (2015).

21. Guo, Z., Xia, Q., Yan, P. & Du, Z. Study on critical ambient temperature of cylindrical battery. *J. Therm. Anal. Calorim.* **119**, 2141–2149 (2015).

22. Waldmann, T. *et al.* Influence of Cell Design on Temperatures and Temperature Gradients in Lithium-Ion Cells: An In Operando Study. *J. Electrochem. Soc.* **162**, A921–A927 (2015).

23. Lee, C. Y. *et al.* A flexible three-in-one microsensor for real-time monitoring of internal temperature, voltage and current of lithium batteries. *Sensors (Switzerland)* **15**, 11485–11498 (2015).

24. Zhang, G. *et al.* Reaction temperature sensing (RTS)-based control for Li-ion battery safety. *Sci. Rep.* **5**, 18237 (2015).

25. Zhang, G. *et al.* In Situ Measurement of Radial Temperature Distributions in Cylindrical Li-Ion Cells. *J. Electrochem. Soc.* **161**, A1499–A1507 (2014).

26. Kim, Y., Mohan, S., Siegel, J. B., Stefanopoulou, A. G. & Ding, Y. The estimation of temperature distribution in cylindrical battery cells under unknown cooling conditions. *IEEE Trans. Control Syst. Technol.* **22**, 2277–2286 (2014).

27. Martiny, N. *et al.* Development of an all kapton-based thin-film thermocouple matrix for in situ temperature measurement in a lithium ion pouch cell. *IEEE Sens. J.* **14**, 3377–3384 (2014).

28. Tippmann, S., Walper, D., Balboa, L., Spier, B. & Bessler, W. G. Low-temperature charging of lithium-ion cells part I: Electrochemical modeling and experimental investigation of degradation behavior. *J. Power Sources* **252**, 305–316 (2014).

29. Hatchard, T. D., Trussler, S. & Dahn, J. R. Building a 'smart nail' for penetration tests on Li-ion cells. *J. Power Sources* **247**, 821–823 (2014).

30. Veth, C., Dragicevic, D. & Merten, C. Thermal characterizations of a large-format lithium ion cell focused on high current discharges. *J. Power Sources* **267**, 760–769 (2014).

31. Mutyala, M. S. K. *et al.* In-situ temperature measurement in lithium ion battery by transferable flexible thin film thermocouples. *J. Power Sources* **260**, 43–49 (2014).

32. Li, Z. *et al.* Examining temporal and spatial variations of internal temperature in large-format laminated battery with embedded thermocouples. *J. Power Sources* **241**, 536–553 (2013).

33. Lin, X. *et al.* Online parameterization of lumped thermal dynamics in cylindrical lithium ion batteries for core temperature estimation and health monitoring. *IEEE Trans. Control Syst. Technol.* **21**, 1745–1755 (2013).

34. Schmidt, J. P. *et al.* Measurement of the internal cell temperature via impedance: Evaluation and application of a new method. *J. Power Sources* **243**, 110–117 (2013).

35. Lee, C. Y. *et al.* In-situ monitoring of temperature and voltage in lithium-ion battery by embedded flexible micro temperature and voltage sensor. *Int. J. Electrochem. Sci.* **8**, 2968–2976 (2013).

36. Sahraei, E., Campbell, J. & Wierzbicki, T. Modeling and short circuit detection of 18650 Li-ion cells under mechanical abuse conditions. *J. Power Sources* **220**, 360–372 (2012).

37. Srinivasan, R., Carkhuff, B. G., Butler, M. H. & Baisden, A. C. Instantaneous measurement of the internal temperature in lithium-ion rechargeable cells. *Electrochim. Acta* **56**, 6198–6204 (2011).

38. Lee, C. Y., Lee, S. J., Tang, M. S. & Chen, P. C. In situ monitoring of temperature inside lithium-ion batteries by flexible micro temperature sensors. *Sensors* **11**,

9942–9950 (2011).

39. Forgez, C., Vinh Do, D., Friedrich, G., Morcrette, M. & Delacourt, C. Thermal modeling of a cylindrical LiFePO4/graphite lithium-ion battery. *J. Power Sources* **195**, 2961–2968 (2010).

40. Zeng, Y., Wu, K., Wang, D., Wang, Z. & Chen, L. Overcharge investigation of lithium-ion polymer batteries. *J. Power Sources* **160**, 1302–1307 (2006).

41. Nakayama, M., Fukuda, K., Araki, T. & Onda, K. Thermal behavior of nickel metal hydride battery during rapid charge and discharge cycles. *Electr. Eng. Japan (English Transl. Denki Gakkai Ronbunshi)* **157**, 30–39 (2006).

42. Leising, R. A., Palazzo, M. J., Takeuchi, E. S. & Takeuchi, K. J. A study of the overcharge reaction of lithium-ion batteries. *J. Power Sources* **97**–**98**, 681–683 (2001).

43. Leising, R. a., Palazzo, M. J., Takeuchi, E. S. & Takeuchi, K. J. Abuse Testing of Lithium-Ion Batteries: Characterization of the Overcharge Reaction of LiCoO[sub 2]/Graphite Cells. *J. Electrochem. Soc.* **148**, A838 (2001).

44. Fellner, J. P., Loeber, G. J. & Sandhu, S. S. Testing of lithium-ion 18650 cells and characterizing/predicting cell performance. *J. Power Sources* **81**–**82**, 867–871 (1999).

45. Wang, Q. *et al.* Thermal runaway caused fire and explosion of lithium ion battery. *Journal of Power Sources* **208**, 210–224 (2012).

46. Bloom, I. *et al.* Mechanisms of impedance rise in high-power, lithium-ion cells. *J. Power Sources* **111**, 152–159 (2002).

47. Wang, Q., Jiang, B., Li, B. & Yan, Y. A critical review of thermal management models and solutions of lithium-ion batteries for the development of pure electric vehicles. *Renew. Sustain. Energy Rev.* **64**, 106–128 (2016).

48. Huat, S. L., Yonghuang, Y. & Tay, A. A. O. Integration issues of Lithium-ion battery into electric vehicles battery pack. *J. Clean. Prod.* **113**, 1032–1045 (2015).

49. Lu, Z. *et al.* Thermal Management of Densely-packed EV Battery with Forced Air Cooling Strategies. *Energy Procedia* **88**, 682–688 (2016).

50. Schwartz, J. *et al.* Embedded Fiber Optic Sensors for In Situ and In-Operando Monitoring of Advanced Batteries. *MRS Online Proc. Libr. Arch.* **1740**, null-null (2015).

51. Ahmed, S. *et al.* Enabling fast charging – A battery technology gap assessment. *J. Power Sources* **367**, 250–262 (2017).

52. Gao, Y. *et al.* Lithium-ion battery aging mechanisms and life model under different charging stresses. *J. Power Sources* **356**, 103–114 (2017).

53. Chu, Z. *et al.* Non-destructive fast charging algorithm of lithium-ion batteries based on the control-oriented electrochemical model. *Appl. Energy* **204**, 1240–1250 (2017).

54. Keil, P. & Jossen, A. Charging protocols for lithium-ion batteries and their impact on cycle life-An experimental study with different 18650 high-power cells. *J. Energy Storage* **6**, 125–141 (2016).

55. Anseán, D. *et al.* Fast charging technique for high power lithium iron phosphate batteries: A cycle life analysis. *J. Power Sources* **239**, 9–15 (2013).

56. Shen, W., Vo, T. T. & Kapoor, A. Charging algorithms of lithium-ion batteries: An overview. *Proc. 2012 7th IEEE Conf. Ind. Electron. Appl. ICIEA 2012* 1567–1572 (2012). doi:10.1109/ICIEA.2012.6360973

57. Stockinger, R. DEMYSTIFYING RTD AND THERMISTOR DIFFERENCES. *Process Cool. Equipment.* p11-13. 3p. (2012).

58. Li, W. *et al.* Flexible parylene packaged intraocular coil for retinal prostheses. *Proc. 2006 Int. Conf. Microtechnologies Med. Biol.* 105–108 (2006). doi:10.1109/MMB.2006.251502

59. Oiler, J., Shock, E., Hartnett, H. & Yu, H. MEMS harsh environment sensor array-enabled hot spring mapping. *Proc. IEEE Sensors* 1–4 (2013). doi:10.1109/ICSENS.2013.6688332

60. Koydemir, H. C., Külah, H. & Özgen, C. Solvent compatibility of parylene c film Layer. *J. Microelectromechanical Syst.* **23**, 298–307 (2014).

61. Raijmakers, L. H. J., Lammers, M. J. G. & Notten, P. H. L. A new method to compensate impedance artefacts for Li-ion batteries with integrated micro-reference electrodes. *Electrochim. Acta* **259**, 517–533 (2018).

62. McTurk, E., Birkl, C. R., Roberts, M. R., Howey, D. A. & Bruce, P. G. Minimally Invasive Insertion of Reference Electrodes into Commercial Lithium-Ion Pouch Cells. *ECS Electrochem. Lett.* **4**, A145–A147 (2015).

63. Belt, J. R., Bernardi, D. M. & Utgikar, V. Development and Use of a Lithium-Metal Reference Electrode in Aging Studies of Lithium-Ion Batteries. *J. Electrochem. Soc.* **161**, A1116–A1126 (2014).

64. La Mantia, F., Wessells, C. D., Deshazer, H. D. & Cui, Y. Reliable reference electrodes for lithium-ion batteries. *Electrochem. commun.* **31**, 141–144 (2013).

65. Atkinson, J. K. *et al.* Thick film screen printed environmental and chemical sensor array reference electrodes suitable for subterranean and subaqueous deployments. *Microelectron. Int.* **30**, 92–98 (2013).

66. Lengsfeld, C. S. & Shoureshi, R. A. LITHIUM RECHARGEABLE CELL WITH REFERENCE ELECTRODE FOR STATE OF HEALTH MONITORING. **1**, (2008).

67. Zhou, J. & Notten, P. H. L. Studies on the degradation of Li-ion batteries by the use of microreference electrodes. *J. Power Sources* **177**, 553–560 (2008).

68. Song, J. Y., Lee, H. H., Wang, Y. Y. & Wan, C. C. Two- and three-electrode impedance spectroscopy of lithium-ion batteries. *J. Power Sources* **111**, 255–267 (2002).

69. Wu, Q., Lu, W. & Prakash, J. Characterization of a commercial size cylindrical Li-ion cell with a reference electrode. *J. Power Sources* **88**, 237–242 (2000).

70. Brecht, W. B. & Wertz, J. a. Reference electrode's use in the analysis of battery performance\nand operation. *Proc. 11th Annu. Batter. Conf. Appl. Adv.* 261–

266 (1996). doi:10.1109/BCAA.1996.485006

71. Fang, W., Kwon, O. J. & Wang, C. Y. Electrochemical-thermal modeling of automotive Li-ion batteries and experimental validation using a three-electrode cell. *Int. J. Energy Res.* **34**, 107–115 (2010).

72. Liu, P. *et al.* Aging Mechanisms of LiFePO[sub 4] Batteries Deduced by Electrochemical and Structural Analyses. *J. Electrochem. Soc.* **157**, A499 (2010).

73. Zhang, Y. & Wang, C.-Y. Cycle-Life Characterization of Automotive Lithium-Ion Batteries with LiNiO2 Cathode. *J. Electrochem. Soc.* **156**, A527–A535 (2009).

74. Nagasubramanian, G. & Doughty, D. H. 18650 Li-ion cells with reference electrode and in situ characterization of electrodes. *J. Power Sources* **150**, 182–186 (2005).

75. Nagasubramanian, G. Two- and three-electrode impedance studies on 18650 Li-ion cells. *J. Power Sources* **87**, 226–229 (2000).

76. Lex-Balducci, A., Henderson, W. & Stefaon, P. Electrolytes for lithium-ion batteries. in *Lithium-ion batteries: advanced materials and technologies* **10**, 149–196 (2012).

77. Reinfelder, A. Thermal In-Cell Measurement for Li-Ion Pouch Cells.

78. Zangl, H., Fuchs, A., Bretterklieber, T., Moser, M. & Holler, G. An investigation on wireless communication and power supply through metal tank walls. *Conf. Rec. - IEEE Instrum. Meas. Technol. Conf.* 1452–1457 (2008). doi:10.1109/IMTC.2008.4547271

79. Graham, D. J. Investigation of Methods for Data Communication and Power Delivery Through Metals. (2011).

80. Zangl, H., Fuchs, A., Bretterklieber, T., Moser, M. J. & Holler, G. Wireless communication and power supply strategy for sensor applications within closed metal walls. *IEEE Trans. Instrum. Meas.* **59**, 1686–1692 (2010).

81. Martiny, N., Hornungy, A., Josseny, A. & Schüßlerz, M. A capacitively coupled

data transmission system for resistance based sensor arrays for in-situ monitoring of lithium-ion battery cells. in **2014**-**Decem**, 535–538 (Institute of Electrical and Electronics Engineers Inc., 2014).

82. Martiny, N., Mühlbauer, T., Steinhorst, S., Lukasiewycz, M. & Jossen, A. Digital data transmission system with capacitive coupling for in-situ temperature sensing in lithium ion cells. *J. Energy Storage* **4**, 128–134 (2015).

83. Wenger, M. M., Filimon, R., Lorentz, V. R. H. & März, M. A robust contactless capacitive communication link for high power battery systems. *IEEE Int. Symp. Ind. Electron.* 1766–1772 (2014). doi:10.1109/ISIE.2014.6864882

84. Ouannes, I., Nickel, P. & Dostert, K. Cell-Wise Monitoring of Lithium-Ion Batteries for Automotive Traction Applications by Using Power Line Communication: Battery Modeling and Channel Characterization - Cell_Wise_Monitoring.pdf. 24–29 (2014).

85. Thelen, D., Martin, J., Allen, S. & SA, S. Battery with an internal microcontroller that draws different currents from the cells internal to the battery based on the temperature of the battery Pub . No .: US 2006 / 0222585 A1. **002**, 7 (2017).

86. Mihailov, S. J. Fiber bragg grating sensors for harsh environments. *Sensors* **12**, 1898–1918 (2012).

87. Dewra, S. & Grover, A. Fabrication and Applications of Fiber Bragg Grating- A Review. **25**, 15–25 (2015).

88. Wnuk, V. P., Méndez, A., Ferguson, S. & Graver, T. Process for Mounting and Packaging of Fiber Bragg Grating Strain Sensors for use in Harsh Environment Applications. *Smart Struct. Conf.* (2005). doi:10.1117/12.601971

89. Fortier, A., Tsao, M., Williard, N. D., Xing, Y. & Pecht, M. G. Preliminary study on integration of fiber optic bragg grating sensors in li-ion batteries and in situ strain and temperature monitoring of battery cells. *Energies* **10**, (2017).

90. Nascimento, M., Ferreira, M. S. & Pinto, J. L. Real time thermal monitoring of

lithium batteries with fiber sensors and thermocouples: A comparative study. *Meas. J. Int. Meas. Confed.* **111**, 260–263 (2017).

91. Raghavan, A. *et al.* Embedded fiber-optic sensing for accurate internal monitoring of cell state in advanced battery management systems part 1: Cell embedding method and performance. *J. Power Sources* 1–8 (2016). doi:10.1016/j.jpowsour.2016.11.104

92. Novais, S. *et al.* Internal and External Temperature Monitoring of a Li-Ion Battery with Fiber Bragg Grating Sensors. *Sensors* **16**, 1394 (2016).

93. Raghavan, A. *et al.* Embedded fiber-optic sensing for accurate internal monitoring of cell state in advanced battery management systems part 2: Internal cell signals and utility for state estimation. *J. Power Sources* 1–9 (2016). doi:10.1016/j.jpowsour.2016.11.104

94. Schwartz, J. *et al.* Embedded Fiber Optic Sensors for In Situ and In-Operando Monitoring of Advanced Batteries. *MRS Online Proc. Libr. Arch.* **1740**, null-null (2015).

95. Sommer, L. W. *et al.* Monitoring of intercalation stages in lithium-ion cells over charge-discharge cycles with fiber optic sensors. *J. Electrochem. Soc.* **162**, A2664–A2669 (2015).

96. Sommer, L. W. *et al.* Fast and slow ion diffusion processes in lithium ion pouch cells during cycling observed with fiber optic strain sensors. *J. Power Sources* **296**, 46–52 (2015).

97. Nascimento, M. *et al.* Lithium batteries temperature and strain fiber monitoring. in **9634**, 96347V-96347V–4 (2015).

98. Meyer, J., Nedjalkov, A., Doering, A., Angelmahr, M. & Schade, W. Fiber optical sensors for enhanced battery safety. in 94800Z (2015). doi:10.1117/12.2183325

99. Sommer, L. W. embedded fiber optic sensing for accurate state estimation in advanced battery management systems. *MRS Symp. Proc.* **1641**, 0–5 (2014).

100. Lochbaum, A. *et al.* Embedded Fiber Optic Chemical Sensing for Internal Cell Side-Reaction Monitoring in Advanced Battery Management Systems. in *MRS Proceedings* **1681**, (2014).

101. Yang, G., Leitão, C., Li, Y., Pinto, J. & Jiang, X. Real-time temperature measurement with fiber Bragg sensors in lithium batteries for safety usage. *Measurement* **46**, 3166–3172 (2013).

102. Bal, H. K., Ladouceur, F. & Brodzeli, Z. State of charge of battery indicator based on fibre optic probe. *35th Aust. Conf. Opt. Fibre Technol.* 1–3 (2010).

103. Zhu, Y. & Wang, A. Miniature fiber-optic pressure sensor. *IEEE Photonics Technol. Lett.* **17**, 447–449 (2005).

104. Fleming, J., Amietszajew, T., Dave, G. & Bhagat, R. Development and evaluation of in-situ instrumentation for cylindrical Li-ion cells using fibre optic sensors. *HardwareX* **3**, 100–109 (2018).

105. De Villiers, G. J., Treurnicht, J. & Dobson, R. T. In-core high temperature measurement using fiber-Bragg gratings for nuclear reactors. *Appl. Therm. Eng.* **38**, 143–150 (2012).

106. De Pauw, B. *et al.* Temperature monitoring using fibre optic sensors in a lead-bismuth eutectic cooled nuclear fuel assembly. *Nucl. Eng. Des.* **297**, 54–59 (2016).

107. McTurk, E., Amietszajew, T., Fleming, J. & Bhagat, R. Thermo-electrochemical instrumentation of cylindrical Li-ion cells. *J. Power Sources* **379**, 309–316 (2018).

108. Amietszajew, T., McTurk, E., Fleming, J. & Bhagat, R. Understanding the limits of rapid charging using instrumented commercial 18650 high-energy Li-ion cells. *Electrochim. Acta* **263**, 346–352 (2018).

109. Duff, M. & Towey, J. Two Ways to Measure Temperature using thermocouples feature simplicity, accuracy, and flexibility. *Analog Dialogue* **44**, 1–6 (2010).

110. Dubarry, M. *et al.* Identifying battery aging mechanisms in large format Li ion

cells. *J. Power Sources* **196**, 3420–3425 (2011).

111. Väyrynen, A. & Salminen, J. Lithium ion battery production. *J. Chem. Thermodyn.* **46**, 80–85 (2012).

112. Al-Thyabat, S., Nakamura, T., Shibata, E. & Iizuka, A. Adaptation of minerals processing operations for lithium-ion (LiBs) and nickel metal hydride (NiMH) batteries recycling: Critical review. *Miner. Eng.* **45**, 4–17 (2013).

113. da Silva Marques, R. *et al.* Corrosion Resistant FBG-Based Quasi-Distributed Sensor for Crude Oil Tank Dynamic Temperature Profile Monitoring. *Sensors (Basel).* **15**, 30693–703 (2015).

114. Dai, H., Jiang, B. & Wei, X. Impedance characterization and modeling of lithium-ion batteries considering the internal temperature gradient. *Energies* **11**, (2018).

115. Jiang, J. *et al.* Electrochemical Impedance Spectra for Lithium-ion Battery Ageing Considering the Rate of Discharge Ability. *Energy Procedia* **105**, 844–849 (2017).

116. Richardson, R. R., Zhao, S. & Howey, D. A. On-board monitoring of 2-D spatially-resolved temperatures in cylindrical lithium-ion batteries: Part II. State estimation via impedance-based temperature sensing. *J. Power Sources* **326**, 377–388 (2016).

117. Information, P. NCP03WF104F05RL Specifications. 4–6 (2018). Available at: https://www.murata.com/en-sg/api/pdfdownloadapi?cate=luNTCforTempeSenso&partno=NCP03WF104F05RL.

118. Jiling, L. & Zhen, Z. Battery Thermal Management Systems of Electric Vehicles. (Chalmers University of Technology, 2014).

119. Wang, Q. *et al.* Thermal runaway caused fire and explosion of lithium ion battery. *J. Power Sources* **208**, 210–224 (2012).

120. Feng, X. *et al.* Thermal runaway mechanism of lithium ion battery for electric

vehicles: A review. *Energy Storage Mater.* **10**, 246–267 (2018).

121. Braun, P. V., Cho, J., Pikul, J. H., King, W. P. & Zhang, H. High power rechargeable batteries. *Curr. Opin. Solid State Mater. Sci.* **16**, 186–198 (2012).

122. Aifantis, K. E., Hackney, S. A. & Kumar, V. *High Energy Density Lithium Batteries: Materials, Engineering, Applications*. (Wiley-VCH Verlag GmbH & Co. KGaA, 2010). doi:10.1002/9783527630011

123. Masaki, Y., Brodd, R. J. & Kozawa, A. *Lithium-Ion Batteries*. *Journal of Chemical Information and Modeling* **53**, (Springer, 2009).

124. Notten, P. H. L., Veld, J. H. G. O. H. & Van Beek, J. R. G. Boostcharging Li-ion batteries: A challenging new charging concept. *J. Power Sources* **145**, 89–94 (2005).

125. Lewenstam, A. & Scholz, F. *Handbook of Reference Electrodes*. (Springer Berlin Heidelberg, 2013). doi:10.1007/978-3-642-36188-3

126. Voutilainen, J., Happonen, T. & Fabritius, T. All Silk-Screen Printed Polymer-Based Remotely. **15**, 723–733 (2015).

127. Ma, B., Ren, J., Deng, J. & Yuan, W. Flexible thermal sensor array on PI film substrate for underwater applications. *Proc. IEEE Int. Conf. Micro Electro Mech. Syst.* 679–682 (2010). doi:10.1109/MEMSYS.2010.5442315

128. Sensors, M. Printed and Flexible Sensors Report from IDTechEx. in *Printed and Flexible Sensors Report from IDTechEx* (2016).

13 Appendix

13.1 Frequency domain analysis of optical instrumented cylindrical cells

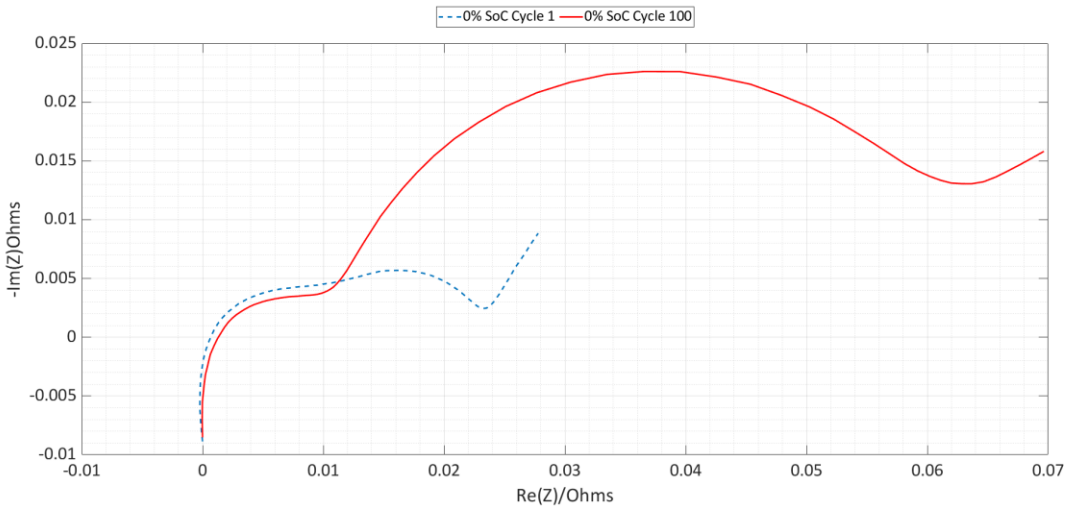

Figure 68 Illustration of an instrumented cells EIS for a 18650 at 0% SoC for cycle 1 and 100

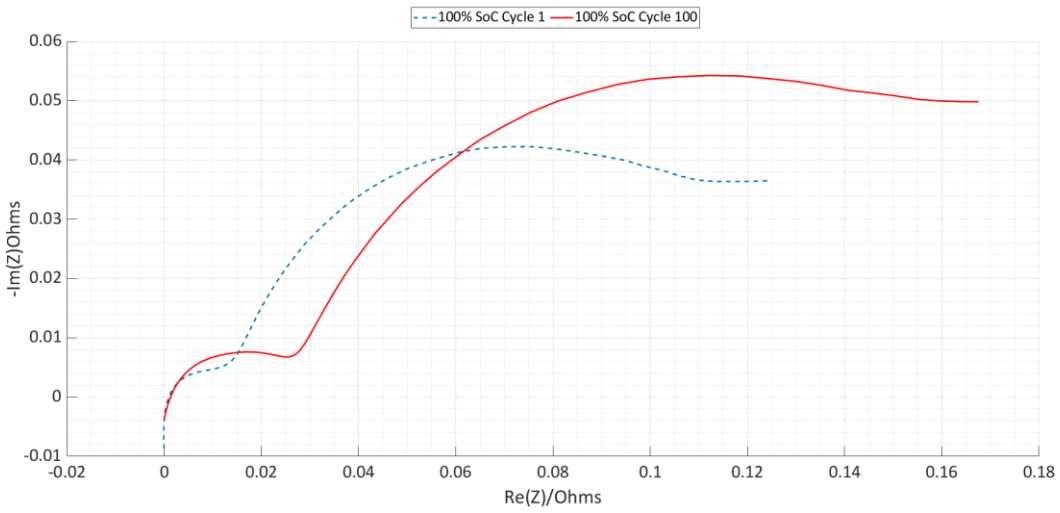

Figure 69 Illustration of an instrumented cells EIS for a 18650 at 100% SoC for cycle 1 and 100

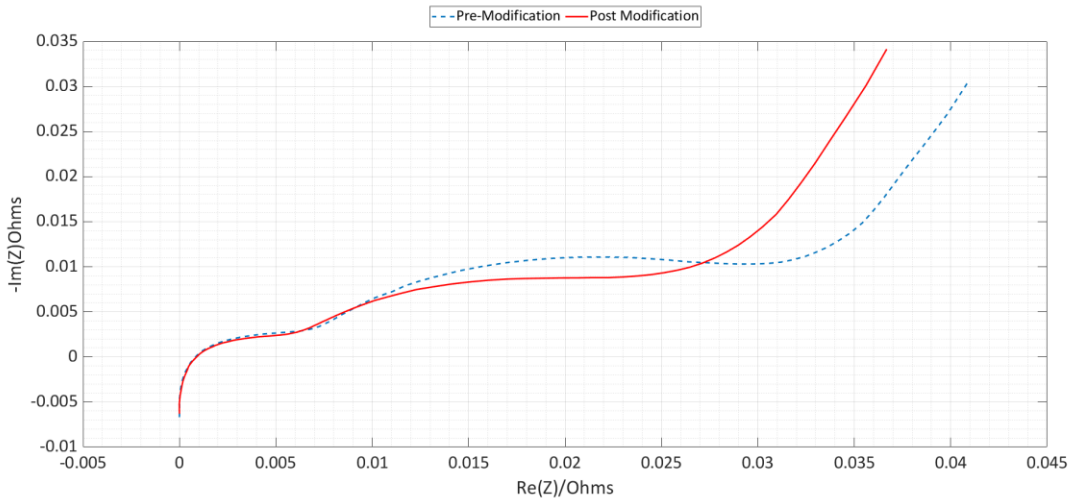

Figure 70 Illustration of an instrumented cell versus a virgin cell EIS for a 18650 at 100% SoC

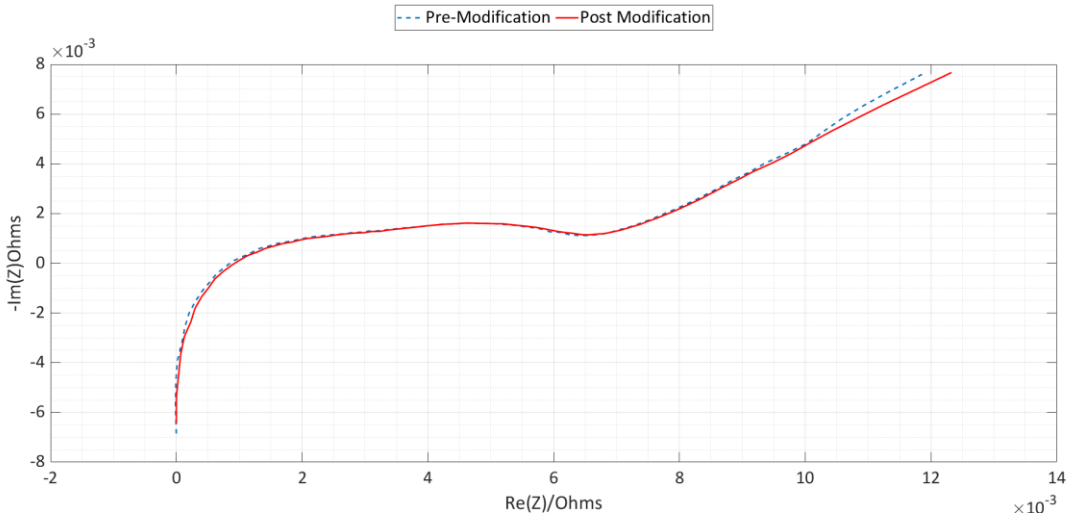

Figure 71 Illustration of an instrumented cell versus a virgin cell EIS for a 18650 at 0% SoC

13.2 Pouch cell instrumented

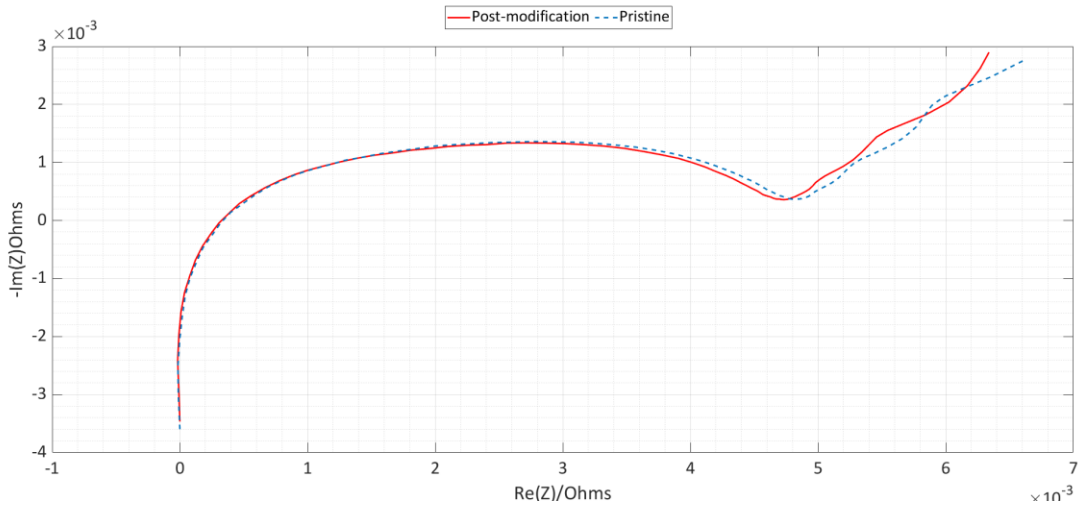

Figure 72 Normalised data for EIS study of an instrumented versus a virgin cell at 0% SoC

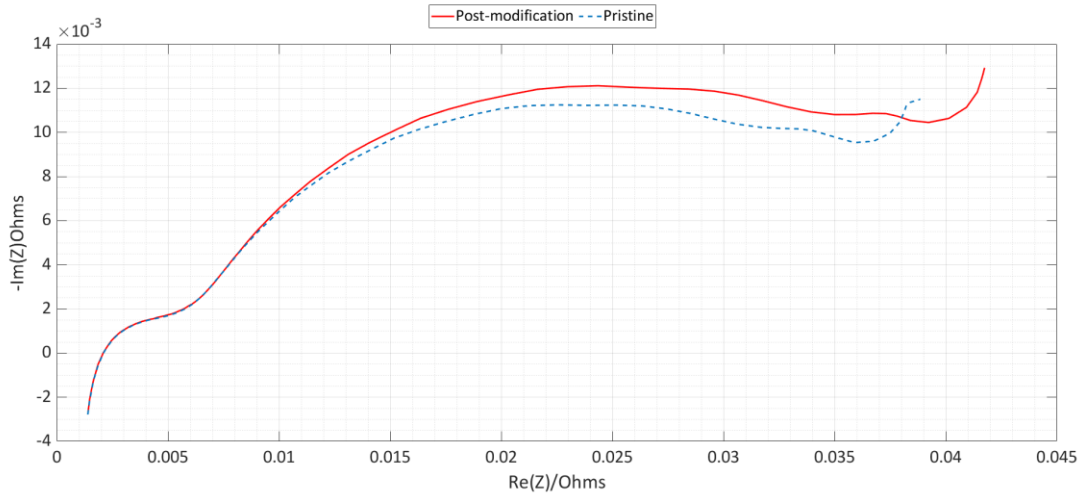

Figure 73 Normalised data for EIS study of an instrumented versus a virgin cell at 100% SoC

13.3 18650 frequency data

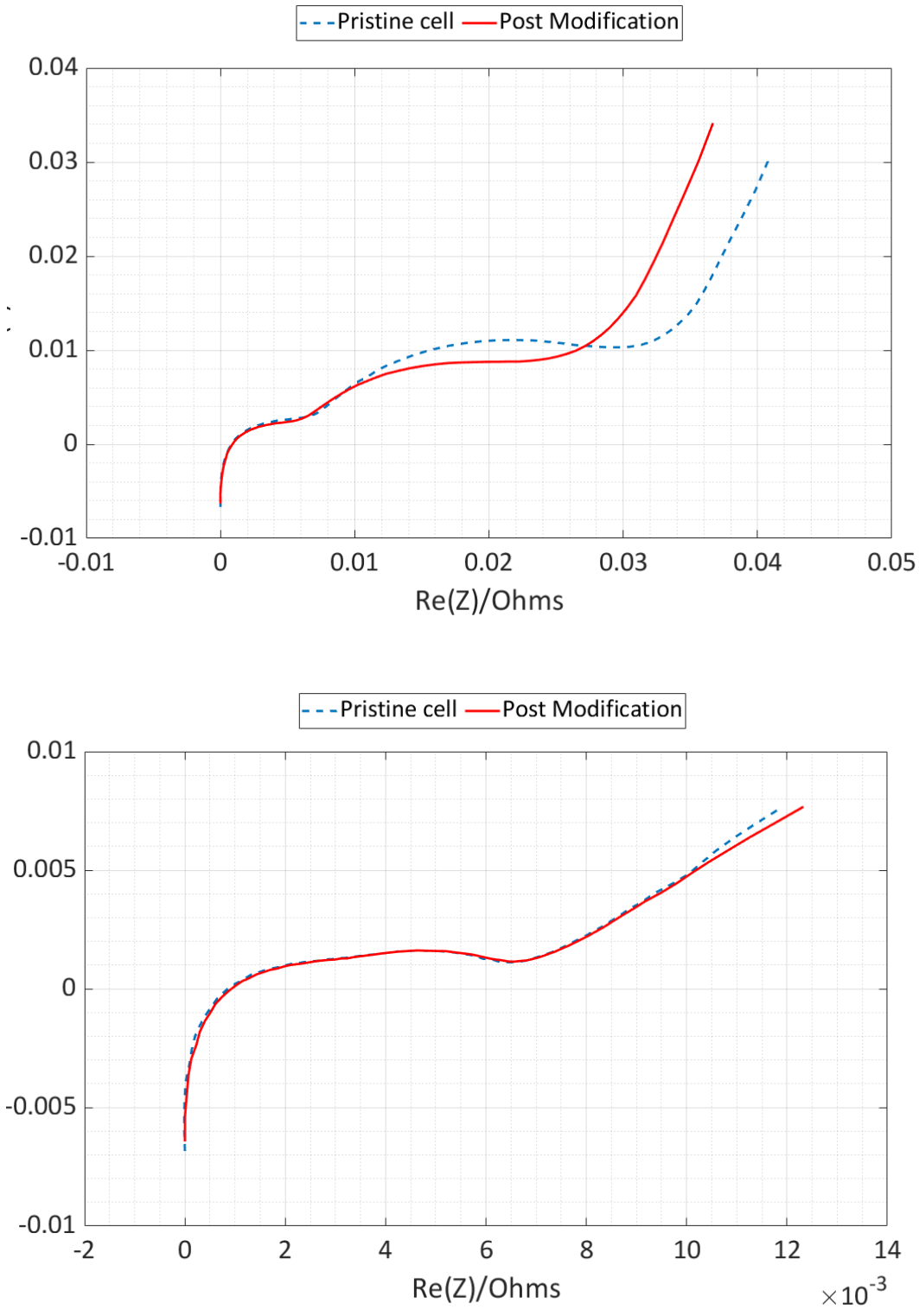

Figure 74 Nominalised data EIS study of an instrumented 18650 cell at 0% (top figure) and 100% (bottom figure) SoC showing a slight drift in the diffusion region of the device compared to an non-instrumented cell